Investigations on Magnetic Nanoparticle Liquid Crystal Composites

A

Thesis

Submitted for the Award of

the Degree of

DOCTOR OF PHILOSOPHY

IN

PHYSICS

Submitted By

Khushboo

Roll No. 951312002

Under the guidance of

Prof. K K Raina
Vice Chancellor
Dehradun Institute of Technology
University, Dehradun
Uttarakhand

Dr. Puneet Sharma
Associate Professor
SPMS
Thapar Institute of Engineering &
Technology Patiala-147004

School of Physics & Materials Science
Thapar Institute of Engineering & Technology
Patiala-147004
(2017)

CERTIFICATE

This is to certify that the thesis entitled ***"Investigations on Magnetic Nanoparticle Liquid Crystal Composites"*** submitted by ***Mrs Khushboo*** in fulfillment of the requirement for the award of the degree of ***Doctor of Philosophy*** in the School of Physics and Material Science, Thapar Institute of Engineering and Technology, Patiala, is an authentic record of candidate's own research work carried out by her under my supervision and guidance.

The matter presented in this thesis has not been submitted in part or full for the award of any degree in any other Institute or University.

Prof. K. K. Raina
Vice Chancellor
Dehradun Institute of Technology University
Dehradun, Uttarakhand, India

Date

Dr. Puneet Sharma
Associate Professor
SPMS
Thapar Institute of Engineering & Technology,
Patiala, Punjab, India

Date

Dedicated

To

My

Family Members

Acknowledgements

Working on the PhD has been a wonderful and often overwhelming experience. It is hard to say whether it has been grappling with the topic itself which has been the real learning experience, or grappling with how to write papers and proposals, give talks, work in a group, stay up until the birds start singing and stay focus.

In any case, I am indebted to many people for making the time working on my PhD an unforgettable experience.

First of all, I am deeply grateful to my supervisors **Prof. K. K. Raina,** Vice Chancellor, Dehradun Institute of Technology University, Dehradun and **Dr. Puneet Sharma,** Associate Professor, SPMS, Thapar University, Patiala for their guidance, constant encouragement, constructive and honest criticism. I am greatly indebted to them for providing me excellent freedom to work of my interest. They have been excellent mentors and very supportive throughout the work. They have always been patient and encouraging in times of new ideas and difficulties. I am also thankful to the family members of my supervisors Mrs. Anju Raina, Dr. Dolly Sharma for providing me the homely feeling and accommodating me.

I am thankful to **Professor Prakash Gopalan**, Director, Thapar University Patiala for providing necessary help and facilities and lots of opportunity for the interaction with national and international scientists in the various conferences and seminars held during the tenure of my Ph D. I also take this opportunity to thank **Professor O P Pandey**, Dean Research and Consultancy for continuous support.

I express my sincere thanks to **Prof. Manoj Sharma**, Head, SPMS, Prof. Kulvir Singh, Prof. N K Verma, Dr. B N Chudasama, DR. Tiwari, Dr. Lovleen Kaur Brar, Dr. Bhunia, Dr. B C Mohanty, Dr. D P Singh for their continuous encouragement and support. I am also deeply thankful to all other faculties' members and staff of the department for their whole hearted support and needful help during the various stages of my PhD.

I am also thankful to Director, Head, DR B R Ambedkar NIT Jalandhar for allow me to work in Liquid Crystal Lab, Physics Department. I gratefully acknowledge my lab mates Dr. Arshdeep Singh, Ms. Divya Jayoti, Mr. Anshu Kumar for their help during

experimental work and thesis writing. I am also thankful to Ms. Indu Gupta, Dr. Supreet Kaur, and for their whole hearted cooperation.

I owe a deep sense of indebtedness to my parents (Sri Sohan Veer Singh, Mrs. Anita Devi), in-laws (Sri C. P. Malik, Mrs. Ishwari Malik), Dr. Aruna Malik, Mrs. Manju, Dr. Poonam Malik, sister in laws, Brother Viky for their affection, wholehearted, untiring and immeasurable support at every stage of my life. I express my sincere thanks to **Dr. Akash Deep**, Scientist, CSIO, Chandigarh, Dr. Samayveer Singh for experimental help and suggestions.

I would like to recognize my husband, **Dr. Praveen Malik**, for his everlasting support on me finishing my dissertation and helping me lighten up when I feel stressed. I look forward to you being with me by my side for many years to come. I am thankful to my loving daughters Ms. Sonakshi Malik and newcomer (Baby) for their love, smile and strengthen me to finish the work in time. Love you beta…..

Finally, I would like to thank the *Invisible Hand* for providing me the enough strength, support, courage to the work hard to add another feather of success to my life and to reach at this destination.

(Khushboo)

Contents

List of Tables

List of Abbreviations and Symbols

LC	Liquid crystal
NLC	Nematic liquid crystal
FLC	Ferroelectric liquid crystal
ITO	Indium tin oxide
NOA	Norland optical adhesive
n_o	Ordinary refractive index
n_e	Extra ordinary refractive index
K	Crystalline
I	Isotropic
N	Nematic
N*	Cholesteric
SmA	Smectic A
SmC	Smectic C
SmC*	Smectic C*
CNT	Carbon nanotube
SWCNT	Single-wall carbon nanotube
MWCNT	Multi-wall carbon nanotube
NiNPs	Nickel nanoparticles
NFNPs	Nickel Ferrite
Δn	Optical anisotropy
$\Delta\varepsilon$	Dielectric anisotropy
P_s	Spontaneous polarization
γ	Rotational viscosity
τ_s	Response time
α	Distribution parameter
ε'	Dielectric permittivity of real part
ε''	Dielectric permittivity of imaginary part
$\Delta\varepsilon_{GM}$	Dielectric strength

σ_o	DC conductivity
ε_∞	Dielectric permittivity at high frequency
ε_o	Dielectric permittivity at low frequency
f_r	Relaxation frequency
E_τ	Activation energy
V_{th}	Threshold voltage
E_g	Band gap
W_P	Polarisation energy coefficients
W_D	Dispersion energy coefficients
σ_{ac}	AC conductivity

List of Publications

Publications in Referred Journals

1. Textural, thermal, optical and electrical properties of iron nanoparticles dispersed 4' –(Hexyloxy)-4-biphenylcarbonitrile liquid crystal mixture**. Khushboo**, Puneet Sharma, Praveen Malik, K. K. Raina, **Liquid Crystals**, 44 **(2017)** 1717-1726.

2. Textural and optical studies of magneto-mesogen material for display applications. **Khushboo**, Praveen Malik, Divya Jayoti, Puneet Sharma, K. K. Raina, **Molecular Crystal Liquid Crystals**, 647 **(2017)** 201-206.

3. Dielectric and polarization switching studies in nickel nanoparticles dispersed ferroelectric liquid crystal mixtures, **Khushboo**, Nikhar Bhargawa, Khayti Anand, Praveen Malik, Puneet Sharma, Divya Jayoti, K. K. Raina, **Integrated Ferroelectrics,** 183 **(2017)** 1-7.

4. Electro-optic, dielectric and optical studies of $NiFe_2O_4$- ferroelectric liquid crystal: a soft magnetoelectric material. **Khushboo**, Puneet Sharma, Praveen Malik, K. K. Raina, **Liquid Crystals**, 43 **(2016)** 1671-1681.

5. Dielectric and electro-optical studies of a nickel ferrite nanoparticles- doped ferroelectric liquid crystal mixture. **Khushboo**, Puneet Sharma, Praveen Malik, K. K. Raina, **Phase Transitions**, 89 **(2016)** 144-154**.**

6. Dielectric studies of iron nanoparticles-ferroelectric liquid crystal mixture, **Khushboo**, Puneet Sharma, Praveen Malik, K. K. Raina, **AIP conference proceeding** 1728 **(2016)** 020670.

7. Size dependent studies in ferromagnetic- ferroelectric liquid crystal mixture, **Khushboo**, Puneet Sharma, K. K. Raina, **Liquid Crystals**, **(2017)** https://doi.org/10.1080/02678292.2017.1397211

Papers Presented in Conferences:

1. Electro-optical and dielectric studies of magnetic nanoparticles-ferroelectric liquid crystal mixtures, **Khushboo**, Puneet Sharma, K. K. Raina, **22 National Conference on Liquid Crystals**, 21-23 Dec., **(2015)**, DIT University, Dehradun, India.

2. Electro-optic and dielectric studies in magnetic nanoparticle doped ferroelectric liquid crystal mixtures for soft magneto-electrics, **Khushboo,** Praveen Malik, Puneet Sharma, K. K. Raina, **International Conference on Soft Materials**, 6-10, Oct, **(2014)**, MNIT Jaipur, India.

Chapter – 1

Introduction

Overview

This chapter deals with the basic features and classification of liquid crystals in general and ferroelectric liquid crystals in particular. The various liquid crystalline phases, order parameters and liquid crystal alignment are presented. The physical properties of liquid crystals are also discussed.

1. Liquid Crystals

Condensed matter that exhibit one or more intermediate thermodynamic phases between the crystalline solid and simple liquid state are called liquid crystals (LCs) [1-2]. These type of phases are named as the liquid crystalline phase; mesophase or mesomorphic phase [3-13]. Liquid crystal materials have unique property i.e. In these phases they retain the ability to flow like ordinary liquids, but also possess long-range orientation order. Some LCs may have positional order as well. The molecular arrangement of solid, liquid and liquid crystal is shown in Figure 1.1.

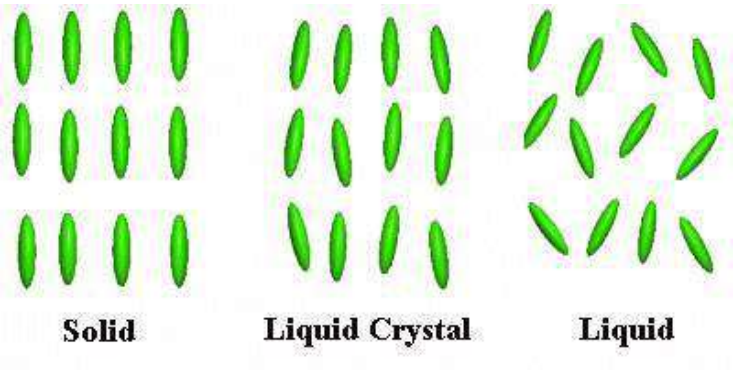

Figure 1.1 Molecular orders in solid, liquid crystal and liquid.

1.1 Classification of liquid crystals

Liquid crystals are classified into two major categories

Lyotropic liquid crystals

Lyotropic liquid crystals are formed by the change in concentration of solvent or solute. e.g. amphiphilic molecules in water. These systems are temperature and concentration dependent and biologically very important [10]. Lytropic liquid crystals are not within the scope of present work, therefore no further details are discussed.

Thermotropic liquid crystals

Thermotropic liquid crystal that exhibits liquid crystalline phase either by heating or cooling and depends on temperature [14]. The phase of a thermotropic liquid crystal changes from crystalline solid to liquid crystal when the temperature is raised above its melting point (T_M). When the temperature is further increased, the phases of the

substance again transform from liquid crystalline phase to isotropic liquid phase. This final temperature is called the clearing point (T_c) (Figure 1.2). Thermotropic liquid crystals which are stable at temperature above the T_M of the compound are called enantiotropic. In certain cases the liquid crystalline state is only stable at a temperature below the T_M point and can be obtained only with decreasing the temperature. Such phases are known as monotropic.

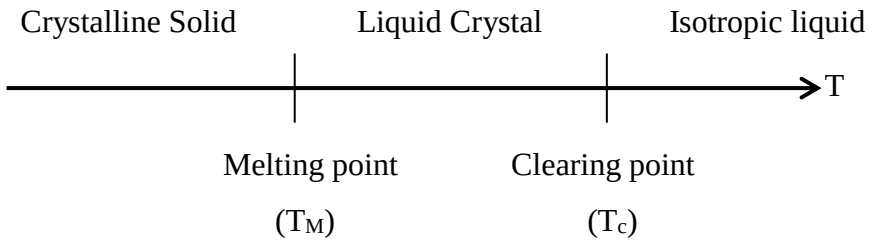

Figure 1.2 Change of phase of substance during heating. T_M and T_C are melting and clearing temperature points.

Thermotropic liquid crystals are of great interest both from basic research & also for their wide applications in electro- optic displays, temperature and pressure sensors etc. Depending upon the molecular structure thermotropic LCs are classified as Calamitic or rod shape like and disc like LCs. The compound formed by rod shaped molecules is called Calamitic liquid crystals. Calamatic stands for rod-like molecules with high length to breath ratio. Calamitic liquid crystal exhibits various phases at different temperature. The commonly used molecules that form LCs are rod shaped molecules. The important property for a calamitic LCs is that the molecule should be rigid for at least some portion of its length, since it must maintain an elongated shape in order to produce interactions that favor alignment. A chemical structure template for calamitic liquid crystal is shown in Figure 1.3.

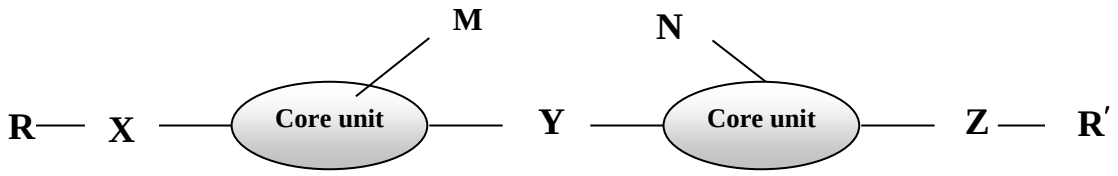

Figure 1.3 Structural template for generating single compound calamitic LCs [10].

- Core units, which are sometimes linked by linkage group (Y) but more often a direct link is used.
- The terminals chains (**R** and **R′**) can be linked to the core, with the groups X and Z but usually the terminals chains are directly linked to the core.
- **M** and **N** are lateral substituents. These are used to modify the mesophase morphology and physical properties of LCs for applications.

On the basis of structure, phase transition, molecular shape and arrangement, classification of liquid crystals is shown in Figure1.4.

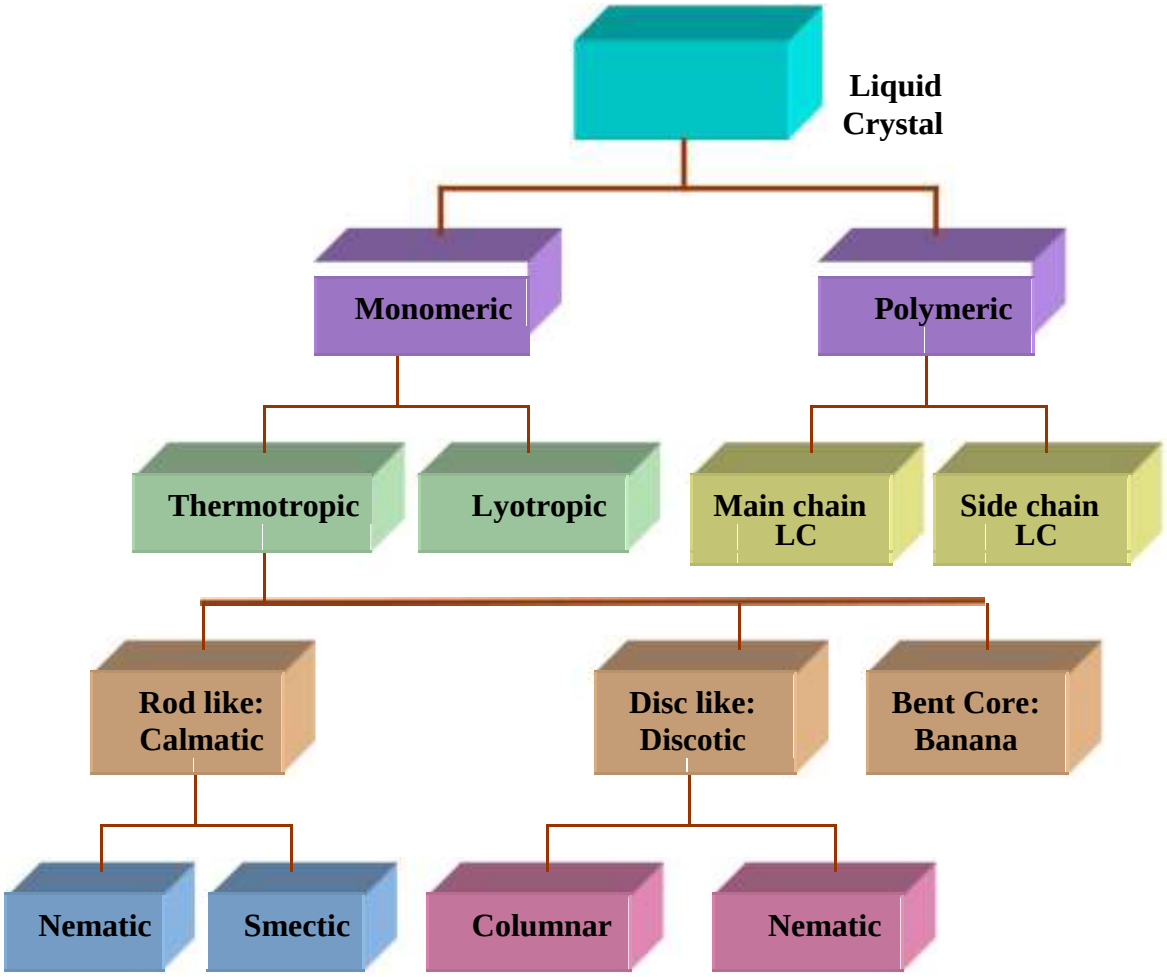

Figure 1.4 Classification of liquid crystals

1.2 Liquid crystal phases

Based on molecular arrangement, liquid crystals are classified into three phases namely Nematics, Smectics and Cholesterics [15].

1.2.1 Non chiral phases

This is a subclass of liquid crystalline phases, which are free from chirality and molecular tilt. However these phases are differ from each other in the type and extent of order and symmetry they possess.

Nematic phase

Amoung all LC phases, nematic phase is simplest one and most commonly used in displays. The word 'nematic' is Greek word means treads. In this phase, the molecules possess only long range orientation but no positional order [Figure 1.5]. Depending on the molecular structure, nematics possess slightly different properties based upon their molecular structure and chemical behaviour like uniaxial and biaxial liquid crystals. Uniaxial nematic liquid crystals have long axes of the molecules tending to align along the director (*n*) as shown in Figure 1.5(a). Biaxial nematic liquid crystal usually consists of molecules that are elongated in one direction and flattered in the perpendicular direction [4,13]. The LC molecules are ordered in two directions: the long axes are oriented around one director and the short axis are oriented around another director perpendicular to the first one.

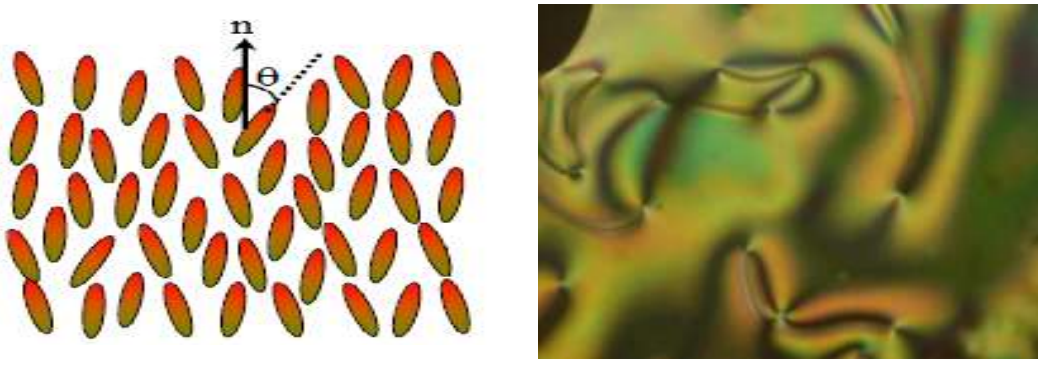

(a) (b)

Figure 1.5 (a) LC molecules possess a preferred direction of orientation (b) Optical texture of nematic liquid crystal under polarizing microscope between crossed polarizers.

A typical example of nematic liquid crystal is p-azoxyanisole (PAA) [16]. The two benzene rings are nearly coplanar. Such a nematic molecule can be considered as a rigid rod. Another liquid crystalline molecule is methoxy benzilidene butyl aniline (MBBA). The chemical structure of PAA, MBBA are shown as

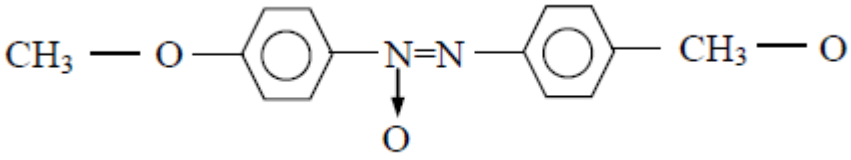

PAA

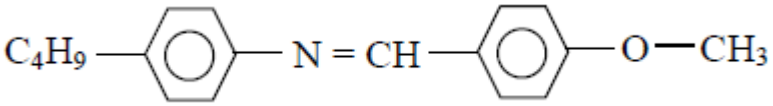

MBBA

Smectic phases

The smectic word is derived from Greek word for ‘soap’. Smectics is the name coined by Friedel [15]. In smectic phase molecules show a degree of translational order and maintain the general orientational order of nematics. From the structural point of view, all the smectics have layered structures and are perpendicular to the layer plane with a well defined interlayer spacing that can be measured using X-ray diffraction technique. The interlayer attractions are weak as compared to lateral forces between molecules and hence layers can easily slide over one another and motion is restricted within these layers or planes. This gives rise to fluidity to the system with higher viscosity than found in nematics and results more ordered smectic phase than nematic. Different type of smectic phases VIZ. Smectic A (SmA), smectic B (SmB), smectic C (SmC), smectic E (SmE) are also observed. Each phase differs from the other in the way of layer formation and existing order inside the layers. [17]. These names are given according the their order of invention. Out of these, SmA and SmC are most common phase and discussed in next section.

Smectic A (Sm A) phase

Sm A phase is least ordered smectic phase in which molecules are arranged in layers having their long molecular axis on average perpendicular to smectic layers. These phases are more ordered than nematics and possess positional and orientation order. These phases usually occur at a temperature below the nematic. In this system the molecules can move freely around the long axes within the layer. Optically Sm A is

uniaxial with the optical axis direction coinciding with the director [Figure 1.6].

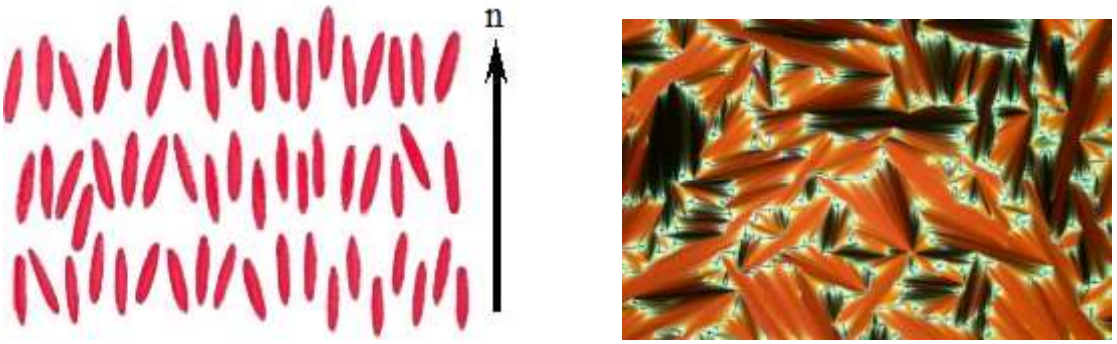

(a) (b)

Figure 1.6 (a) Molecular arrangement in SmA phase. The long axes of the molecules in each layer, on an average, are perpendicular to the layer plane containing the molecules (b) Texture of SmA phase [18].

Smectic C (Sm C) phase

In this phase molecules are organized like the SmA phase, but the only difference is the long axes of the molecules are arranged at an angle θ to the layer normal as illustrated in Figure 1.7 [20]. As in Sm A, the molecules in Sm C can also revolve freely about their long molecular axis within the layer. Optically, SmC is biaxial with one of the axes coinciding with the director, and one along the surface normal. On the temperature scale, SmC is usually located lower than SmA. The microtexture of SmC phase is also seen in Figure 1.8. In SmA and SmC, no positional order exisits within the layer but the positional order is limited only up to one dimension. While others smectic LC phases posses three dimensional orders, they are Smectic B, Smectic E. The molecular arrangement in other smectic phase is shown in Figure 1.9.

Figure 1.7 Molecular arrangement in SmC Phase

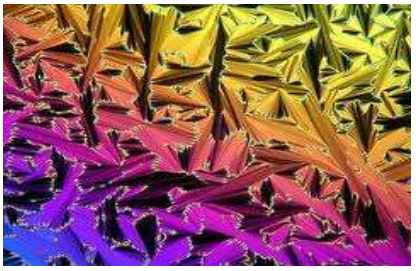

Figure 1.8 Texture of SmC phase [19].

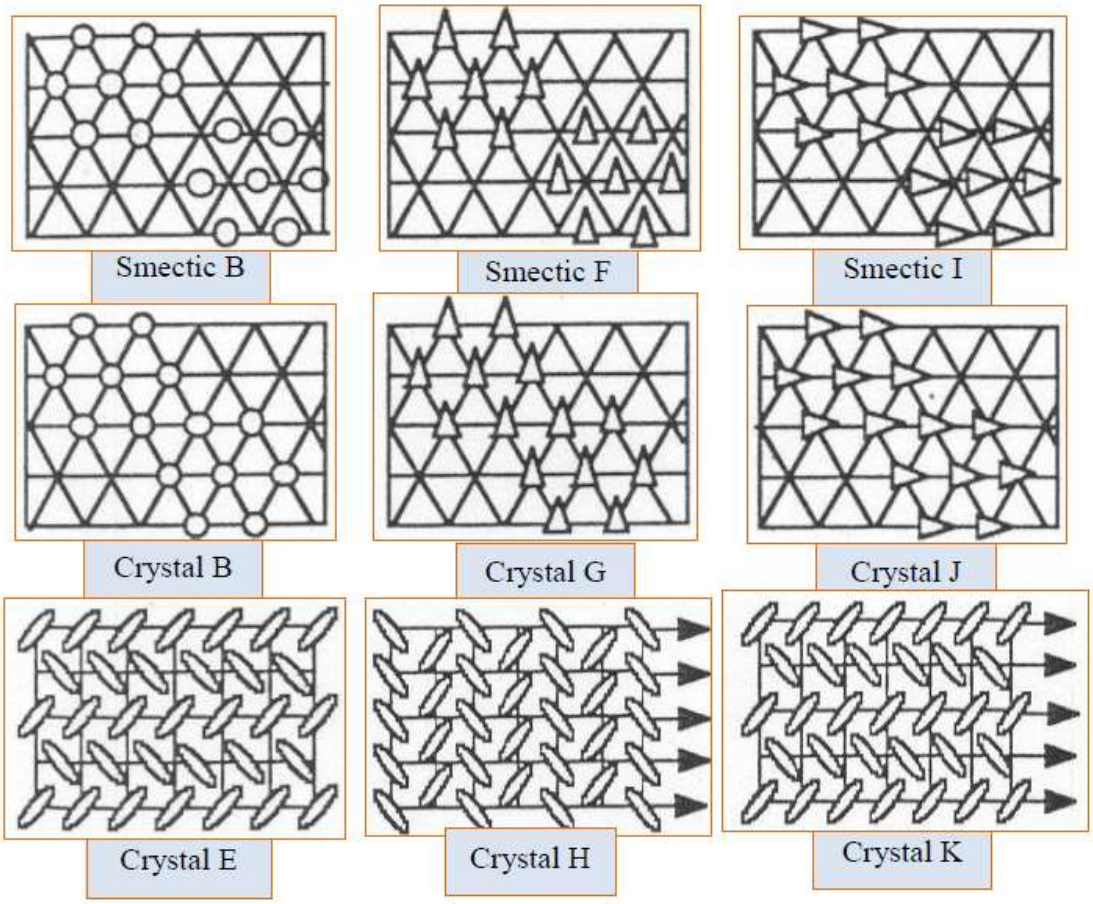

Figure 1.9 (a) Classification of smectic liquid crystal and their molecular arrangement in SmC phase.

1.2.2 Chiral phases

The molecules which are not identical to its mirror image are called *Chiral molecules*. Chiral molecules are optical active and when induced into LC phases, a variety of new phases (chiral phases) is formed. Such material exhibit unusual properties and have wide range of applications [3,8]. Cholesteric replaces nematic phase and smectic phases are replaced by their chiral versions.

Cholesteric or chiral nematic phase

This phase can be generated by adding a small amount of chiral molecules to nematic liquid crystal. These chiral molecules produce intermolecular forces that favor alignment between molecules at a slight angle with respect to one another. This leads to the formation of a structure similar to thin two dimensional nematic like layers with the director in each layer twisted with respect to those above and below. In this structure, the directors form in a continuous helical pattern about the layer normal. The pitch *p* (the distance along the layer normal needed to reach the same molecular orientation) can be adjusted to any desired value by adding suitable amount of a chiral compound to a nematic. Pitch is an important characteristic of this phase and expressed as [21].

$p = 1/(HTP \cdot X_c)$

where HTP and X_c repregents the helical twisting power and concentration of the chiral agent, respectively. The helical pitch controls the selective reflections of the cholesteric phase and makes them suitable for electro-optic display devices. It is represented by N* (* repregents chiral) and the arrangement of molecules is shown in Figure 1.10.

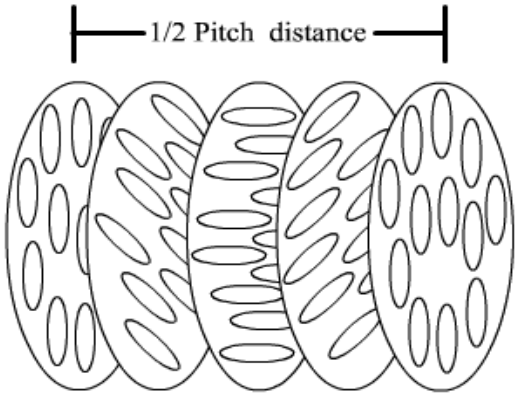

Figure 1.10 Molecular arrangement in Cholestric liquid crystals.

Chiral smectic phase (SmC*)

When chiral molecules are induced into smectic LCs, tilted smectic phase or chiral smectic phase form a helical structure. as a direct result of the molecular chirality of the constituent molecules. In these phases the director rotates from layer to layer through a change in tilt direction and describes a helix [3,8,10]. SmG*, SmH*, SmJ* and SmK* SmC*, SmF* and SmI* are also chiral smectic phases. In case of low symmetry chiral smectic phases (SmC*, SmF* and SmI*), the orientations of molecules tend to form a macroscopic helical structure while moving from one layer to next successive layer [10]. Out of these, SmC* is most common smectic phase.

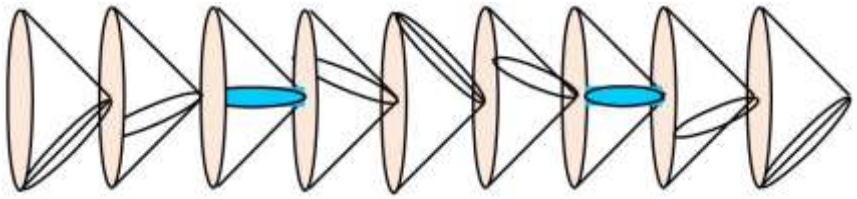

Figure 1.11 Molecular arrangement in Chiral liquid crystals.

1.3 Ferroelectric liquid crystals (chiral smectic C phase)

Ferroelectric liquid crystals (FLCs) or chiral smectic C (SmC*) liquid crystals possessing low symmetry are novel materials owing to their fundamental significance and promising applications in electro-optic displays [22, 23]. FLCs are successfully used in fast response light shutters and displays, image convertor, waveguides etc. The molecules of FLCs possess permanent dipole moment. Meyer *et al*. demonstrate the origin of ferroelectricity both theoretically as well as experimentally in the SmC* phase.

In 1975, Meyer *et al*. used symmetry arguments and demonstrated that chiral titled smectic phases exhibit ferroelectric properties (spontaneous polarization). SmC* phase is formed by the addition of chiral molecules in the ordinary SmC molecules. When the molecule is chiral, successive tilted smectic layers show a gradual change in the direction of tilt, such that the director (*n*) precesses about the layer normal (Z) from layer to layer, always lying on the surface of a hypothetical cone of angle *2θ (θ- tilt angle; the angle between n and Z).* The angle around the circle of precession is known as the *azimuthal angle* (*Φ).* This creates a helical structure in the SmC* with the pitch being the distance along the layer normal needed to reach the same molecular orientation. There is no change in the amplitude of *θ*, only azimuthual angle changes along the helix axis. Although the SmC* phase is actually weakly biaxial, to a good approximation, it can be treated as a uniaxial material. Figure 1.12 shows the basic geometry of the SmC* phase.

The permanent electric polarization *P* is perpendicular to the director and parallel to the smectic layers, where *C* gives the direction and magnitude of the tilt. The magnitude of the polarization depends on temperature, generally decreasing with decreasing the temperature as the tilt angle goes to zero at the SmC- SmA phase transition.

In addition to producing this helical structure, chirality results in a spontaneous molecular polarization. The presence of helical structure in the LC material is responsible for its fascinating optical properties.

Another most exciting feature of FLCs is that the symmetry of the SmC* phase permits the existence of spontaneous polarization within the layer plane and perpendicular to the director. Since spontaneous polarization is coupled with the director, it also rotates. It will lead to the cancellation of microscopic polarization in the bulk sample, but each layer is

spontaneously polarizaed. [24, 25]. By supporting (unwinding) the helix with the external electric field, this phase will exhibit macroscopic polarization and as a result net spontaneous polarization is obtained. The value of spontaneous polarization in these materials is quite small, usually about one or two orders of magnitude less than that of a solid ferroelectric.

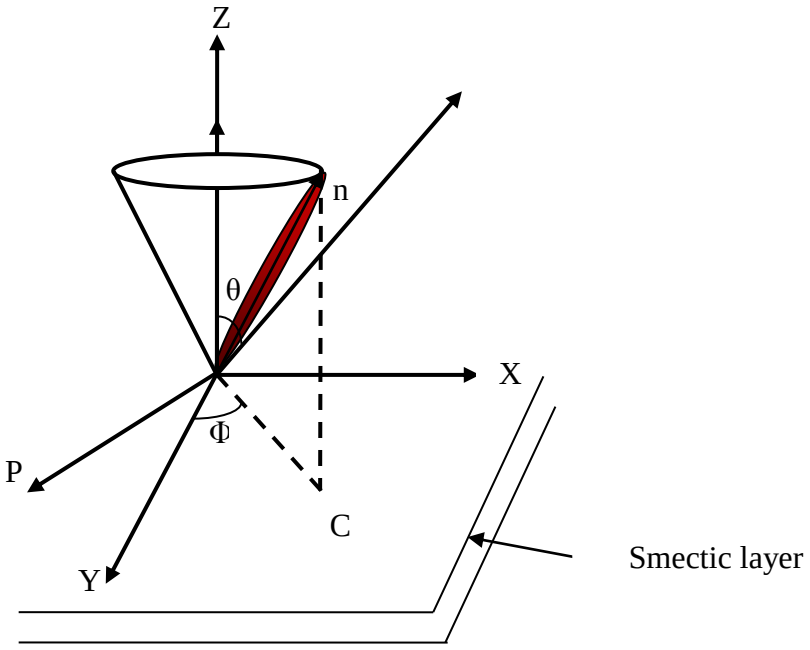

Figure 1.12 Basic geometry of the SmC* phase showing layer normal (Z), tilt angle (θ), molecular director (n), polarization (P) along (z x n) and azimuthal angle (Φ) of P about z. Directions of both n and P vary spatially in a helical manner**.**

Properties of FLCs and chiral

The essential material requirements to be used as a good ferroelectric host mixture are; [10].

-low melting point (below room temperature)

-wide SmC range with no underlying ordered smectic phases

-cooling phase sequence of I – N – SmA – SmC

-low viscosity

-tilt angle of 22.5^{o}

-low to moderate optical anisotropy

-negative dielectric anisotropy, high dielectric biaxiality

-high chemical and photochemical stability

Out of all the materials that exhibits SmC phase, phenylpyrimidines and difluroterphenyls and diflurophenlprimidines) are commonly used materials as ferroelectric host [26]. The proper selection of chiral dopant is an important creteria because it should provide some additional physical properties (reasonably high spontaneous polarization (P_S), long pitch and good solubility and compatibility between ferroelectric host and chiral dopant).

The most important chiral dopants for ferroelectric mixtures have a polar group on the chiral centre (e.g. Cl, F, and CN). The fluoro-substituent is widely employed at a chiral centre in dopant materials because of its small size and high electro-negativity. To get the high P_s (10 nC/cm^2 with 20% dopant) and retain the stability of SmC* phase, chiral phenylpyrimidine systems having fluoro-substituents at the chiral centre are normally used. DOBAMBC (p-decyloxybenzylidene-p‘-amino-2-methylbutylcinnamate, first FLC material exhibit ferroelectric LC properties was synthesized in 1974 [10]. This material received much scientific attention but photochemically unstability, high viscosity and low P_s were the main issues which makes it unsuitable for use in displays. Later on, analogous to DOBAMBC, Schiff base compounds were prepared which enriched the understanding of molecular dynamics on phase morphology, transition temperature and magnitude of spontaneous polarisation. A typical structure of a chiral, calamitic, rod-like liquid crystalline compound, which has two flexible aliphatic chains attached to a rigid aromatic

or quasi-rigid alicyclic core is shown in Figure1.13.

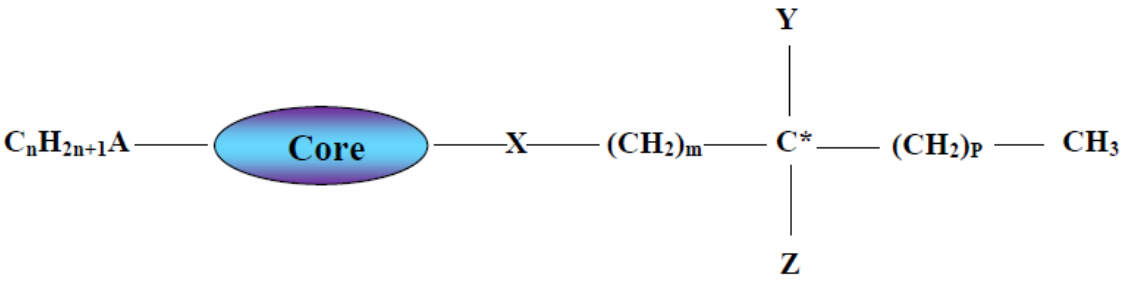

Figure 1.13 A typical structure of a chiral, calamitic, rod-like liquid crystalline compound. Here n, m and P are integers; A and X are polar groups; Y and Z are different substituent; * denotes a chiral centre [10].

1.4 Other Types of Liquid Crystal Phases

Blue Phase

Blue phases (BPs) in liquid crystals was first observed by F. Reinitzer and exist in a very narrow temperature range of the order of 1°C [27]. BPs have created enormous interest due to its exotic optical properties like optically isotropic voltage off state, fast switching, high contrast ratio, no need for alignment layer, and selective reflection of circularly polarized light [28]. These properties make them a suitable candidate for various applications such as fast response displays, mirror-less lasers, tunable photonic band gap materials, and light modulators due to electrically controllable Bragg's diffraction [29-32].

Blue phase liquid crystals (BPLCs) have high twist power (HTP) [33-38]. Three thermodynamically stable distinct blue phases BP-III, BP-II and BP-I, respectively are observed under cooling condition from isotropic liquid [39-41]. BP-III is amorphous and it appears like bluish fog under polarizing microscope. A number of models have been proposed to account for the structure of BP-III but microscopic structure of this phase has not yet established. The structure of BP-I is body centered cubic while that of BP-II is simple cubic [42-43]. This cubic symmetry of BPs is comprised of double twist cylinders (DTCs) which represent a structure of minimum free energy [44]. DTCs are arranged mutually perpendicular to each other that results in creation of a defect [45]. Thus a cubic

lattice of DTC or line defects is formed with lattice parameters of several hundred nanometers. BPs are isotropic but they become anisotropic on application of electric field. A DTC, defect and BPLC having wide temperature range (10-60 K) is shown in Figure 1.14 [46].

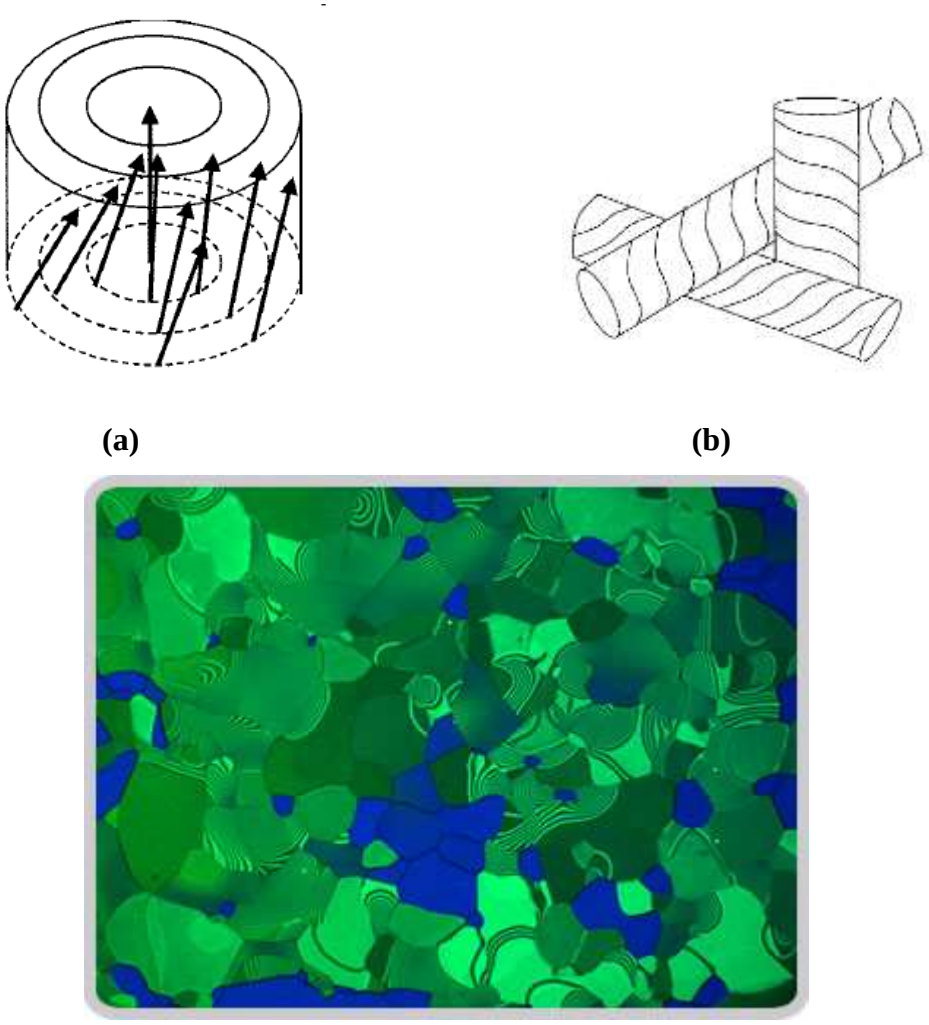

(a) **(b)**

(C)

Figure1.14 (a) Double twist cylinder (b) Local arrangement of three DTCs forming a defect region. (c) A Blue phase liquid crystal of wide temperature range from 16-60ºC.

Twisted Gain Boundary Phases

Twist grain boundary (TGB) phases are frustrated defect phases, which can be observed in often only at narrow temperature range between cholesteric and SmA* phase or between SmA and isotropic phase of highly chiral liquid crystals. TGBA phase were first predicted theoretically by Renn and Lubensky [47, 48] and experimentally by Goodby *et al*. [13-15] [49-51]. These phases exhibit simultaneously a helical twist and block of smectic layers. The TGB is formed when the layers of a smectic A phase are forced to twist by the presence of chiral molecules. The system accommodates the conflicting demands of constant layer spacing and a net twist by breaking up into a sequence of blocks, each with intact layers and no twist, but each rotated by a fixed angle relative to its neighbouring blocks (Figure 1.15 (a)). The interface between adjacent blocks is a twist grain boundary. Depending on the charachter of the smectic blocks (SmA*, SmC, SmC*), TGBA*, TGBC and TGBC* phases are predicted. For the existence of these phases molecule should have strong molecular chirality. Planar TGB TGBA* phase is shown in Figure 1.15 (b). Here TGBA* helix axis is perpendicular to the substrate plane, i.e. out of the plane of the image.

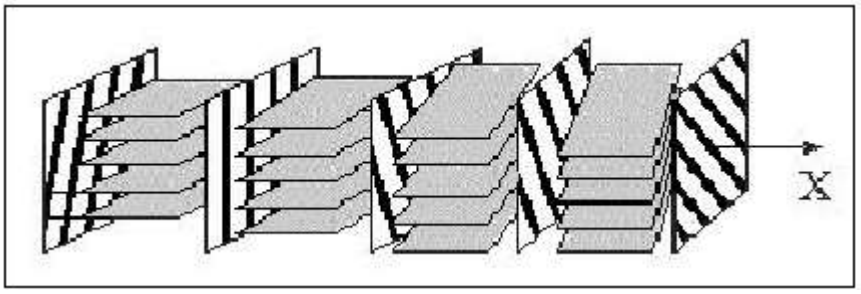

(a)

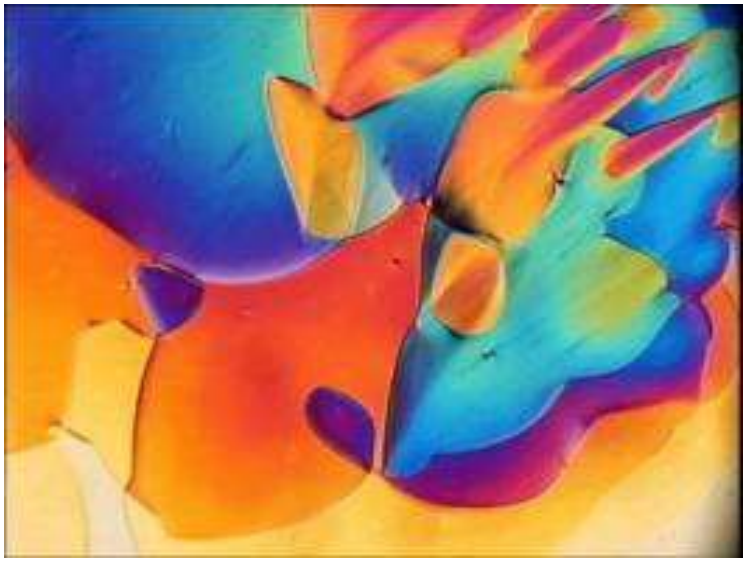

(b)

Figure 1.15 (a) A sequence of twisting of smectic blocks in TGBA phase; (b) Planar twist grain boundary TGBA* phase

Banana-shaped or bent-core liquid crystals

Bent-core liquid crystal were synthesized by Vorlander in 1930 and received much interest due to its unusual polarity behaviour and show ferroelectricity. These are achiral, but the special molecular packing induces chirality into the smectic layers and show ferroelectric behaviour [52]. These organic molecules due to their bent core or V shape are called 'Bananas'. Bend-core molecules basically consists of a V-shaped core and alkyl tags at the two ends of the V-bend. Various phases were observed for this new kind of mesophase, and referred as B1, B2…. B7 [53,54]. Recently it has been reported that the smectic phase of achiral banana –shaped molecular systems could form helical superstructures [55]. Matsunaga and co-workers synthesized banana shaped materials and reported that they can form smectic LCs but they did not pay any attention to the electrical properties [56,57]. Watanable *et al*. reported that a ferroelectric smectic phase with C_{2v} symmetry might be formed for chain types of LC polymers, if two different aliphatic spacers with odd numbers of carbons are incorporated into the backbone in regularly alternating fashion and they segregate into different mono-domains. They also

prepared homologous series of banana-shaped molecules, which form the SmA_b, $HexB_b$ and smectic BP in order of decreasing temperature, and then discovered the ferroelectricity in the SmA_b and $HexB_b$ phases. They reported spontaneous polarization more than 150 nC/cm^2 even in the higher order smectic phase below the SmA_b phase, and concluded that this phase is also ferroelectric. These materials, which form smectic phase are particularly interesting because of their shape, they form a peculiar smectic phase in which the banana-shaped molecules are closely packed and are aligned in the direction of bending. A banana-shaped structure is shown in Figure1.16.

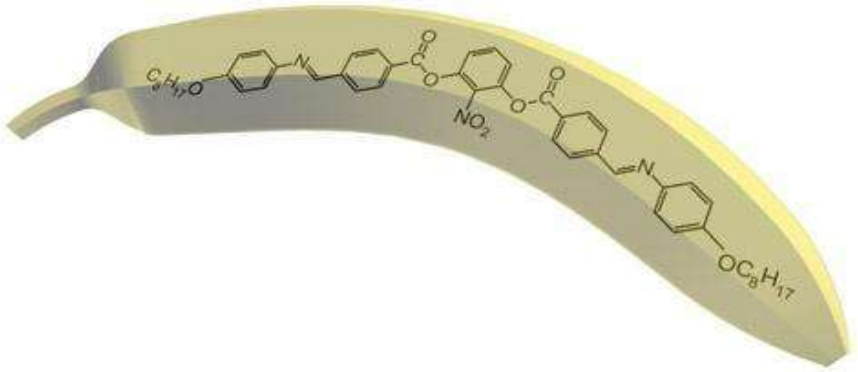

Figure 1.16 A typical banana-shaped molecule

Disc shaped

Discotic liquid crystals are formed by disc shaped molecules, in which one molecular axis is shorter than other two. The first evidence of mesomorphic behaviour in disc shaped molecules (hexa-alkanoylbenzene) was discovered in 1977 by S. Chandrasekhar [8]. Such compounds known as discotic LCs and again rigidity in the central part of the molecule is essential. The core of a typical discotic LC molecule is usually based on benzene, triphenylene or truxene with 6 or 8 chains, each resembling a typical calamitic LC molecule. Figure 1.17 shows a general structural template for discotic LCs. The disc shaped central core unit is usually benzene or a polyaromatic such as triphenylene or phthalocyanime, but columnar phases have been generated with alicyclic cores such as

cyclohexane and carbohydrate. In order to maintain the disc-like structure, the central core is usually symmetrical and the peripheral dendritic units are present in number that is appropriate for the central core [10].

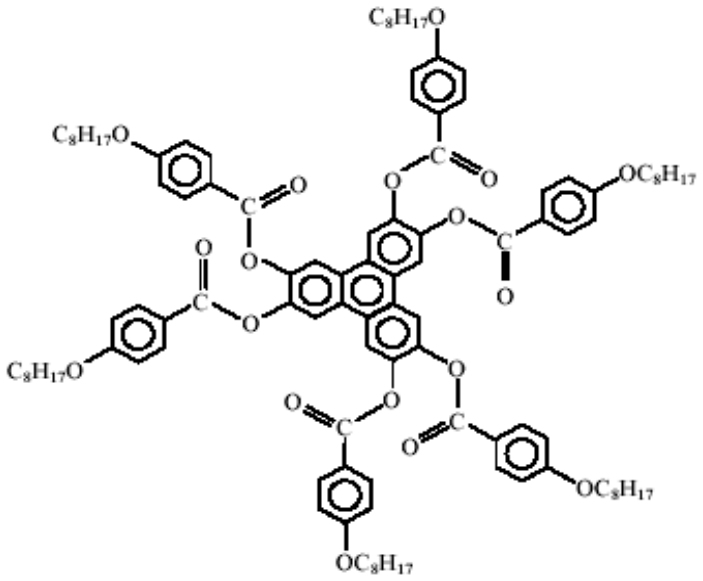

Figure 1.17 A general structural template for discotic liquid crystal.

1.5 Physical Properties of Liquid Crystals

Order parameter

The amount of orientation order in liquid crystals can be obtained by averaging macroscopic molecule orientation with respect to director. The order parameter (S) can be defined as the average of the second Legendre

$$S = (\frac{1}{2}) < 3\cos^2\theta - 1 > \qquad (1.1)$$

Where θ is the angle between the rod axis of a molecule and the director as shown in Figure 1.18. If all liquid crystal molecules align perfectly parallel to the director then S = 1. If all the molecules orient completely at random directions, then S = 0.

Typically, the order parameter in liquid crystal phases ranges from 0.3 to 0.9 [Figure 1.18(b)].

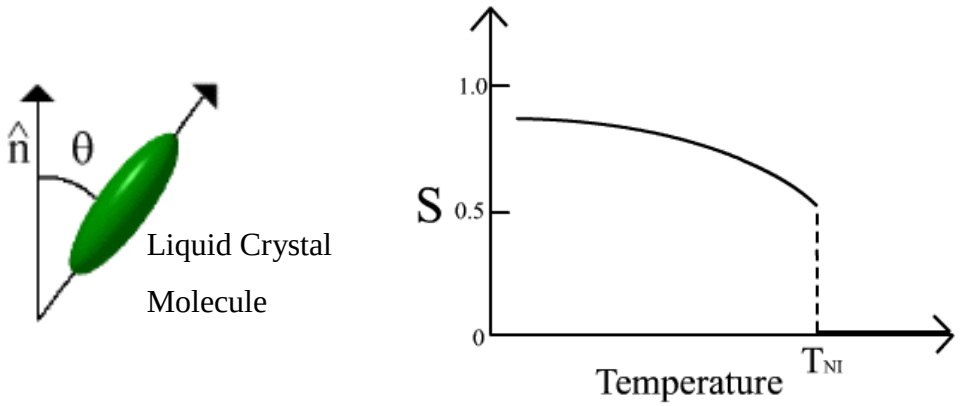

Figure 1.18 (a) Geometry defining order parameter of a liquid crystal (b) Variation of order parameter of nematic liquid crystal as a function of temperature.

Anisotropy

Due to the presence of small degree of order among their molecules, LCs are anisotropic in nature. This property distinguishes them from ordinary liquids.

When an electromagnetic wave passes through the nematic LC material, the outgoing wave gets split into two rays; one along parallel to the nematic director and other perpendicular to the direction of nematic director. These rays are called ordinary ray (O-ray) and extraordinary ray (e-ray) respectively. The optical anisotropy (Δn) can be explained by a typical example of birefringence as illustrated in Figure 1.19.

The optical anisotropy is determined by

$$\Delta n = n_e - n_o \tag{1.2}$$

Where n_e and n_o gives the indices of refraction in the direction parallel (extra ordinary) and perpendicular (ordinary) to the nematic axis respectively. If Δn is positive then material is said to be positive uniaxial LC and if negative then materials is said to be negative uniaxial.

The effect of electric field gives rise to dielectric anisotropy $\Delta\varepsilon$ in these systems. It is given by

$$\Delta\varepsilon = \varepsilon_{II} - \varepsilon_{\perp} \tag{1.3}$$

Where $\varepsilon_{\perp}$ and ε_{II} refer to the dielectric constant perpendicular and parallel to the

nematic axis respectively. The response of nematics to an electric field depends upon both the sign and magnitude of $\Delta\varepsilon$. If $\Delta\varepsilon$ is positive, lowest energy state in the presence of field will be that in which the nematic axis is parallel to field and for negative value of $\Delta\varepsilon$, the lowest energy state will be the one in which the nematic axis is perpendicular to the electric field [10].

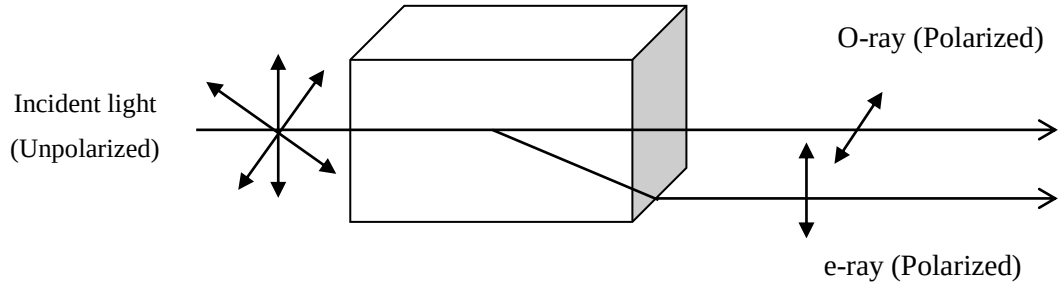

Figure 1.19 Bifurcation of incident light into an ordinary and extra ordinary rays due to the anisotropy in a birefringent liquid crystal.

Electric and magnetic field effects

When an external electric field is applied to the LCs, the dipole molecules tend to orient themselves along the direction of applied electric field. As shown in Figure 1.20, the black arrows represent the electric field vector and the other arrows show the electric force on the molecule.

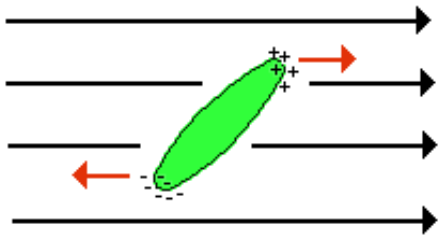

Figure 1.20 Effect of external electric field on liquid crystal molecules.

Even if a molecule does not form a permanent dipole, it can still be influenced by an electric field. In some cases, the field produces slight re-arrangement of electrons and protons in molecules such that an induced electric dipole. While not as strong as permanent dipoles, orientation with the external field.

The effects of magnetic fields on LCs molecules are analogous to electric fields. Because magnetic fields are generated by moving electric charges, permanent magnetic dipoles are produced by electrons moving about atoms. When a magnetic field is applied, the molecules will tend to align with or against the field.

References:

[1]. O. Lehmann, “Uber fliessende krystalle,” Z. Phys. Chem. 1889; 4: 462–472.

[2]. F. Reinitzer, “Beitrage zur kenntniss des cholesterins,” Monatsh. Chem.1888; 9: 421–441.

[3]. P G De Gennes. The Physics of Liquid Crystal: Oxford University Press;1975.

[4]. B. M. Mulder, Liq Cryst. 1986; 1: 539-551.

[5]. D. C. Wright, N. D. Mermin, Rev Mod Phys. 1989;61, 385-432.

[6]. J.W. Goodby, M.A. Waugh, S.M. Stein, E. Chin, R. Pindak, J. Patel, Nature 1989;337; 449-452.

[7]. K.J. Ihn, A.N. Zasadziinski, R. Pindak, A.J. Slaney, J.W. Goodby. Science. 1992; 258: 275-278.

[8]. S. Chandrasekhar, Liquid Crystal 2nd Edn. Cambridge: Cambridge University Press (1992).

[9]. J.W. Goodby, I. Nishiyama, A.J. Slaney, C.J. Booth, K.J. Toyne, Liq Cryst. 1993; 14: 37-66.

[10]. P. J. Colling, M. Hird, “Introduction to Liquid Crystal, Chemistry and Physics,”Taylor and Francis Ltd. (1997).

[11]. A. Jakli, M. Muller, D. Kruerke, G. Heppke, Liq Cryst. 1998;24; 467-472.

[12]. C.K. Lee, A. Primak, A. Jakli, E.J. Choi, W.C. Zin, L.C. Chain, Liq Cryst. 2001;28: 1293 1299.

[13]. B.R. Acharya, A. Primak, S. Kumar, Phys Rev Lett. 2004; 92: 145506.

[14]. G. Vortogch and W. De Jeu, Thermotropic liquid crystal fundamentals, Springer Verlag, New York, (1998).

[15]. G. Friedel, Ann Physique 1992;18: 273.

[16]. Neeraj, Ph.D. Thesis, Thapar University, Patiala (2011).

[17]. P. J. Collings, Liquid Crystals: Nature‘s Delicate Phase of Matter, Princeton University Press (1990).

[18]. S.F. Tandel, http://www.eng.cam.ac.uk/photocomp/2008/sf386_9.shtml (2008).

[19]. Weblink,http://photonicswiki.org/index.php?title=File:F%C3%A4chertextur.jpg (2005).

[20]. S. Kumar, Phys Rev A 1981; 23: 3207.

[21]. P. G. De Gennes and J. Prost, The Physics of Liquid Crystals, 2nd edition, Oxford, Clarendon Press 1973.

[22]. Meyer RB, Liebert L, Strzelecki L, Keller P, J Phys Lett. 1975; 36: 69-71.

[23]. I Musevic, R Blinc, B Zeks, The Physics of Ferroelectric and Antiferroelectric Liquid Crystals, World Scientific Publishing Company, (1999).

[24]. I.C. Khoo, Liquid Crystals: Physical Properties and Non-Linear Optical Phenomenon, John Wiley and Sons Inc. New York (1995).

[25]. Marek Matuszczyk, Ph.D. Thesis, Chalmers University of Technology, Goteborg, Sweden (1996).

[26]. L.A. Bersnav, L.M. Blinov, M.A. Osipov and S.A. Pikin, Mol Cryst Liq Cryst. 1988; 158A: 1.

[27]. F. Reinitzer, Monatsh Chem. 1888; 9; 421.

[28]. I. Dierking, W. Blenkhorn, E. Cruruba, Bedland, W. Drake, R. Kociuruba, B. Kayser and T. Michael, Soft Matter. 2012; 8: 4355.

[29]. F. Castles, F. V. Day, S. M. Morris, D. H. Ko, D. J. Gardiner, M. M. Qaasim, S. Nousheen, P. J. W. Hands, S. S. Choi, R. H. Friend and H. J. Coles., Nat Mater. 11, 599 (2012).

[30]. J. Yan, L. Rao, M. Jiao, Y. Li, H. C. Cheng and S.T. Wu., J. Mater. Chem. 2011; 21:7870.

[31]. S. Yokohama, S. Mashiko, H. Kikuchi, K. Uchida and T. Nagamra, Adv Mater. 2006; 18: 48.

[32]. W. Cao, A. Munoz, P. P. Muhoray and B. Taheri, Nat. Mater. 2002; 1: 111.

[33]. P. G. de Gennes, The Physics of Liquid Crystals (Clarendon Press, Oxford, (1974).

[34]. V. A. Belyakov and V. E. Dmitrienko, Sov. Phys. Usp. 1985; 28: 535.

[35]. G. W. Gray, J. Chem. Soc. 1956; 3733.

[36]. Y. Chen and S. T. Wu, J Appl Polym Sci. 2014; 131: 40556.

[37]. A. Saupe, Mol Cryst Liq Cryst. 1969; 7: 59.

[38]. D. Coates and G. W. Gray, Phys Lett. A 1973; 45: 115.

[39]. D. Armitage and F. P. Price, J Phys. 1975; 36: 133.

[40]. J. Thoen, Phys Rev. A 1988; 37: 1754.

[41]. S. Meiboom and M. Sammon, Phys Rev. A 1981; 24: 468.

[42]. H. S. Kitzerow, Ferroelec. 2010; 395: 66.

[43]. I. Dierking, Textures of Liquid Crystals (Wiley-VCH Verlag GmbH, Germany, (2003).

[44]. J. Yan and S.T. Wu, Opt. Mater. Express 2011; 1; 1527.

[45]. S. Meiboom, J P. Sethna, P W. Anderson and W. F. Brinkman, Phys Rev Lett. 1981; 46: 1216.

[46]. H. J. Coles and M. N. Pivenko, Nat Mater. 2005; 436: 997.

[47]. S. R. Renn and T.C. Lubensky, Phys Rev A, 1988; 38: 2132.

[48]. T. C. Lubensky and S. R. Renn, Phys Rev A, 1990; 4: 4392.

[49]. J. W. Goodby, M. A. Waugh, S. M. Stein, E. Chin, R. Pindak and J. Patel, Nature, 1989;337: 449.

[50]. K. J. Ihn, J. A. N. Zasadzinski, R. Pindak, A. J. Slaney, and J. Goodby, Science, 1992;258: 275.

[51]. J. W. Goodby, I. Nishiyama, A. J. Slaney, C. J. Booth, and K. J. Toyne, Liq Cryst., 1993; 14: 37.

[52]. A. Jakli, M. Muller, D. Kruerke and G. Heppke, Liq Cryst., 1998; 24: 467.

[53]. G. Pelzl, S. Diele, and W. Weissflog, Adv Mater., 1999; 11: 707.

[54]. W. Weissflog, H. Nadasi, U. Dunemann, G. Pelzl, S. Diele, A. Eremin, and H. Kresse, J Mater Chem. 2001; 11: 2748.

[55]. C. K. Lee, A. Primak, A. Jakli, E. J. Choi, W. C. Zin, and L. C. Chien, Liq Cryst., 2001;28:1293.

[56]. H. R. Brand, P. E. Cladis and H. Pleiner, Eur Phys J B. 1998;6: 347.

[57]. W. Helfrich, Phys Rev Lett., 1970; 24:201.

[58]. R. Blinc, M. Copic, I. Drevensek, A. Levstik, I. Musevic, B. Zeks, Ferroelec 1991; 113: 59-76.

Chapter – 2

Magnetic nanoparticles –liquid crystals

Overview

This chapter describes an introduction of nanotechnology and doped liquid crystals systems. A historical perspective of doped liquid crystal particularly polymer dispersed liquid crystal and nanomaterials doped liquid crystal is presented. Different type of nanoparticles doped liquid crystal mixtures are discussed and a review of cited work is highlighted. The main emphasis of this chapter is to discuss the magnetic nanoparticles dispersed liquid crystals composites. In last, aim of the thesis is also specified.

2.1 Nanoparticles

The origin of term *Nanotechnology* was started with the revolutionary talk of R. Feynman's, "*There is plenty of room at bottom*" in 1959. The terminology nanotechnology was used by Norio Taniguchi in 1974. At this time, most of the scientific community realized that nanomaterials would be the new forthcoming materials for next generation [1-2].

Nanoparticles are a part of nanomaterials of at least one dimension of 100 nm or less. Nanomaterials attain unique physical properties as their size approaches to nanometer scale dimensions. The nanomaterials can be of nanoscale along 1, 2 and 3 dimensions and exist in single, fused, aggregated forms like spherical, tubular, and irregular shapes. Common types of nanomaterials include nanotubes, dendrimers, quantum dots and fullerenes. Spherical, rod like and disc type are the most familiar forms of nanomaterials. In recent years, these novel materials have created vast research interest due to their unusual chemical, mechanical, electrical, optical, magnetic properties and promising applications. Nanomaterials have widespread applications includes display as well as non-display such as biomedical imaging, functional coatings, optoelectronics & photovoltaic devices and many other functional composites in the field of science and engineering [3-6].

During the past decade, liquid crystal science has become an interdisciplinary topic of research and made enormous contributions to nanoscience and nanotechnology [7]. At this time, the assembly between nanoscience and liquid crystals is so deep that a new term *''liquid crystal nanoscience''* has come into common practice.

2.2 Doped liquid crystals: A historical perspective

This section simply summaries the important stage and development in doped liquid crystal systems. Doped liquid crystal system consist of dispersion of small amount (< 1%) of dopants (polymer or dyes or nanomaterials) as guest into liquid crystals (host). Historically the research in doped liquid crystal area was initiated due to the increasing demand of growing display industry. Organic dyes were the first doping materials used as guest into LCs. The approach of doping of dyes into different types of liquid crystalline mixtures was introduced in order to improve the physical properties of LCs. Various groups observed the electro-optic guest-host effect and measurable change in the optical responses (absorbance) by dyes [7-9].

Another important class of doped liquid crystal is *polymer dispersed liquid crystals* (PDLCs), were invented by J. W. Doane and coworkers [10-13]. PDLCs consist of micron or submicron size randomly oriented LC droplets dispersed in polymer matrix. These films can switch from an opaque to transparent state with the application of external electric field. PDLCs are used in flexible displays, switchable windows, holographic grating etc. [14-17].

Liquid crystal nanocomposites are considered to be extremely promising materials in which the properties of LC, are modified/ improved by the presence of various NPs. There are various scientific reports showing that doping of a LC with even a small amount of NPs affects the properties of LCs. The idea behind the doping or dispersion of nanomaterials and further detailed investigation of such composites are (i) to understand the role of nanomaterials in liquid crystals (ii) coupling between nanomaterials and LCs (iii) improve the distinctive optical, electrical and electro-optic properties of LCs for display applications [18].

Suspension of metal, dielectric and semiconductor NPs in various nematic LC mixtures, have been investigated by many authors and, in particular, doping of nematics with ferroelectric NPs is known to enhance dielectric and optical anisotropy, increase the electro-optic response and improve the photorefractive properties.

Suspension of para- and ferromagnetic particles in nematics are promising candidates for magnetically tunable structures, and doping of ferroelectric LCs with metal and silica NPs enables one to improve the spontaneous polarization and dielectric permittivity and to decrease switching times [19,20]. Various groups dispersed a variety of nanomaterials such as clay mineral/CdSe nanorods, gold nanoparticles, nanodot arrays, inorganic particles (Pd, Ag, MgO, SiO_2), nanotubes (single/double wall), ferroelectric nanoparticles ($Sn_2P_2S_6$, $BaTiO_3$) in a controlled amount ($\leq 2\%$) into nematic as well as in ferroelectric LCs and observed significant effect on LC properties [19-29]. In addition lytropic and cholesterics LC were also dispersed with nanomaterials and observed a changes in LC properties. In brief, there is enough experimental evidence to believe that nanomaterials will have high impact on physicochemical properties of LCs [30-38].

The improvement/ modification in LC properties depends on several factors i.e. nanoparticles surface coating, synthesis method, concentration of nanoparticles in LCs,

intrinsic characteristics, type and amount of surfactant, chemical and physical stability of nanomaterials, compatibility and miscibility, mutual interaction between nanomaterials and LCs [18]. The effect of nanomaterial doping, form, size, shape and concentration on structural, phase transition temperature, electro-optic, dielectric, optical responses and thermal properties in nematic liquid and ferroelectric liquid crystals were extensively studied.

2.3 Magnetic nanoparticles in liquid crystals

Most of the liquid crystal display (LCD) devices are based on the reorientation of LC molecules in external electric or magnetic fields. Despite the fact that early theoretical and experimental works addressed magnetic reorientation, in practice, the majority of LC devices are driven by electric field. This is because the sensitivity of LC to an external field is too high: only small amount of applied voltage is required to trigger the LC reorientation and optical responses. In contrast, the sensitivity of LC in magnetic field is very high. Although, some previous studies also suggest that optical and other properties of LC can be controlled by magnetic field [39-43], but usually it cannot be employed due to (i) Low sensitivity to magnetic field and (ii) very week anisotropy of diamagnetic susceptibility ($\chi_a \sim 10^{-7}$). Therefore, rather a high magnetic fields (H > 1 kOe) must be applied to get a magneto-optical response comparable to its electro-optical analog. As a consequence, increasing the magnetic sensitivity of liquid crystals is an important issue for the development of new devices.

In 1970, Brochards and De-Genes theoretically proposed that doping of nanometer size magnetic nanoparticles (in low volume) would increase the sensitivity of nematic LC based devices and named them *"ferronematics"* (i.e. suspension of magnetic particles in nematic liquid crystals) [44]. Subsequently Burylov and Raikhler [45], projected that the ferronematics should respond to a low field (order of tens of G). This low magnetic field would has no substantial effect on the undoped nematic, but sufficient to align or rotate the magnetic moments of the doped particles inside the ferronematic suspensions. The realignment or rotation effect of nanoparticles could then be transferred into the nematic through coupling between the nanoparticles and the liquid crystal molecules. It should be noticed that in these systems the realignment effect of nematic host was supposed to be completely determined by the ferromagnetic properties of nanoparticles instead of nematic

properties. Later on in 1983 the first experimental realization of ferronematic materials was carried out by Chen and Amer [46]. Currently similar to the ferronematics the term "ferrosmectics" (dispersion of magnetic nanoparticles into smectic liquid crystals) is also in use and studied.

Magnetic nanoparticles (MNPs) of different size and shape, including rod-like [47], spherical and chainlike particles [40], as well as magnetically functionalized [48] or magnetically filled nanotubes [49] were used to prepare ferronematic suspensions. The results suggest that the performance of ferronematic suspensions and consequently devices depends not only on the NPs properties, but also on their coupling with LC molecules.

A stronger interaction was achieved when the particles had anisotropic shapes [41]. In addition, Cordoyiannis *et al.* [50] demonstrated that the degree of interaction was also strongly influenced by the particle surface chemistry. The dispersion of MNPs in a NLCs and their molecular arrangement is shown in Figure 2.1.

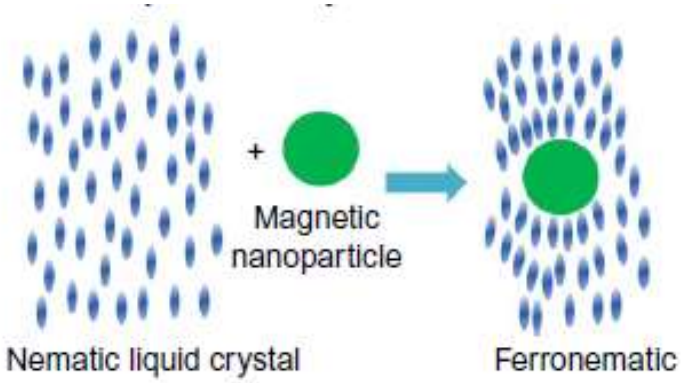

Figure 2.1 Dispersion of MNPs into nematic liquid crystal

2.4 Aim of Thesis:

The present work is focus on synthesis and systematic study of MNPs dispersion effect on physical properties of nematic and ferroelectric liquid crystals. Efforts are made to study the MNPs doping on the phase sequences, structural transitions, electro-optic (switching time, polarisation, viscosity, threshold voltage, order parameter etc.), dielectric, magnetic properties and understanding the physics involved between guest and host materials. The effect of size of magnetic nanoparticles on physical parameters of ferroelectric liquid crystal is also discussed.

The objectives of this work were

- Preparation of magnetic nanoparticles- liquid crystal composites.
- To study the size dependent structural and electro-optical properties.
- To study the dielectric and magnetic properties of prepared composites.

References

[1]. G. Cao, "Nanostructures & Nanomaterials: Synthesis, Properties & Applications", Imperial College Press, London (2004).

[2]. B. Bhushan (Ed.), "Handbook of Nanotechnology", Springer (2004).

[3]. C. P. Poole, J. F. J. Owens, Introduction to Nanotechnology, John Wiley & Sons, (2003).

[4]. M. Aliofkhazaei, "Hand Book of Nanoparticles" Springer (2015).

[5]. S. Thomas , N. Kalarikkal, A. M. Stephan, B. Raneesh, Advanced Nanomaterials: Synthesis, Properties, and Applications, CRC Press, (2014).

[6]. T. Hegmann, H. Qi and V. M. Marx, J. Inorganic and Organometallic and Polymer Materials, 2007;17: 483 – 508.

[7]. L. Lucchetti, M. Gentili, L. Tifi, F. Simoni, Liq. Cryst. 2008; 489(1**)**: 280/ [606]–290/ [616].

[8]. G. H. Heilmeier, L. A. Zanoni, Appl. Phys. Lett. 1968; 13 (3): 91–92.

[9]. G. H. Heilmeier, J. A. Castellano, L. A. Zanoni, Mol. Cryst. Liq. Cryst. 1969; 8: 293–304.

[10]. J. W. Doane, N.A. Vaz, B. G. Wu, S. Zumer, Appl. Phys. Lett. 1986; 48(4): 269–271.

[11]. J. L. Fergason, Encapsulated Liquid Crystal and Methods, US Patent (1984) 4435047.

[12]. B. G. Wu, J. L. West and J. W. Doane, J. Appl. Phys. 1987; 62: 3925.

[13]. J. W. Doane, A. Golemme, J. L. West, J. B. Whitehead, and B. G. Wu, Liq. Cryst. 1988; 165: 511-532.

[14]. P. S. Drazic, J. Appl. Phys. 1986; 60: 2142.

[15]. P. S. Drazic, Liquid Crystal Dispersion, World Scientific, Singapore (1995).

[16]. F. Simoni, Non Linear Optical Properties of LC & PDLCs, World Scientific, Singapore, (1997).

[17]. M. Mucha. Prog. Polym. Sci. 2003; 28: 837.

[18]. T. Hegmann, H. Qi and V. M. Marx, J. Inorganic and Organometallic and Polymer Materials, 2007; 17: 483 – 508.

[19]. H. H. Liang, Y. Z. Xiao, F. J. Hsh, C. C. Wu and J. Y. Lee, Liq. Cryst, 2010; 37:255-261.

[20]. K. Chen, Y. Williams, J. H. Park, I. C. Khoo, B. Lewis and T. E. Mallouk. Proceedings of SPIE, 2005; 5936: 593613.

[21]. F. Li, J. West, A. Glushchenko, C. I. Cheon and Y. Reznikov. J Soc. Inf. Disp. 2006; 14: 523-527.

[22]. S. Kobayashi, T. Miyama, N. Nishida, Y. Sakai, H. Shiraki, Y. Shiraishi and N. Toshima. J Soc. Inf. Disp., 2006; 2: 121-129.

[23]. S. Sano, T. Miyama, K. Takatoh and S. Kobayashi. Proceeding of SPIE, Liquid Crystal Materials Devices and Applications XI, 2006; 6135: 613501-613505.

[24]. F. Haraguchi, N. Toshima, K. Inoue, S. Kobayashi and K. Takatoh. Jpn. J. Appl. Phys., 2007; 46: L796-L797.

[25]. T. Joshi, A. Kumar, J. Prakash and A. M. Biradar. Liq. Cryst, 2010; 37: 1433-1438.

[26]. S. N. Paul, R. Dhar, R. Verma, S. Sharma and R. Dabrowski, Mol. Cryst. Liq. Cryst. 2011; 545**:** 105-111.

[27]. A. S. Pandey, R. Dhar, S. Kumar and R. Dabrowski. Liq. Cryst., 2011; 38:115-120.

[28]. Q. H. Wang, A. A. Setlur, J. M. Lauerhaas, J. Y. Dai, E. W. Seelig and R. P. H. Chang. Appl. Phys. Lett. 1998; 72**:** 2912-2913.

[29]. F. V. Podgornov, A. M. Suvorova, A. V. Lapanik and W. Haase. Chem. Phys. Lett. 2009; 479: 206-210.

[30]. Neeraj and K. K. Raina, Opt. Mater. 2013; 35: 531-535.

[31]. P. Malik, A. Chaudhary, R. Mehra and K. K. Raina. J. Mol. Liq. Cryst. 2011; 541: 243-251.

[32]. B. Kinkead and T. Hegmann. J. Mater. Chem.2010; 20: 448-458 .

[33]. Neeraj and K. K. Raina, Phase Trans. 2010; 83: 615-626.

[34]. A. Kumar and A. M. Biradar. Phys. Rev. E 2011; 83: 041708-041716.

[35]. T. Joshi, A. Kumar, J. Prakash and A. M. Biradar. Appl. Phys. Lett. 2010; 96: 253109-253112.

[36]. A. Chaudhary, P. Malik, R. Mehra and K. K. Raina. J. Mol. Liq. 2013 188, 230–236.

[37]. A. Chaudhary, P. Malik, R. Mehra and K. K. Raina. Phase Trans. 2013; 86**:** 1256-1266.

[38]. A. Chaudhary, P. Malik, R. Mehra, K. K. Raina, Phase Trans. 2012;85:44-254 .

[39]. P. Kopcansky, N. Tomasovicova, M. Koneracka, et al. Int. J. Thermodyn. 2011; 32**:**807-817.

[40]. P. Kopčanský, N. Tomašovičová, M. Koneracká, V. Závišová, et al. Phys. Rev. E. 2008; 78: 011702-011707.

[41]. N. Tomasovicova, M. Koneracka, P. Kopcansky, L. Tomko, et al. J. Phys. Condens. Matter. 2008; 20: 204123.

[42]. M. S. Zakerhamidi, S. Shoarinejad and S. Mohammadpour. J. Mol. Liq. 2014; 191: 16-19.

[43]. Yu. Garbovskiy, J. R. Baptist, J. Thompson, T. Hunter, et al., Appl. Phys. Lett. 2012; 101:181109-5.

[44]. F. Brochard and P.G. De Gennes, J. of Phys. 1970; 31**:** 691-708.

[45]. (a) S. V. Burylov, Y. L. Raikher. Mol. Cryst. Liq. Cryst. 1995; 258, 107-122.

(b) S. V. Burylov and Yu. L. Raikher. Mol. Cryst. Liq. Cryst. 1995; 258: 123–141.

[46]. S. H. Chen, N. M. Amer, Phys. Rev. Lett. 51(25), 1983; 2298–2301 (1983)

[47]. P. Kopˇcansk´y, N. Tomaˇsoviˇcov´a, M. Konerack´a, M. Timko, et al. J. Magn. Magn. Mater. 2010; 322: 3696–3700.

[48]. Z. Mitr´oov´a, N. Tomaˇsoviˇcov´a, M. Timko, M. Konerack´a, et al. New J. Chem. 2011; 35: 1260–1264.

[49]. O. Buluy, S. Nepijko, V. Reshetnyak, E. Ouskova, et al. Soft Matt. 2011; 7: 644–649.

[50]. G. Cordoyiannis, L. K. Kurihara, L. J. Martinez-Miranda, C. Glorieux, J. Thoen. Phys. Rev. E, 2009; 79:011702.

Chapter – 3

Experimental

Overview

This chapter describes the detail of materials (magnetic nanoparticles and liquid crystals) and experimental techniques used to study the physical properties of magnetic nanoparticles dispersed liquid crystals composites. The physical properties of both materials and structural characterization (TEM) of Iron, Nickel and Nickel Ferrite nanoparticles are presented. The detailed method of preparation of liquid crystal sample cells, magnetic NPs- LCs composite materials are also discussed. A brief description of various instruments used for morphological, electro-optical, dielectric and optical characterization are also presented in this chapter.

3.1 Introduction

In the last few years, a wide range of nanosize materials have been the subject of current research due to their interesting properties and technological applications. Nanomaterial as a guest, in liquid crystals (LCs) may open a new era for the LCs based display devices because of their unique structural, electrical and mechanical properties. In this series, the proper selection of nanomaterials and LCs play an important role on the performance of liquid crystal display devices. The selection of used materials in the present work has been made on the basis of size, state and compatibility with liquid crystals.

3.2 Materials

In the present work, commerciably available ferroelectric liquid crystals (FLCs) trade name ZLI 4851-000 and W206 E purchased from BDH, UK [1] and Warsaw Poland [2] respectively are used. Nematic liquid crystal (6OCB) was also procured from Sigma Aldrich, India. The 6OCB molecules possess large longitudinal dipole moment caused by the cyano (CN) group. For dispersion purpose, Iron, Nickel ferrite and Nickel magnetic nanoparticles were used as dopants. Iron and Nickel nanoparticles were obtained from Sigma Aldrich, India [3]. However Nickel ferrite nanoparticles were synthesized in our lab. Nickel nanoparticles of two different sizes (~ 20 nm and 40 nm) were also used. The detailed physical, chemical properties of liquid crystals and nanomaterials are summarized in Tables 3.1 to 3.5. The TEM images of Iron and Nickel NPs are given in Figures 3.1, 3.2. The magnetic properties of Nickel NPs is shown in Figures 3.3.

Synthesis of nickel ferrite nanoparticles

To prepare nickel ferrite nanoparticles (NF-NPs), nickel nitrate hexahydrate ($Ni(NO_3)_2.6H_2O$) and iron nitrate nonahydrate ($Fe(NO_3)_3.9H_2O$) purchased from Sigma Aldrich (99.99%) were dissolved in 2-methoxyethanol and citric acid. The molar ratio of metal nitrates to citric acid was kept at 1:2. The solution was continuously stirred at 80^oC using a magnetic hot plate to form a dark reddish gel. The obtained gel was dried at 250^oC and subsequently calcined at 700^oC in the furnace. Figure 3.4 shows the X-ray diffraction (XRD) pattern of synthesized NF-NPs. All diffraction peaks are matched with

the standard JCPDS data card no. 742081 and indicate a single phase $NiFe_2O_4$. The crystallite size of the NF was calculated by the Debye-Scherrer formula.

$$\boldsymbol{t = \frac{0.9\lambda}{\beta\, cos\theta}} \tag{3.1}$$

The size of synthesized particles were found ~ 45 nm. In Equation (3.1), t is the crystallite size, β is full width of the diffraction line at half of the maximum intensity, λ is the x-ray wavelength and θ is Bragg angle. Figure 3.5 shows the scanning electron micrograph of NF-NPs. Since the particles are insulators, a thin film of Au was deposited to avoid electron charging. It is clear from Figure 3.5 that the particles are fine and appear to be agglomerated due to surface forces. However, particles were deagglomerated before dispersing them in the FLC [5]. The magnetic behavior of synthesized NF-NPs is also presented in Figure 3.6.

Table 3.1 Physical properties of ferroelectric liquid crystal materials [1, 4]

Ferroelectric liquid crystals	***Physical Properties***	***Values***
ZLI-4851-000*	Phases	-10°C SmC* 64°C SmA 70°C N* 74°C Isotropic
	θ (degree)	24.0
	P_s (nC/cm^2) at 20°C	-4
W206E	Phases	$K \longleftrightarrow SmC^* \xleftrightarrow{86.6°C} SmA \xleftrightarrow{92.5°C} N^* \xleftrightarrow{97.6°C} I$
	θ (degree)	28
	P_s (nC/cm^2)	17
	$\Delta\varepsilon$	0.31

* Sourse- E Merck Data Sheet

θ = Tilt angle; P_s = Spontaneous polarization; $\Delta\varepsilon$ = Optical birefringence

Table 3.2 Physical properties of nematic liquid crystal [3]

Nematic Liquid crystal	***Physical Properties***	***Values***
4′-(Hexyloxy)-4-biphenylcarbonitrile (6OCB)	Phases	Crystal (Cr) 58°C - nematic (N) 76°C - Isotropic
	Chemical Structure	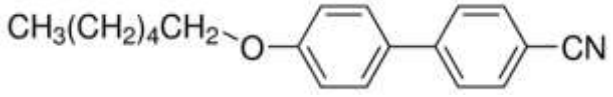

Table 3.3 Physical properties of nickel nanoparticles [3]

Properties	Nickel Nanoparticles
Form	Powder, gray to Black color
Size (nm)	20, 40
Density (g/cm^3)	8.90
Molecular weight (g/mol)	58.69
Surface area (m^2gm^{-1})	12.0
Morphology	Spherical

Table 3.4 Physical properties of nickel ferrite nanoparticles

Properties	Nickel Ferrite Nanoparticles
Form	Powder
Particle size (nm)	~ 45
Molecular weight (g/mol)	234.38
Density (g/cm^3 at 25ºC)	5.36
Morphology	Spherical

Table 3.5 Physical properties of Iron nanoparticles

Physical Properties	**Iron Nanoparticles**
Form	Powder
Particle size (nm)	~ 45-60
Restivity (μΩ-cm)	9.71
Molecular weight (g/mol)	55.84
Density (g/ml at 25ºC)	7.86
Melting Point (ºC)	1535
Morphology	Spherical

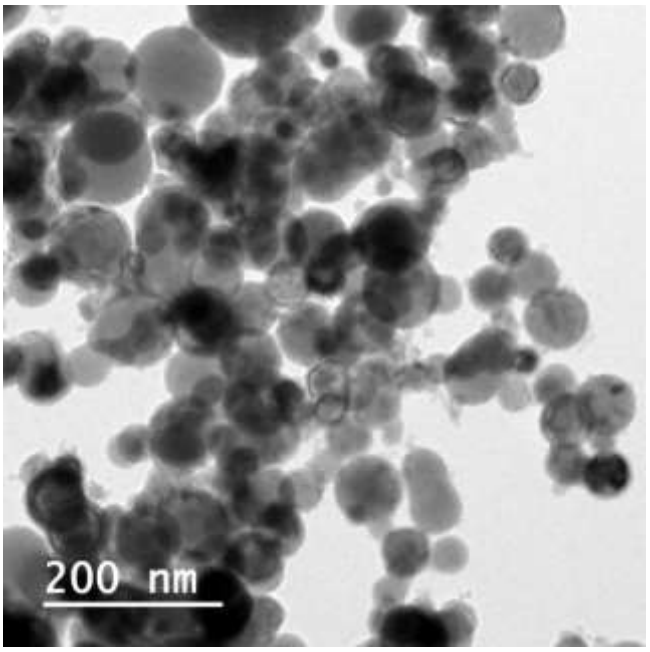

Figure 3.1 TEM image of Iron Nanoparticles

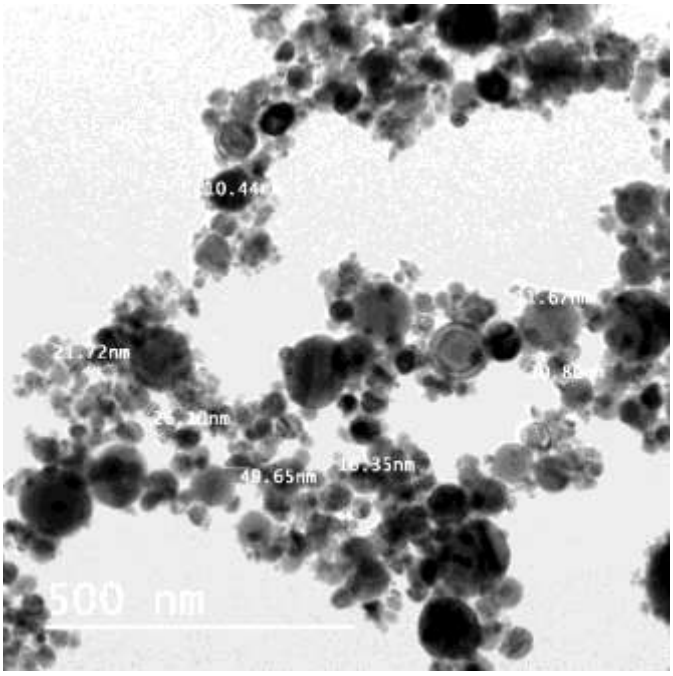

(a)

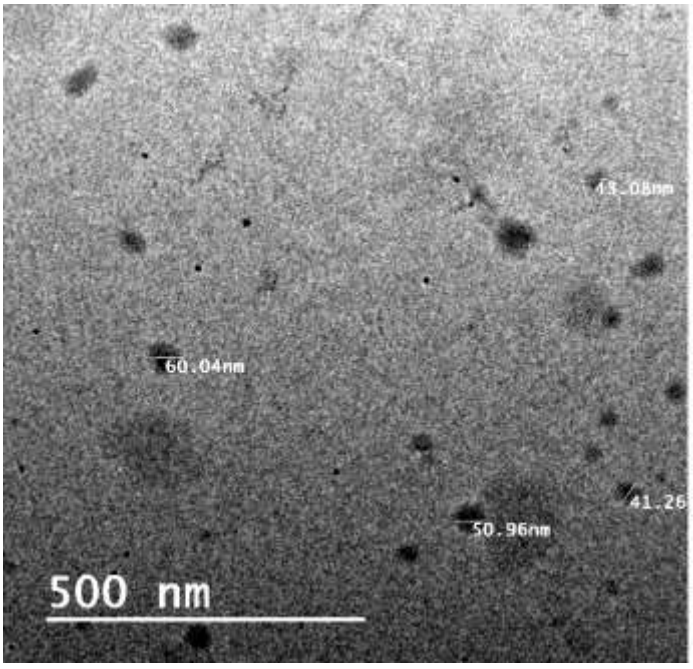

(b)

Figure 3.2 TEM image of Nickel nanoparticles of size (a) 20 nm, (b) 40 nm

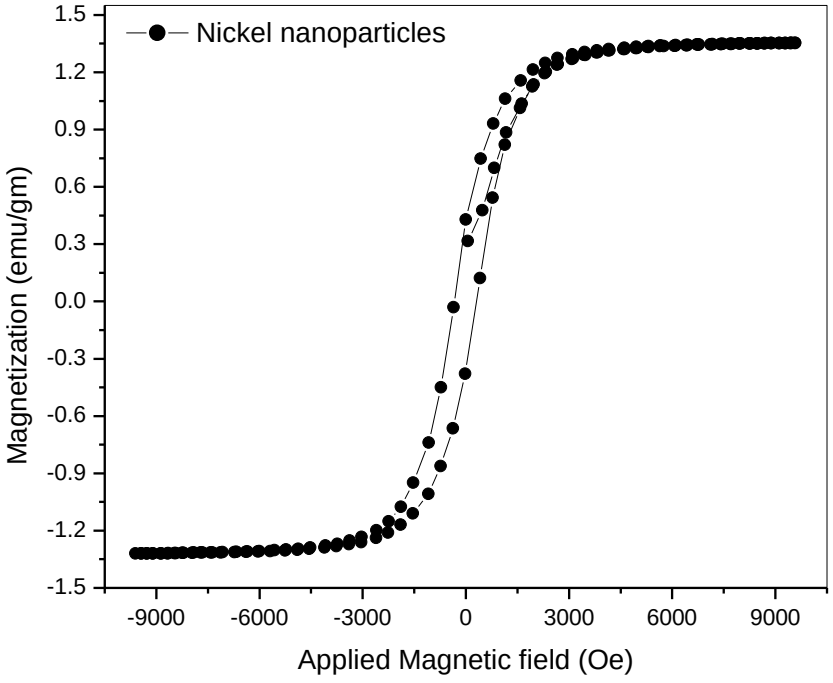

Figure 3.3 Magnetic behavior of nickel nanoparticles

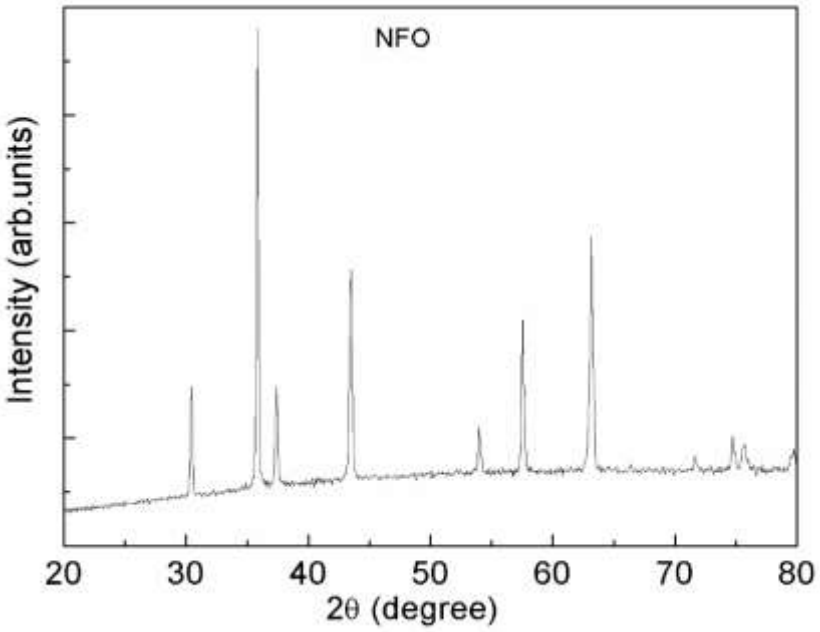

Figure 3.4 XRD pattern of nickel ferrite- nanoparticles

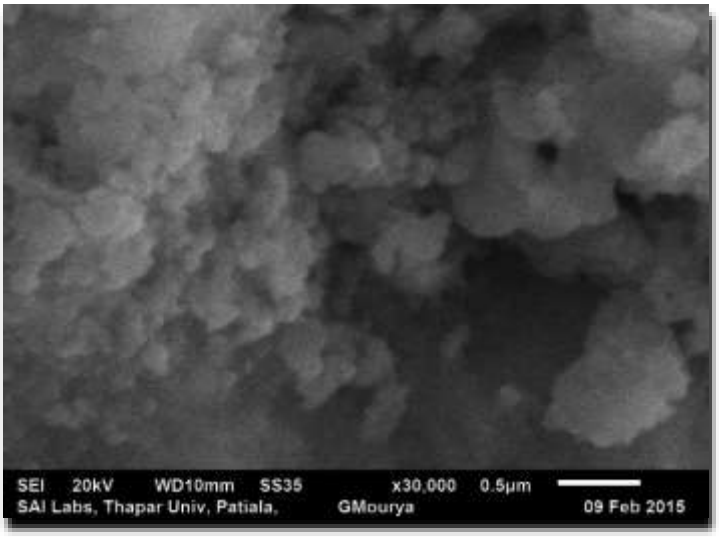

Figure 3.5 SEM image of Nickel Ferrite nanoparticles.

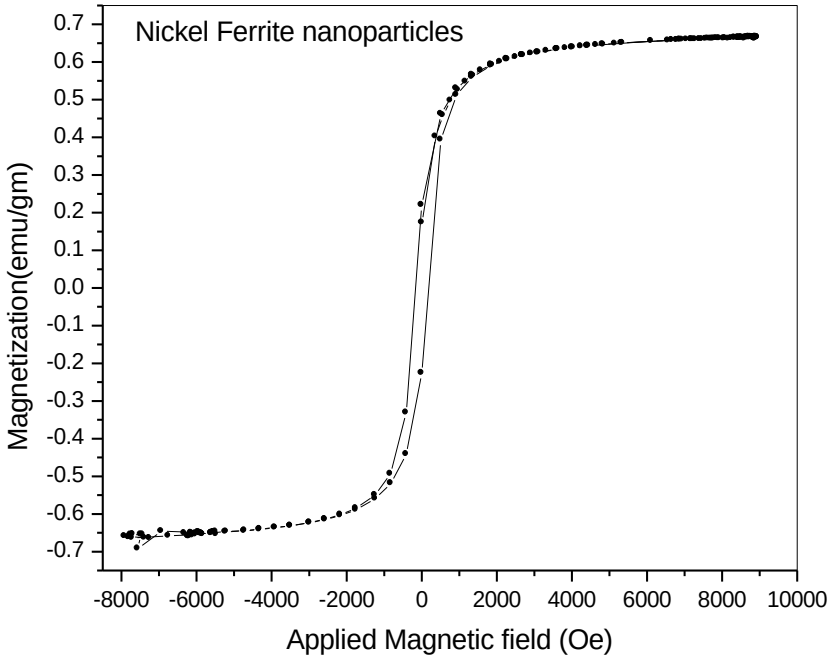

Figure 3.6 Magnetic behavior of nickel ferrite nanoparticles

3.3 Preparation of liquid crystal cells

Liquid crystal cell alignment

Surface alignment is necessary for maximizing the contrast of the display so that the orientation of the molecules is same throughout the liquid crystal sample whether the field is Off or On. In the liquid crystals, different methods have been proposed by various research groups to obtain uniform alignment. In LCDs alignment of surfaces with polyimide / PVA is most commonly used method. Basily there are two types of alignments used for aligning LC molecules [6-10].

1. Homeotropic alignment
2. Homogeneous alignment

Depending on the pre-treatment of the substrate, the optic axis of the LC molecules are oriented either parallel (homogenous) or perpendicular (homeotropic) to the surface of

the substrate. If the substrate is covered with a thin film of amphiphilic molecules, which deposit their polar end to the substrate, LC molecules will be aligned such that the director is perpendicular to the supporting substrates. This configuration is called *Homeotropic alignment*. If the supporting substrate is applied with a thin layer of polymer stretched in one direction by rubbing with a nylon cloth, the LC molecules will be aligned such that the director is parallel to the supporting substrates in the direction of the rubbing. This configuration is named as Homogenous (planar) alignment. Both type of configurations are illustrated in Figure 3.7. [11-13]

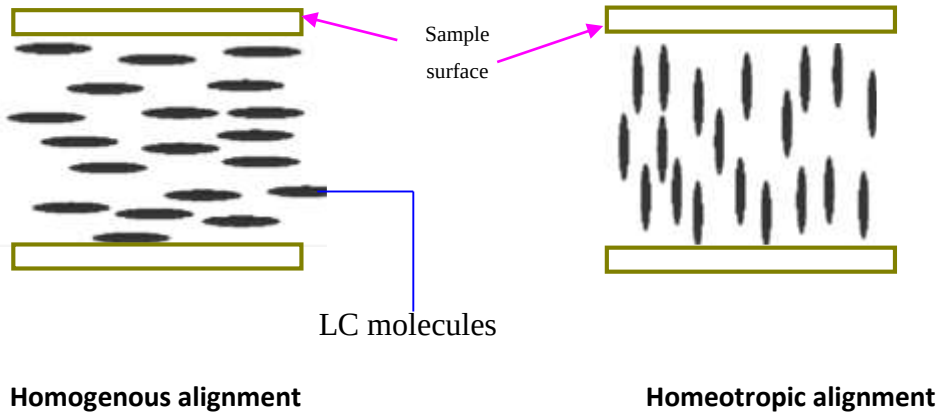

Figure 3.7 Homogeneous and homeotropic alignment [7-10].

In the present work, liquid crystal sample cells were prepared using indium tin oxide (ITO) coated highly transparent (> 85-90%) glass substrates of sheet resistance 30-60 Ω/□. These substrates were purchased from Sigma Ardrich India. The substrates were initially washed with soap rinsed with acetone (purity 99.9%), distilled water and then dried in a vacuum chamber. Cleaned ITO substrates were then put in laminar flow chamber (Figure. 3.8) to ensure proper cleaning conditions. Out of the two basic forms of LC alignment i.e. homeotropic and homogenous, the homogenous alignment method was adopted.

To get a homogenous (planar) aligned LC cell, a drop of homogeneous solution was spin coated (speed 1400 rpm) on conducting side of ITO substrates. Homogenous solution

consist of 0. 5 % (wt. to vol.) of polyamide (Nylon 6/6) in 60% m-cresol and 40% methanol (vol. to vol.) was used [14-15]. The excess amount of solution left on substrates was evaporated by keeping the substrates in an oven at a temperature of ~130^{o}C for about an hour. These substrates were then rubbed unidirectionally with a nylon cloth for planar alignment.

For assemble of LC cell, coated side of glass substrates were joined together and separation between the substrates was maintained with the help of mylar spacer. To obtained the uniform and desired thickness, small sheet of maylar spacer are placed on the edges of substrates. The sides of substrates were sealed with Norland optical adhesive (NOA-65) and then kept at room tempearure for dryness. For measurement, an electrical connections were made at the ITO coated substrate surface using Indium ingots. In this work, few commercially available LC cells of different thickness and configurations obtained from M/S Instec Inc., USA were also used. The detail of these cells are given in respective chapters. Figure 3.9 illustrate the essembly of empty LC cell.

3.4 Preparation of magnetic nanoparticles dispersed liquid crystal samples

Magnetic nanoparticles (MNPs) dispersed liquid crystal samples were prepared by dispersion of small amount of MNPs in different ratio into liquid crystal mixtures. Initially 1-2 drop of surfactant (chloroform or oleic acid) was added into MNPs followed by ultrasonification at a frequency of 36 kHz for one hour. The purpose of surfactant is to avoid the problem of aggeration in MNPs. Now these MNPs were then added into LCs and ultasonication was repeated. The prepared homogenous mixture was then filled between empty LC sample cells by capillary action at the isotropic temperature of LC and finally sealed using araldite/ norland optical adhesive. The electrodes (copper wire) were connected to the ITO surface of the cells by indium. These samples were assigned as magnetic nanoparticles doped liquid crystal sample cells. The complete step-step methodology of cell fabrication process is shown in Figure 3.10. An essembly of empty and filled LC sample cells are shown in Figure 3.11. In the present work, following magnetic nanoparticles dispersed LC composites are prepared and studied.

(i) Iron nanoparticles dispersed nematic liquid crystal composites

(ii) Nickel-ferrite nanoparticles dispersed ferroelectric liquid crystal composites

(iii) Nickel nanoparticles dispersed ferroelectric liquid crystal composites.

The experimental details of above composites are discussed in respective chapters 4-6.

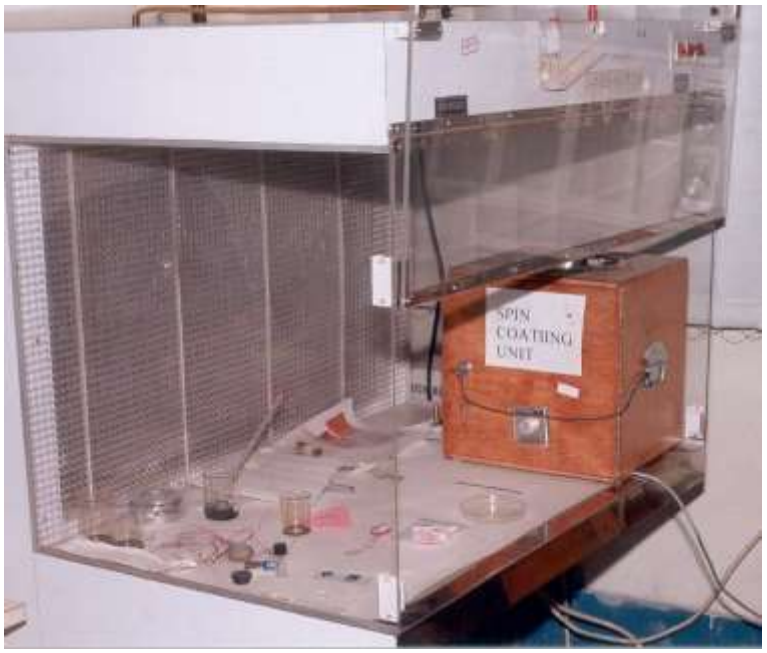

Figure 3.8 Laminarr flow chamber for preparation of LC cells

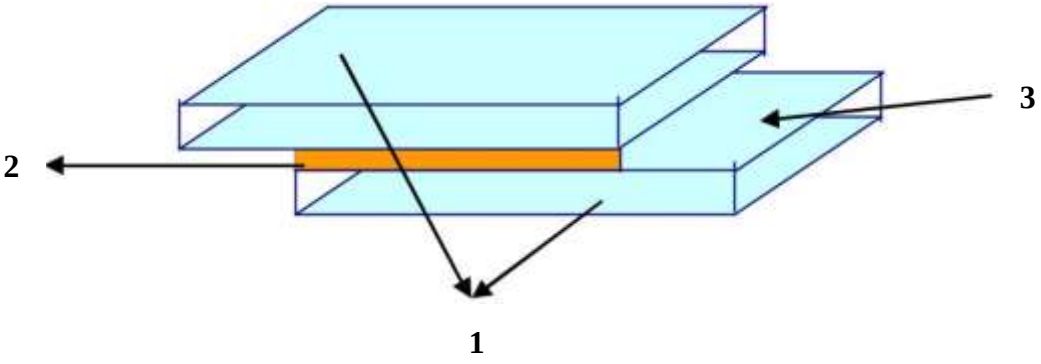

1. **Glass substrates**
2. **Mylar spacer**
3. **ITO coated surface**

Figure 3.9 An illustration of empty LC cell

Methodology

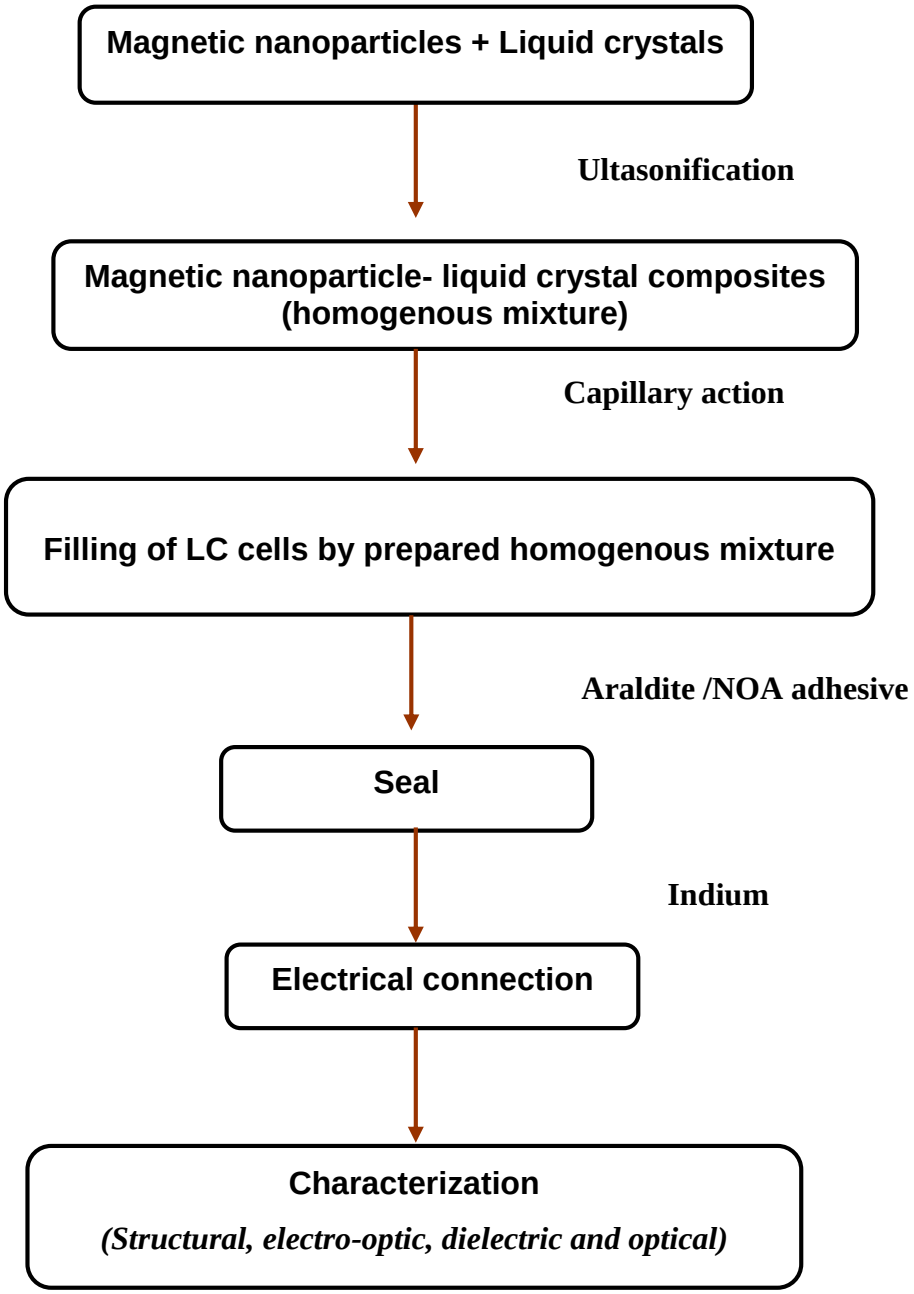

Figure 3.10 Flow chart showing preparation and characterization of magnetic nanoparticles dispersed LCs samples.

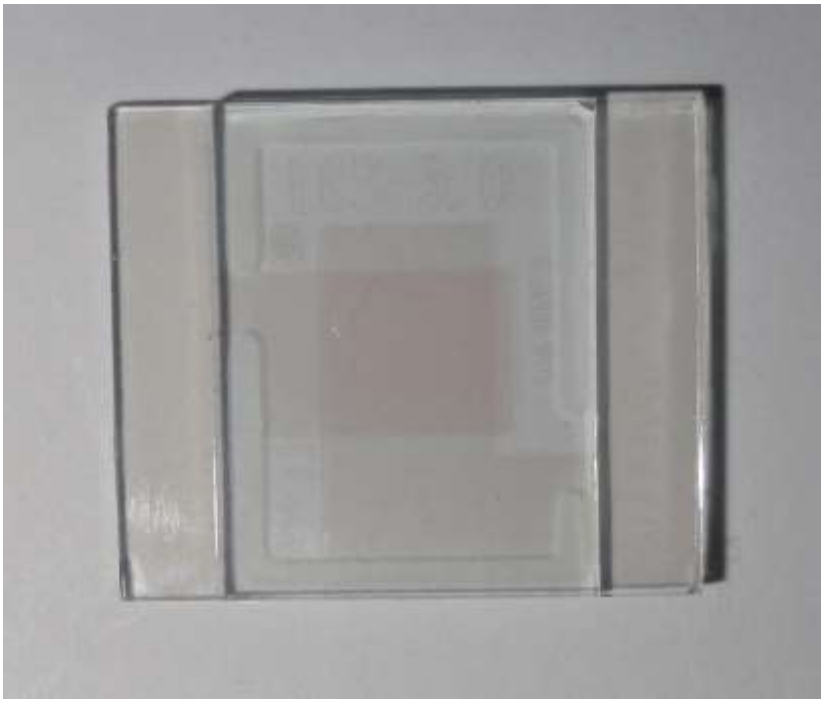

(a)

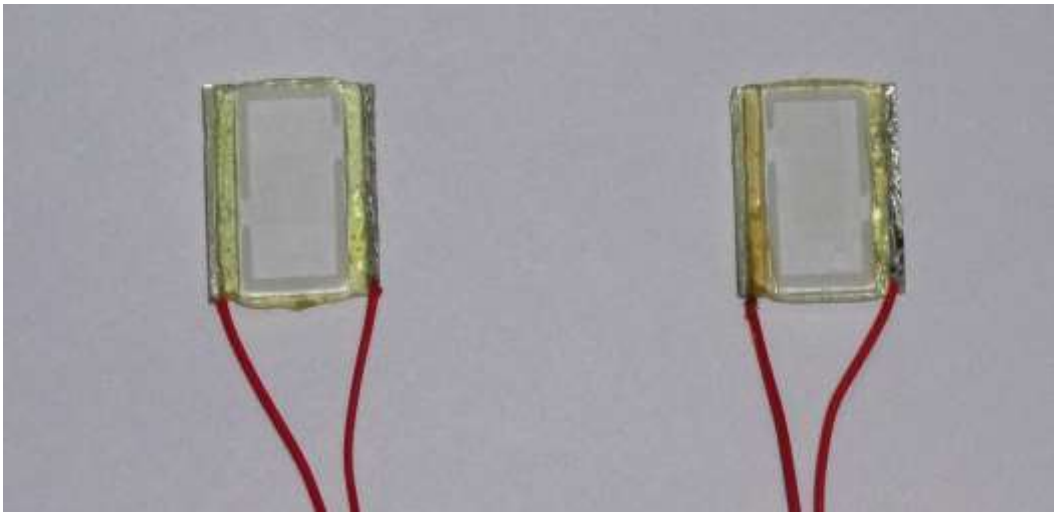

(b)

Figure 3.11 An assembled (a) unfilled (b) filled liquid crystal cells.

3.5 Instruments Details and Experimental Techniques

Polarizing optical microscopy

Polarizing optical microscopy is a powerful tool to identify various phases and phase transition temperatures of LCs. Polarizing microscope (Model- Nikon Eclipse LV100) equipped with CCD camera (Make: Q imaging, Model: Q28378) is used. The microscope consist of an eyepiece of 10x, objectives (10x, 20x, 50x and 100x) and attachced with digital camera interfaced with computer. All the texture and change in LC phases were recorded in the computer using Linksys software. The hotstage can be placed on the rotating stage fixed on the microscope. The texture are studied as a function of temperature and applied electric field at a magnification of 10x under crossed polarizers using long working distance objective lens at 10X. The complete experimental set-up for the investigation of textures, electro-optic and optical responses is shown in Figure 3.12.

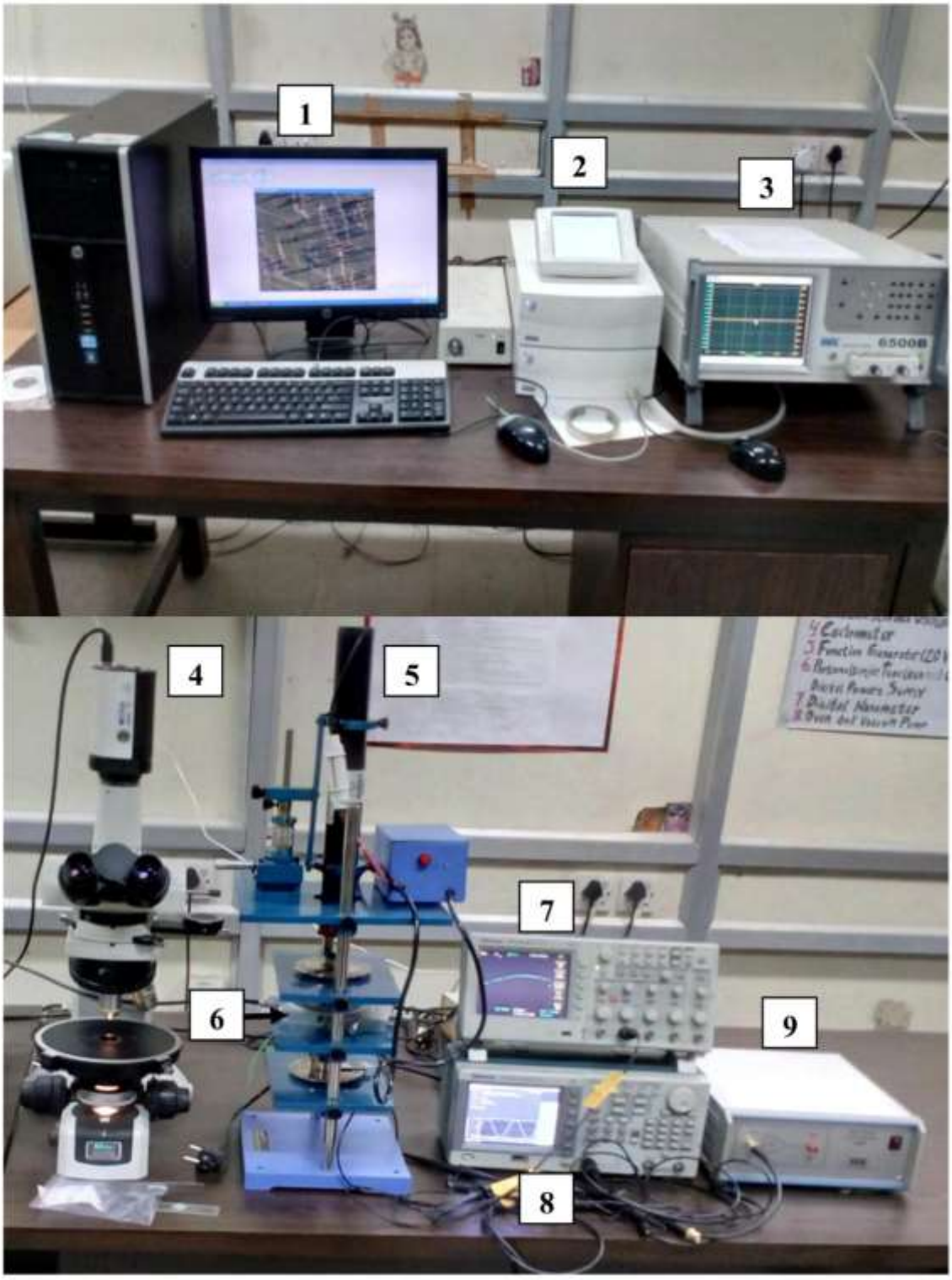

Figure 3.12 Experimental setup (1) Computer attached with Linksys software, (2) Temperature controller, (3) Impedance analyzer, (4) Polarizing optical microscope, (5) He-Ne laser setup assembly for electro-optic studies, (6) Hot stage (7) Oscilloscope, (8) Function generator, and (9) Power amplifier.

Temperature programmer cum heating/freezing stage

Temperature controller cum heating & freezing stage is an essential experimental tool to study the phase transition temperature of liquid crystals. Here a programmable temperature controller cum hot stage (Make- Linkam, model- TP95, THMSE600). TP95 has temperature range of -196 to 600^{o}C and specifically designed to control the temperature of heating/freezing stages with an accuracy of ± 0.1^{o}C [16]. The stage sensor is digitally linearized to give accurate temperature readout, the controls and their functions have been carefully selected for simple and easy operation. The heating or cooling rates can be changed almost instantly using the three rate keys. The different heat rates are

From 0.1 to 0.9^{O}C/min at 0.1 degree intervals

From 1.0 to 9.0^{O}C/min at 1.0 degree intervals

From 10 to 90^{O}C/min at 10.0 degree intervals

A varying dc signal is used to control the stage and results in an even application of power, which avoids the bursts seen with conventional burst fire ac techniques. An optional remote control gives single key control of three programmable heating/cooling rates and the HEAT, COOL and HOLD functions. The three programmable heating/cooling rates are held in memory when power is switched OFF. The temperature and limit values can also be stored and recalled using the remote control facility.

Transmission electron microscopy (TEM)

TEM is a very powerful tool used for determination and analyze the the quality, shape, size and density of nanomaterials like quantum dots, quantum wires, nanoparticles, carbon nanotubes etc. The principle of TEM is similar to light microscope but it uses electrons instead of light. TEM consists of high energetic beam of electrons accelerated through a potential difference (up to 300 kV) focussed on a thin-section of the specimen of a material. The electron beam undergoes many interactions and an image is formed by the electrons transmitted through the specimen. A diagram of the TEM is shown in Figure 3.13. Various components of the TEM are described as:

1. Electron source (gun): It consists of a V-shaped filament usually made up of tungsten which emits the electrons when heated up.

2. Condenser lens: The stream of the electrons from the electron gun is then focused to a small, thin, coherent beam by the use of magnetic lenses also called condenser lenses. These lenses determine the size of spot striking on the sample.

3. Objective lens: The main role of the objective lens is to focus the transmitted electrons from the sample into an image.

4. Sample: The beam from the condenser lens strikes the sample and the electron sample interaction takes place in three different ways: (i) unscattered electrons (transmitted beam), (ii) elastically scattered electrons (diffracted beam), and (iii) inelastically scattered electrons.

5. Objective aperture: The role of objective aperture is to block the electrons diffracted at large angles.

6. Projector lens: The projector lenses are used to expand the beam onto the phosphor screen.

7. Screen: Imaging systems in a TEM consists of a phosphor screen, which may be made of zinc sulphide for direct observation by the operator. In the present study, the morphology and size of used NPs were determined by using the TEM (Make- FEI, Model-FEI Tecnai G^2 20 S-Twin).

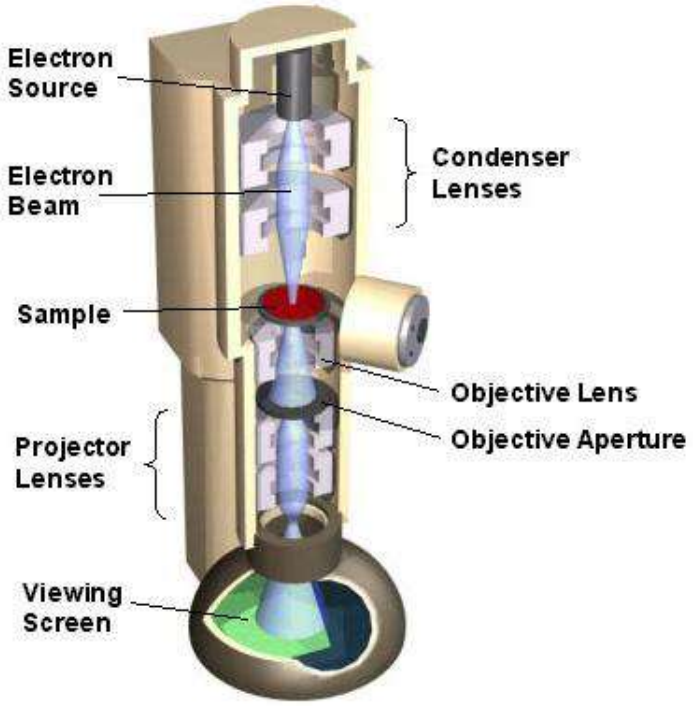

Figure 3.13 Schematic diagram showing various sections of TEM.

Vibrating sample magnetometer (VSM)

VSM is used to measure one of the most fundamental quantity is magnetic moment of solids. When a magnetic material is placed under magnetic field a dipole momemt is produced in the sample. The generated moement is directly proposnal to the product of susceptibility of sample and appled magnetic field. If the sample is made to undergo sinusoidal motion as well, an electrical signal will be induced in attached pick-coils. The obtained signal is proposnal to the magntic moment, vibration amplitude and frequency. The used VSM is make of Quantum Design (model PAR 155).

Differential scanning calorimetry (DSC) measurements

Differential scanning calorimetry (DSC) is a versatile instrument to study the phase transition temperature, glass and melting points, enthalpy, heat capacity and specific heat of sample. DSC is based on thermal analysis that measurers the heat flow to and from a specimen as a function of temperature and time. During heating/cooling process transition temperature, enthalpy, heat capacity, specific heat, type of chemical reactions can be calculated from a single data run. Using DSC, we are able to examine the phase transitions and thermodynamic parameters of the pure nematic and ferroelectric liquid crystals and magnetic nanoparticles doped liquid crystal composites. The phase transition temperatures studied through DSC were also confirmed using optical microscopy. In our work, experimental datas are taken using computer controlled DSC (Mettler DSC 821, EXSTAR).

3.6 Polarisation switching studies:

Current reversal method is one of the accurate technique used for the measurement of several electro-optic parameters. The main parameters are spontaneous polarization and response time. [15,17]. Triangular wave method offers a direct measurement of spontaneous polarization while square wave method measures response time along with polarization. The experimental setup used for the measurement of electro-optic parameters is shown in the Figure 3.14. Here an input triangular voltage (V_{IN}) is applied across the sample and output (V_o) is taken across a standard resistor (R). The electric

field was applied to the LC sample cell through an electrode (copper wire in our case) connected to ITO substrates. The e-field is applied through a function generator (Make: Tektronix, Model: AFG3021B) attached with power amplifier (Make: FLC, Model: A400) to LC cell and output trace is acquired on digital storage oscilloscope (Tektronix TDS 2024B). Function generator, oscilloscope and LC sample cell are fully interfaced with computer and data acquisition was done using the help of wavestar and Origin 6.0 software.

In order to study the molecular re-orientation processes associated with the helix dynamics, the symmetric triangular or square wave pulses were applied to the samples. It reorients the dipoles between two stable polarization states (Up and Down). As the field is switched ON, molecular alignment in the form of voltage drop is detected on the storage oscilloscope. In the SmC* phase, for a certain applied field, the output current response across the standard resistor R comprise of three components;

(a) capacitive term I_C (a differentiating component which shows an abrupt jump when the slope of applied voltage changes abruptly)

(b) ionic conduction term I_R

(c) the third term is polarization current I_P, due to the charge induced by the dipole realignment in the form of polarization hump.

A schematic representation of these output responses is shown in Figure 3.15. The instantaneous value of the output current over resistor R can be presented as

$$I = I_R + I_C + I_P = \frac{V_{IN}}{R} + C\frac{dV_{IN}}{dt} + \frac{dP}{dt} \qquad (3.2)$$

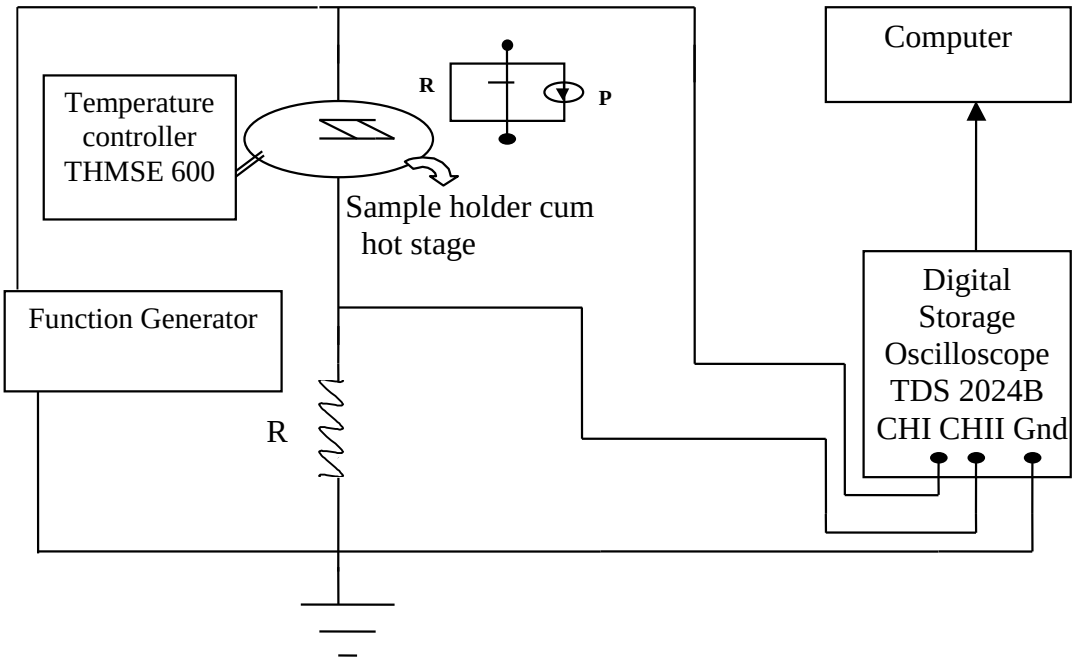

Figure 3.14 Experimental setup to study the spontaneous polarization and response time using reversal method.

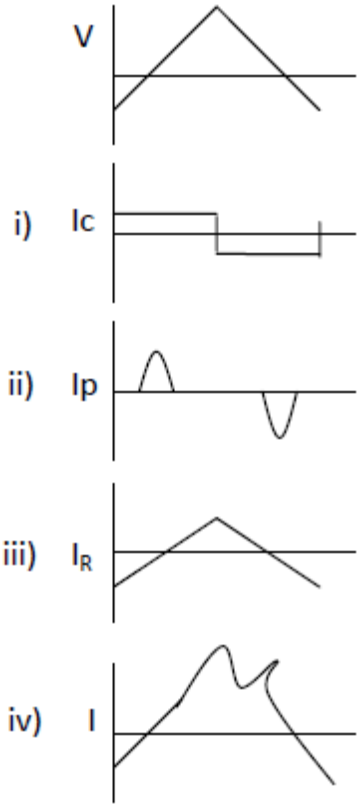

Figure 3.15 Illustration of current induced on application of triangular wave

Measurement of spontaneous polarization

The spontaneous polarization (P_s) is the macroscopic polarization, which the sample attains due to coupling between molecular polarization P with applied electric field E. Here sample gets poled and attains a macroscopic polarization. At this stage the helix of the FLC in the cell of a particular thickness unwinds, the macroscopic polarization becomes non-zero and the sample gets spontaneously polarized. This polarization is determined by applying the symmetric triangular wave and separating the resistive and capacitive term from the polarization term by drawing a base line. The occurred polarization hump is directly associated with dipole reorientation, corresponding to the switching between uniform stable states. Every reorienting dipole imparts a charge impulse and contributes to the polarizing reversal peak. Thus the peak incorporates total contribution of reorientation dipoles while switching between uniform states. The area under the hump is a measure of the spontaneous polarization, which is given by

$$P_s = \frac{A(i \times t)}{R(Area\,of\ Sample)} \tag{3.3}$$

Where, *A (i×t)* represent the area under the curve measured by integrating the polarization hump in terms of current and time [18,19]. Thus by calculating the area of the curve by knowing current and time representing along the Y, X-axes, respectively the P_s can be measured. The magnitude of P_s in the ferroelectric phase of FLC and doped-FLC samples decreases with the increasing the temperature and finally becomes zero at the SmC*-SmA transition temperature (T_c*A). It obey the power law and expressed by the equation.

$$P_s = P_o(T_c - T)^{\beta} \tag{3.4}$$

From mean field theory, the critical exponent β should be 0.5.

Response time

Another important parameter, i.e. response time (τ) which is delayed switching between two stable states is measured by appliying a symmetric square pulse to LC cell. Response time is calculated by applying a square pulse in the input and ouput is noted across the LC cell. Figure 3.16 show a view of obtained output waveform at certain voltage (30V). Response time can also be measured by electro-optic switching (i.e. the time required to change the optical transmission from 10 to 90%).

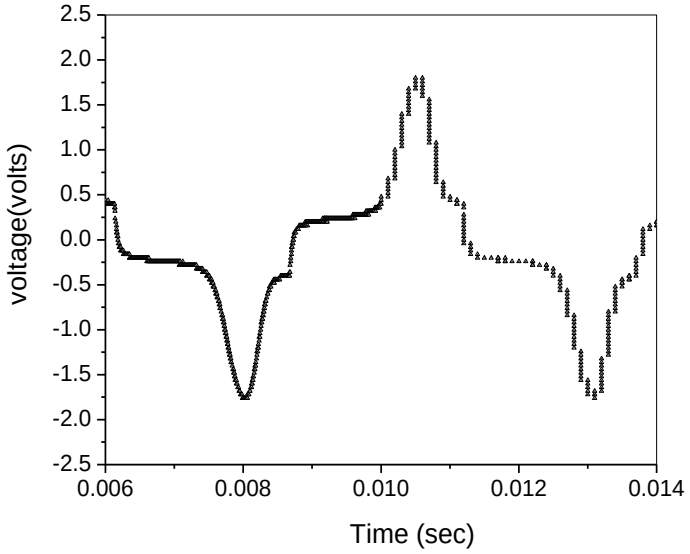

Figure 3.16 A view of output waveform at 30V.

Rotational Viscosity

Rotational viscosity (γ) corresponds to the molecular rotation of the director about its layer normal and given by the expression;

$$\gamma = P_s E \tau_s \quad (3.5)$$

Here γ is effective rotational bulk viscosity and E is applied electric field to LC cells.

3.7 Dielectric spectroscopy

Dielectric spectroscopy or impedance spectroscopy is one of the important tools to study the molecular dynamical process over a wide range of characteristic time for 10^{-12} s to 10^{15} s. This provides the information of intermolecular (dipoles) interaction and establish a link between properties of individual constitutes with bulk properties of sample [20].

This section describe the dielectric measurement technique and some imperative points concerning dielectric spectroscopy. In the present work, dielectric properties have been studied by Impedance Analyzer (Make: Wayne Kerr, Model: 6500B) having frequency range of 20Hz- 10MHz. A complete experimental setup is shown in Figure 3.12. The instrument is capable to determine capacitance (C), inductance (L), resistance (R), reactance (X), conductance (G), susceptance (B), dissipation factor (D), quality factor (Q), impedance (Z), admittance (Y), and phase angle (ϕ). All the above functions can be

selected via manual front panel control or controlled remotely via GPIB or LAN interfaces for fully automated high speed testing.

Calibration of cell

To measure the dielectric properties of investigated samples, the terminals (connecting wires) of filled LC sample cell are connected to Impedance analyzer by a text fixture. The values of capacitance (C), conductance (G) and dissipation factor (D) of the investigated samples are recorded by interfacing software which is further processed by Origin software 6.0.

Liquid crystal sample cell is considered as a parallel plate capacitor, whose capacitance (C) is given by

$$C = \frac{\epsilon A}{d} \tag{3.6}$$

A is area of cell, ϵ is the dielectric permittivity of the material and d cell thickness. However in practice, a stay capacitance (C_s) which is very important term to consider, arises when cell is subjected to an electric field due to wire attached and non homogeneities of the field lines at the edges of the active area [21-23].

The air capacitance of the cell can be written as

$$C_{air} = C_L + C_s \tag{3.7}$$

Where, C_L is live capacitance (capacitance of the empty cell without C_s).

C_s is measured by using the relative permiitivity of known standard liquids i.e. Benzene and CCl_4.

$$C_{sL} = \epsilon'_{SL} C_L + C_s \tag{3.8}$$

C_{sL} = capacitance of the cell filled with standard with Benezene or CCl_4.

Using Equations (3.7 & 3.8), the C_L is calculated as

$$C_L = \frac{C_{SL} - C_{air}}{\epsilon'_{SL} - 1} \tag{3.9}$$

The relative permittivity (ϵ') and dielectric loss ($\epsilon^{"}$) is calculated by using the values of capacitance, conductance and live capacitance. The equations for these calculations are as follow

$$\epsilon' = \frac{C_m - C_{air}}{C_L} + 1 \tag{3.9}$$

$$\epsilon^{"} = \frac{G_m - G_{air}}{2\pi f C_L} + 1 \tag{3.10}$$

Where C_m and G_m are the capacitance and conductance respectively of the cell filled with liquid crystal material. C_{air} *and* G_{air} are the capacitance and conductance, respectively of empty cell.

Data Analysis

In liquid crystals, the measurement of dielectric data and their analysis with full accuracy is a great concern because these materials have some amount of ionic impurities and affects more or less the dielectric properties. Basically, the obtained data suffers from two basic problems. The first one which is due to the presence of free ionic charge carrier exist in the low frequency region. There are two main type of ionic contributions i.e. ionic space charge polarization and charge buildup at the electrodes [24-25]. The second is due to the ITO coated sheet and connecting wires. These two issues can be resolved by best fitting the data as discussed below [26].

Low and high frequency Problem

The presence of ionic charge carriers are effective in the low frequency region (≈ 10 Hz-1 kHz) and offers additional conductivity in the liquid crystal and influcences the dielectric results significantly. The effect of this additional conductivity can be resolved by adding a resistance parallel to the cell. In addition to ionic conductivity, electrode polarization also takes places in low frequency region.

After adding the correction terms associated with the ionic conductance and electrode polarization in the low frequency region, the real and imaginary part of the dielectric permittivity can be written as [26].

$$\varepsilon^{*} = \varepsilon' \pm j\varepsilon'' \tag{3.11}$$

Where,

$$\varepsilon' = \frac{\varepsilon'(dc)}{f^{n}} + \left(\varepsilon'(\infty) + \frac{\delta\varepsilon}{1+(2\pi f\tau)^{(1-\alpha)}} \right) \tag{3.12}$$

and

$$\varepsilon'' = \frac{\sigma(dc)}{\varepsilon_0 2\pi f^{k}} + \mathrm{Im}\left(\varepsilon'(\infty) + \frac{\delta\varepsilon}{1+(2\pi f\tau)^{(1-\alpha)}} \right) \tag{3.13}$$

Here f is measuring frequency and σ is specific conductivity of sample. n and k are the fitting parameters. The first term of equations 3.12 and 3.13 represents the contribution due to ionic conductivity, while second terms of equations 3.12 & 3.13 repregents real

and impaginary part of the cole-cole equation. In the high frequency region .i.e beyond 10 MHz, the ionic contribution is negligible but ITO sheet resistance come into existence which significantly affect the dielectric absorption. In this region due to ITO effect, absorption suddenly increase to very high value. After including the contribution of pristine ITO absorption, the experimentally observed absorption can be written as

$$\varepsilon'' = Af^{m} + \mathrm{Im}\left(\varepsilon'(\infty) + \frac{\delta\varepsilon}{1+(2\pi f\tau)^{(1-\alpha)}}\right) \tag{3.14}$$

A, m are fitting parameters.

The total contribution due to ionic conductivity and ITO resistance can be written as

$$\varepsilon' = \frac{\varepsilon'(dc)}{f^{n}} + \left(\varepsilon'(\infty) + \frac{\delta\varepsilon}{1+(2\pi f\tau)^{(1-\alpha)}}\right) \tag{3.15}$$

and

$$\varepsilon'' = \frac{\sigma(dc)}{\varepsilon_0 2\pi f^{k}} + Af^{m} + \mathrm{Im}\left(\varepsilon'(\infty) + \frac{\delta\varepsilon}{1+(2\pi f\tau)^{(1-\alpha)}}\right) \tag{3.16}$$

By fitting the equations (3.15) and (3.16), with the experimental data, it is possible to substract the ionic and ITO effects from the dielectric spectrum in the low and high frequency region. Therefore for corrected dielectric results, ITO resistance should be as low as possible [26,28].

After getting the correction terms from these fitting equations, we correct the experimental data using following equations:

$$\epsilon'(corrected) = \epsilon'(experimental) - \frac{\epsilon'(dc)}{f^{n}}$$

$$\epsilon''(corrected) = \epsilon''(experimental) - \left(\left(\frac{\sigma(dc)}{2\pi\epsilon_0 f^{k}}\right) + (Af^{m})\right)$$

From the final calculated values of real and imaginary part of permittivity, other dielectric parameters can also be estimated by cole-cole plot.

The dielectric strength is written as

$$\delta\epsilon = (\epsilon_0 - \epsilon_\infty) \tag{3.17}$$

Where, ϵ_0 and ϵ_∞ are the the low and high frequency limit of permittivity respectively [29, 30].

3.8 Electro-optical studies

Electro-optic studies were performed to measure parameters such as transmission, birefringence, constrast ratio, threshold voltage etc. Figure 3.13 shows the experimental setup employed for electro-optical measurements. The setup consist of He-Ne laser (Make: Melles Griot, 5 mW, 632.8 nm), a pair of polarizers, power amplifier (Make: FLC, Model: A400), function generator (Make: Tektronix, Model: AFG3021B), digital storage oscilloscope (Make: Tektronix, Model: TDS2024B), photo-detector (Make: Instec, Model: PD02), Digital multimeter. An ac rectangular field at low frequency was applied to the sample using function generator coupled with power amplifier, and change in intensity which transmit through LC cell was measured with the help of photo-detector connected to the digital multimeter.

3.9 UV-VIS Spectrophotometer for absorbance studies

Ultraviolet-visible spectrophotometry (UV-VIS) refers to absorption spectroscopy in the ultraviolet-visible spectral region. It uses light in the visible and adjacent (near-UV and near-infrared) ranges. The absorption in the visible range directly affects the perceived color of the materials involved. Molecules undergo electronic transitions in this region of the electromagnetic spectrum. Absorption measures transitions from the ground state to the excited state. The UV-VIS absorbance spectra of pure LCs and magnetic nanoparticles-liquid crystal composites were investigated at room temperature using UV-VIS spectrophotometer (Make: Agilent; Model: Carry 100) in the wavelength range of 190-800nm. The output responses were obtained on the computer interfaced to the spectrophotometer. The bang gap of samples were also calculated using obtained spectra.

References:

[1]. BDH, UK.

[2]. R. Dabrowski, Warsaw, Poland.

[3]. Sigma Aldrich, Germany.

[4]. Kingston Chemicals, UK.

[5]. Khushboo, P. Sharma, P. Malik, K. K. Raina, Liq. Cryst. 2016; 43: 1671-1681.

[6]. B. Bahadur, Liquid Crystals: Applications and Uses, World Scientific, Singapore, Vol. 3 (1992).

[7]. S. Chandrasekhar, Liquid Crystals, 2nd Edn, Cambridge University Press (1992).

[8]. P. G. De Gennes, Physics of Liquid Crystals, Oxford University Press (1975).

[9]. I.C. Khoo, Physics of Liquid Crystalline Materials (Amsterdam: Golden and Breach) (1991).

[10]. P. J. Collings, Liquid Crystals: Nature‘s Delicate Phase of Matter, Princeton University Press (1990).

[11]. K. Hiroshima, Jpn. J Appl Phys. 1982; 21: L761.

[12]. W. Urbach, M. Boix and E. Guyon, Appl Phys Lett. 1974 25, 479.

[13]. S.S. Bawa, A.M. Biradar and S. Chandra, Jpn J Appl Phys. 1986; 25:L446.

[14]. J.K. Ahuja and K.K. Raina, Jpn J Appl Phys. 2000; 39: 4076.

[15]. J.K. Ahuja, Ph.D. Thesis, Thapar Institute of Engineering and Technology (2000).

[16]. Manual of Linkam Temperature Controller (TP95) and Hot Stage (THMSE 600).

[17]. P. Malik, Ph.D. Thesis, Thapar Institute of Engineering and Technology (2005).

[18]. K.K. Raina and J. K. Ahuja, Mol Cryst Liq Cryst. 2001; 338: 125.

[19]. P. Malik, K. K. Raina, A. K. Gathania, Thin Solid Films 2010; 519: 1047-1051.

[20]. W. Haase, S. Wrobel, Relaxation Phenomena, Springer Press (2003).

[21]. A. K. Thakur, PhD Thesis, University of Delhi, 2004.

[22]. S. Mastsumoto, M. Kawamoto and N. Kaneko, Appl Phys Lett. 1975; 27: 268.

[23]. A. K. Srivastava, PhD Thesis, University of Lucknow, (2008).

[24]. M. Iwamoto, J Appl Phys. 77 (1995) 5314.

[25]. S. Murakami, H. Iga and H. Naito, J Appl Phys. 1996; 80: 6396.

[26]. F. M. Gouda, PhD Thesis, Chalmers University of Technology, (1992).

[27]. D. P. Singh, PhD Thesis, University of Lucknow, (2015).

[28]. S. L. Srivastava and R. Dhar, Ind. J. Pure & Appl. Phys. 1991; 29: 745.

[29]. K.S. Cole and R.H. Cole, J. Chem. Phys. 1941; 9:341.

[30]. C. Wakai, A. Oleinikova, M. Ott, and H. Weinga1rtner, J. Phys. Chem. B2005; 109**:** 17028.

CHAPTER - 4

Iron magnetic nanoparticles doped nematic liquid crystal

Overview

In this chapter, the effect of Iron nanoparticles (Fe NPs) dispersion in nematic liquid crystal (6OCB) physical properties is discussed. Dispersion of Fe NPs (0.25 wt. %) in 6OCB on textures, isotropic- nematic transition temperature ($T_{I\text{-}N}$), electro-optical and dielectric properties have been investigated in planar aligned cell. The threshold voltage (V_{th}) and $T_{I\text{-}N}$ decrease after dispersion of Fe NPs. Dielectric spectroscopy show that in nematic phase, relaxation frequency also decreases in Fe NPs doped 6OCB composite. The band gap and AC conductivity in case of 6OCB-Fe sample increase over pure 6OCB sample. A decrease in activation energy is also noticed.

4.1 Introduction:

Dispersion of nanosize materials in LCs has been explored owing to their promising applications in diverse fields including photonics, biomedical, electronics, optics etc. [1–3]. The research activity enriched in this area has increased exponentially due to the two emerging fields, namely LCs and nanoscience. The idea behind dispersion of NPs in LCs is two fold; first one is to improve or alter the physical and chemical properties of LC for display applications; and secondly to study the molecular interaction between NPs and LCs, effect of size, shape and concentration of NPs on the phases, phase transition temperatures, optical, electrical, thermal and magnetic properties of LCs [4–6]. In the past years, carbon nanotubes (CNTs), gold NPs, graphene, graphene oxides, oxides, ferroelectric, quantum dots were dispersed in LCs and their physical properties are extensively studied [7-18]. It is well established that doping of NPs has considerable effect on enhancement in transmittance, birefringence, contrast ratio, switching time, threshold voltage, polarization, permittivity, dielectric strength, conductivity and photoluminance.

Conventional thermotropic LCs are usually diamagnetic in nature with small value of anisotropy of diamagnetic susceptibility (~ 10^{-7}). Therefore, rather high magnetic field (~ 1 Tesla) is needed to change the orientation of LC director [19]. Consequently, a great scientific interest in suspension of magnetic particles in nematics (ferronematics) has created due to their fundamental points of view and unique features. The operation of ferronematics is based on the effect of a mechanical coupling between magnetic particles and LC director (i.e. magnetic particles share their properties with LCs). The coupling between magnetic particle and LC molecule orientations then transfers the magnetic orientation effect on the underlying LC matrix. The magnetic particles of different nature (ferromagnetics, ferrimagnetics, paramagnetics and superparamagnetics) are used as guest/dopants in host (nematics LCs). These materials have attracted considerable interest because, in principle, they should exhibit higher magnetic susceptibilities than undoped liquid crystals, resulting in evident device applications. The first experimental attempts was carried out by Chen and Amer in 1983 [20, 21]. They prepared a ferronematic suspension consisting of magnetic nanopartilces, γ-Fe_2O_3 needle (~ 70× 500 nm), volume fraction of particles 10^{-6}- 0^{-7} and magnetization M = 340 G and NLC MBBA (N-(4-Methoxybenzylidene)-4-butylaniline)). These needles were coated with a surfactant DMOAP. A reduction in effective

Frederiks threshold voltage [20]. In spite of low threshold voltage, this work have not received much scientific attention due to the problem of unstability of suspension which occurs due to particle agglomeration. More recently, studies of ferronematics suspension using different thermotropic liquid crystal matrices were reported by P. kopcansky and others. Various MNPs, Fe_3O_4 (diameter ~10 nm, coated with oleic acid, volume concentration 10^{-3} to 10^{-5}) in ZLI 1695 and 6CHBT; Fe_3O_4 (needle like covered with surfactant) in 5CB; FeCo in 8CB [22-25] were investigated. Fe_3O_4 of different shapes (spherical- 12 nm, rod like- 80 nm, chain like 500 nm) in 6CHBT, and functionalised CNTs with magnetic particle of Fe_3O_4 were also studied in 6CHBT [26]. In addition to the many works on the physics of LC doped with MNPs, the ability of magnetic NPs to form mesophases and MNPs decorated by LCs were prepared and studied, but these works are beyond the scope of our thesis. Continous efforts have been made by several groups to investigate and understand the role of MNPs in LCs in detail [29-32]. Further, a modification/improvement in LC physical properties after dispersion of MNPs has been reported and discussed.

In this chapter, our aim is to study the effect of Fe NPs dispersion in nematic liquid crystal (6OCB) on the micro-textures, phase transition temperature, thermal, dielectric, electro-optical properties. The effect of applied voltage on transmission and behaviour of dielectric permittivity, conductivity as a function of frequency is also discussed.

4.2 Experimental Detail

NLC, 4′-(Hexyloxy)-4-biphenylcarbonitrile (trade name 6OCB) has a phase sequence; Crystal (Cr) 58°C–nematic (N) 76°C– Isotropic (I). The molecules of 6OCB possess large longitudinal dipole moment caused by the cyano (CN) group. This CN group produced a pronounced relaxation in the range of MHz [33]. Fe MNPs, (powder form) was used for dispersion purpose. The physical properties of 6OCB and Fe NPs are shown in Table 3.2, 3.5 of chapter 3.

To characterise the size and morphology of Fe NPs, Transmission Electron Microscopy (Tecnai G^2, FEI) at an accelerating voltage of 200 kV was used. For TEM, small quantity of Fe NPs were dissolved in solvent (ethanol) and then ultrasonification was done for about 30 min. A drop (solution of Fe NPs and solvent) was put on carbon-coated grid (400-mm mesh) for investigation. Microscopy shows that Fe NPs are of spherical shape of size ~ 45– 60 nm. The corresponding TEM image is shown in Figure 3.1. Since NPs has a tendency to form a aggerates, therefore to avoid the formation of

agglomeration, 1-2 drops of oleic acid (surfactant) were added in Fe NPs followed by ultrasoniocation. 6OCB-Fe composite was prepared by dispersion of small concentration (0.25 wt. %) of Fe into 6OCB. For complete dispersion, Fe and 6OCB were thoroughly mixed above the isotropic temperature of 6OCB followed by ultrasonification for 1 hr. The mixture of 6OCB-Fe was then kept at room temperature for 24–36 h so that surfactant may be completely removed from the mixture.

Planar aligned LC cells (purchased from Instec, USA) consisting of highly transparent ITO glass substrates were used. The thickness and active area of LC cell is 5.0 μm, 0.5 × 0.5 cm^2 respectively. Both 6OCB and 6OCB-Fe mixtures were introduced into LC cell by capillary action above the isotropic temperature of 6OCB. Now these filled LC cells were kept in hot stage. The temperature of filled LC cells was controlled using temperature controller. The micro-textures and phase transition temperatures were observed through an optical polarising microscope (objective 10x) interfaced with a Q-imaging camera. The phase transition temperatures were also studied using differential scanning calorimeter. Both mixtures, 6OCB and 6OCB-Fe were initially heated and then cooled down in two cycles at the scan rate of 2.0°C/min in the range of 40- 80°C. The intensity of transmitted light passing through filled LC cells was measured using high resolution photodetector. For optical measurements, LC cells were kept in hot stage between crossed polarizer and analyzer. The output of cell is attached with digital multimeter (DMM). The transmitted intensity in the form of voltage was measured using six-half digit DMM. A function generator was used to apply alternating electric field to LC cells. The experimental setup used for electro-optical studies is also shown in Figure 4.1. Dielectric properties were measured by impedance analyser in the frequency range of 10–20 MHz. To reduce the low- and high-frequency corrections, experimental datas were calibrated with air and benzene [34]. The optical band gap (E_g) was also measured in the wavelength range of 200–450 nm at room temperature by UV–visible spectrometer.

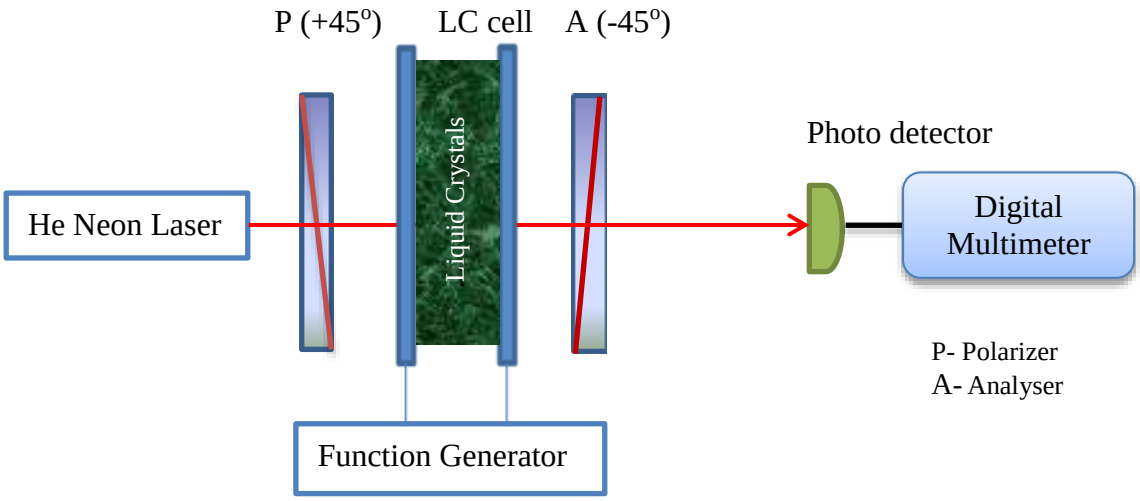

Figure 4.1 Experimental setup to study the electro-optical responses of liquid crystal.

4.3. Results and Discussion

4.3.1. Effect of applied volatge on textural behaviour

The effect of applied voltage (frequency 1 kHz, square wave) on textures of 6OCB-Fe cells at 65°C is shown in Figure 4.2. Figure 4.2 (a) illustrate a typical NLC phase at 0 V and exhibit a bright state. However, on increasing the voltage from 0 to 12 V (6OCB-Fe), these bright states gradually change to bright cum dark state and finally change to complete dark states (figure 4.2 (f)). Initially, at 0 V, LC molecules have parallel orientation (homogenous) to the glass substrates and on further increasing the applied voltage, LC molecules start to change their orientation from parallel to perpendicular to the glass substrates. In this case, since LC molecules have their orientation just perpendicular to glass substrates, therefore light coming through the LC does not pass up to the analyser and appears as a dark state (Figure 4.2(f)).

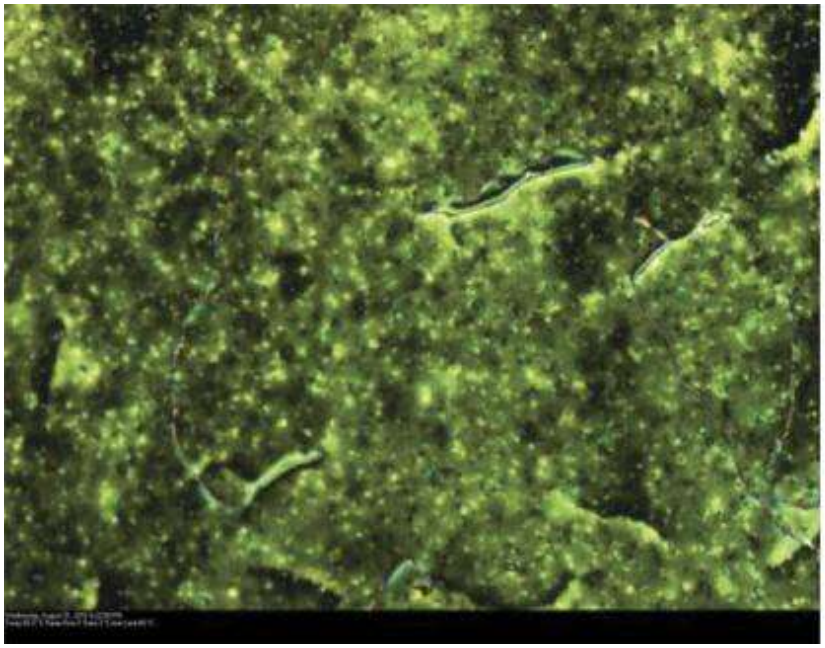

(a)

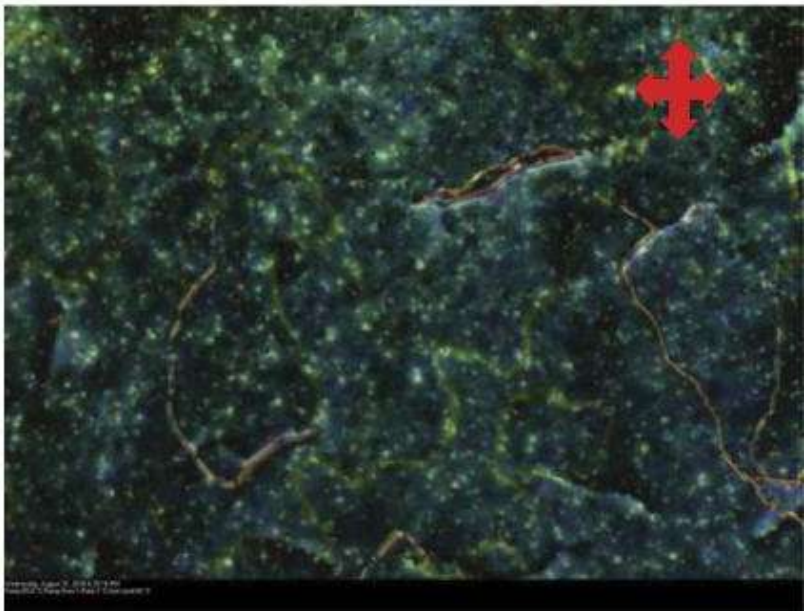

(b)

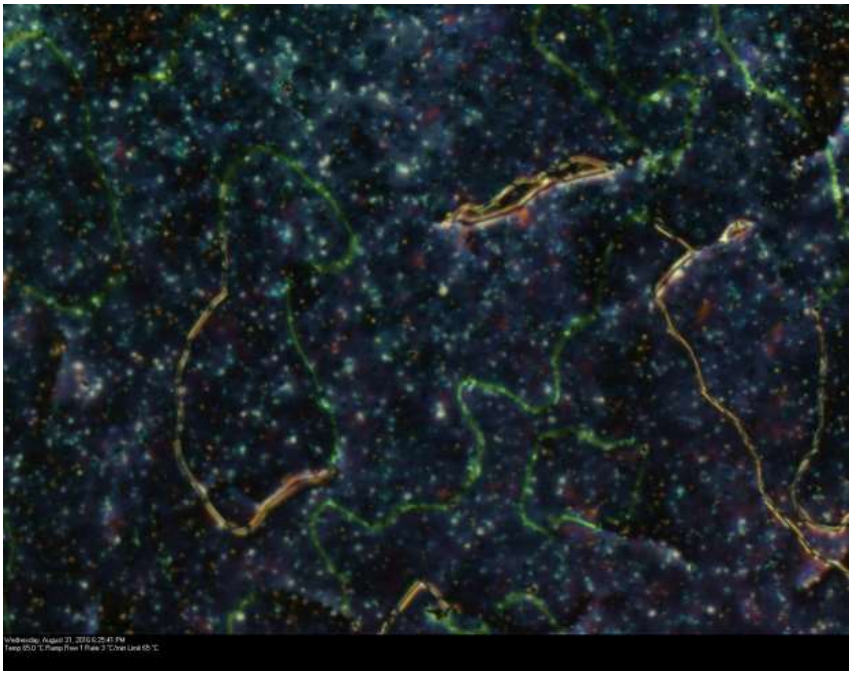

(c)

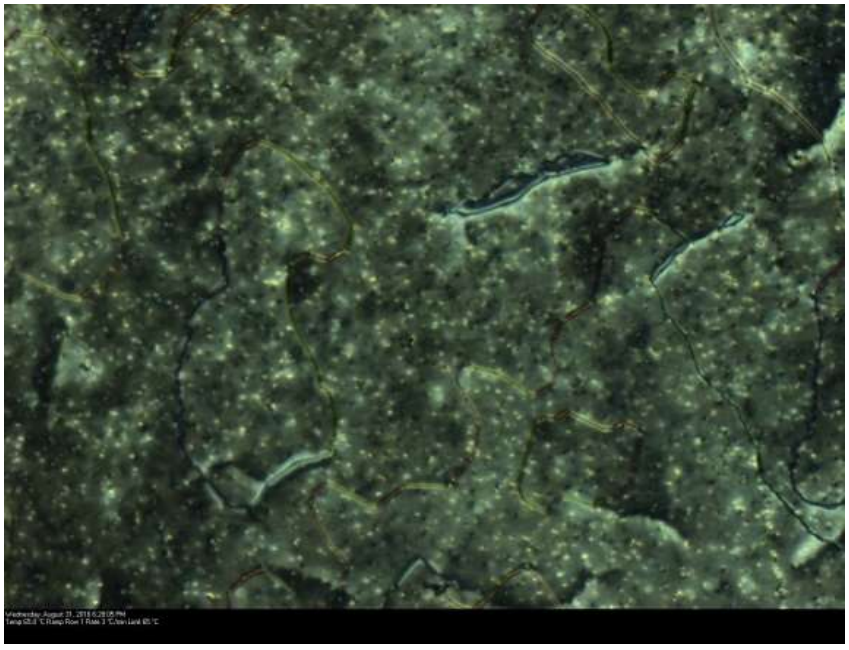

(d)

(e)

(f)

Figure 4.2 Texture of 6OCB-Fe mixture under polarizing microscope at 10x (a) 0 (b) 1.8 (c) 2.0 (d) 4 (e) 8 (f) 12 V at 65ºC. Cross arrow indicates the position of polarizer and analyzer.

4.3.2 Voltage-Transmittance (V-T) Study

The intensity of transmitted light passing through the LC cell can be expressed as [35-37].

$$I_t = \frac{sin^2 2\theta}{2}(1 - cos\Delta\varphi) \quad (4.1)$$

Where θ is the angle between the polarizer and optic axis. $\Delta\varphi$- phase difference. The birefringence (Δn) is calculated using the Equation (4.1).

$$\Delta\varphi = \frac{2\pi}{\lambda}\Delta n.d \quad (4.2)$$

d- cell thickness and λ is wavelength of incident light (λ for Helium Neon laser 632.8 nm). The effect of applied voltage on transmission (V-T curve) in nematic phase is also shown in Figure 4.3. Here LC cells were placed at an angle of 45^o with the optic axis of incident light. Initially, in the low voltage range (~0-1.5V), transmitted intensity through LC cells is found nearly constant and a decrease in intensity is seen from 1.5-2V. The threshold voltage (V_{th} - the required voltage at which the cell turns from bright to dark state) was found ~1.4V and 1V for 6OCB and 6OCB-Fe sample cells, respectively. The extended view of V-T curve in low voltage region (0-2 V) is also presented in Figure 4.3 (inset). Birefringence (Δn) is also measured in nematic phase (temperature, 65^{0}C) at an applied voltage of 2V. The calculated values of Δn for 6OCB and 6OCB-Fe sample cells are found 0.24 and 0.76, respectively. The obtained values of Δn in both samples match well with earlier published data [38].

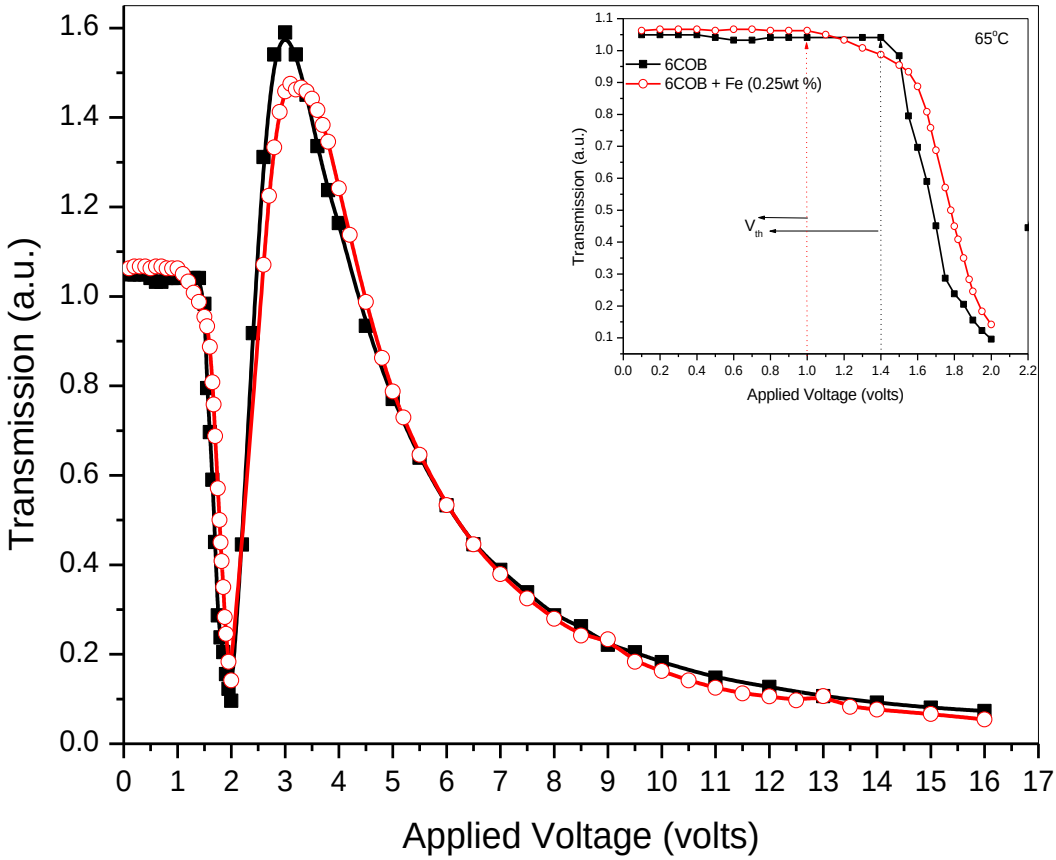

Figure 4.3: Voltage- transmission (V-T) behavior for 6OCB and 6OCB-Fe sample cells under crossed polarizer at applied voltage (frequency- 1 kHz) at 65°C. The inset shows an extended view of V-T curve at lower applied voltage. Arrow indicates a threshold voltage (V_{th}).

4.3.3. Phase Transition Studies

The crystal–nematic and nematic–isotropic phase transition temperatures of 6OCB and 6OCB-Fe samples were also studied by DSC thermograph and shown in Figure 4.4. The thermal data are taken during heating as well as in cooling cycles at the rate of 2.0°C/min under nitrogen atmosphere. The obtained transition temperatures in both samples is given below:

6OCB Crystal ↔ 57.64°C ↔ Nematic 75.8°C ↔ Isotropic

6OCB-Fe Crystal ↔ 57.69°C ↔ Nematic 76.0°C ↔ Isotropic

The observed phase sequence indicates that dispersion of Fe NPs does not affect the Crystal to nematic (Cr–N) and nematic to isotropic (N–I) transition temperatures. The Cr–N and N–I phase transitions were also confirmed by polarising microscopy and our results match well with earlier reported works [38–41].

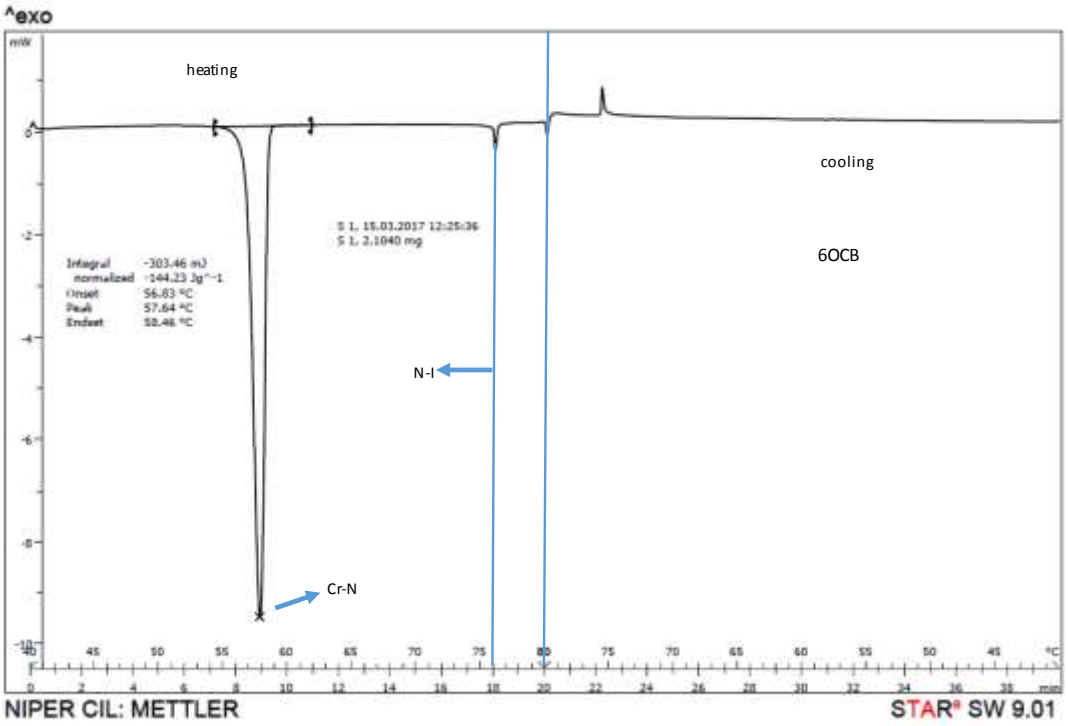

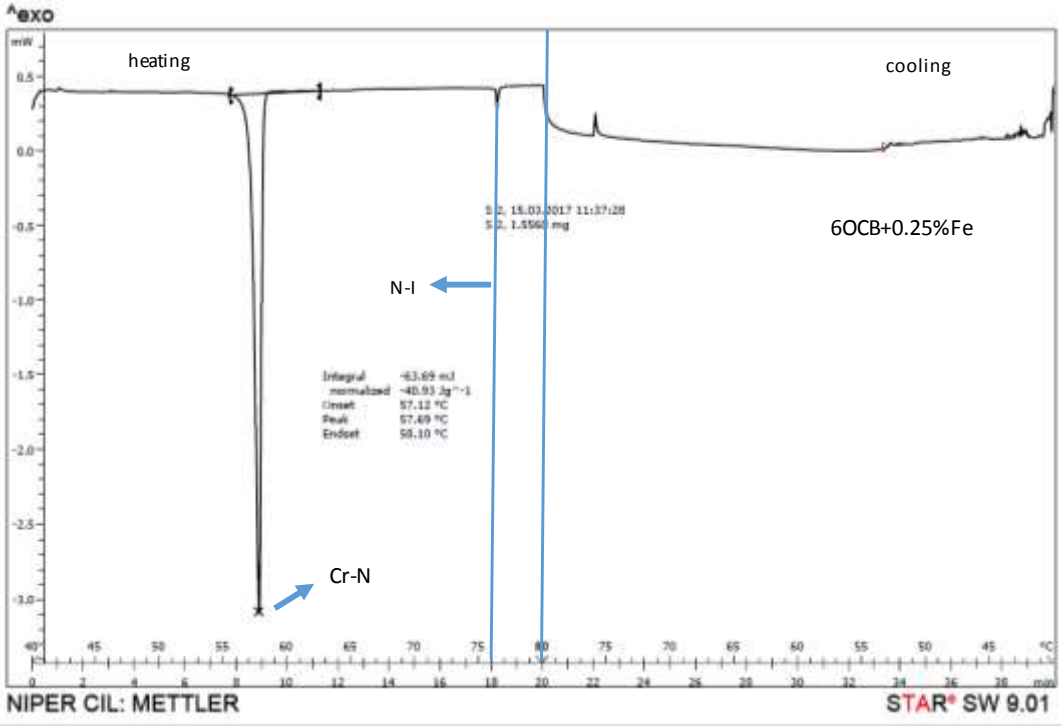

Figure 4.4 DSC thermograms of 6OCB and 6OCB-Fe samples at a scan rate of 2^{o}C/min.

4.4.4 Dielectric Investigations

The dielectric relaxation spectrum can be described with the help of the following generalized Cole– Cole equation as [42-43].

$$\varepsilon^* = \varepsilon'(\infty) + \sum \frac{\delta\varepsilon}{1+(j\omega\tau)^{(1-\alpha)}} + \frac{A}{\omega^n} - j\frac{\sigma_{ion}}{\varepsilon_0\omega^k} - jB\omega^m \quad (4.3)$$

The real (ε') and imaginary part (ε'') of Equ. (4.3) can be expressed as

$$\varepsilon' = \varepsilon'(\infty) + \sum \frac{\delta\varepsilon[1+(\omega\tau)^{(1-\alpha)}\sin(\alpha\pi/2)]}{1+(\omega\tau)^{2(1-\alpha)}+2(\omega\tau)^{(1-\alpha)}\sin(\alpha\pi/2)} + \frac{A}{\omega^n} \quad (4.3.1)$$

$$\varepsilon'' = \sum \frac{\delta\varepsilon(\omega\tau)^{(1-\alpha)}\cos(\alpha\pi/2)}{1+(\omega\tau)^{2(1-\alpha)}+2(\omega\tau)^{(1-\alpha)}\sin(\alpha\pi/2)} + \frac{\sigma_{ion}}{\varepsilon_0\omega^k} + B\omega^m \quad (4.3.2)$$

Where, ε_0, ε_∞ are the low and high frequency limiting values of dielectric permittivity, $\delta\varepsilon$, α ($0 < \alpha < 1$) represents the dielectric strength and distribution parameter, respectively. The third and fourth terms in equation (4.3), represent the contribution due to electrode polarization capacitance and ionic conductivity at low frequencies. The measured dielectric absorption contains a contribution above 100 kHz due to finite resistance of electrodes and wire inductance. Therefore, an additional imaginary term ($B\omega^m$) is included in equation (4.3) in order to partially to account for high frequency effect. Here *A*, *B*, *m*, *n* and *k* are the fitting parameters. $\varepsilon_0 = \left(8.85 \times 10\text{^}(-12)\,\frac{\mathrm{F}}{\mathrm{m}}\right)$, permittivity of free space, ω - angular frequency and τ is relaxation time. The frequency -dependence behavior on the dielectric permittivity and dielectric loss for both samples in nematic phase at 68°C is shown in Figure 4.5. The measured values of dielectric permittivity and dielectric loss are separately fitted with equations 4.3.1 and 4.3.2 using origin 6.1 software. During fitting process, efforts were made to get the best fit values of chi-square ($\chi^2 \rightarrow 0$) and correlation coefficients ($R^2 \rightarrow 1$). Using fitted value of parameters, the low and high frequency correction terms were calculated and then subtracted from the measured data to get the corrected (free from low- and high -frequency effects) values. The purpose of fitting was to eliminate the low-(ionic conductance) and high-frequency corrections (electrode and lead conductance) factors from the experimental values of permittivity and dielectric loss. It is seen in Figure 4.5 that inclusion of Fe NPs in 6OCB increases the dielectric permittivity from 6.13 to 7.01. From the analysis of absorption spectra, it is clearly seen that a relaxation mode in the range of ~1-2 MHz exists in the nematic phase of both samples. The relaxation frequencies (f_r) of 6OCB and 6OCB-Fe corresponding to detected modes at 68°C are

found 1.80 MHz and 1.65 MHz, respectively. The f_r was also calculated at other temperatures in nematic phase. It is seen that f_r decreases with increasing the temperature and addition of Fe NPs. A marginal decrease in relaxation frequency after dispersion of $BaTiO_3$ NPs in 5CB NLC was also notice than pure 5CB [44]. Mainly two dynamical processes occurs in LCs (i) the low-frequency process connected with the molecular rotation around the short axis and (ii) high-frequency processes corresponding to much faster rotation of around the long axis of LC molecules. We believe that such type of observed relaxation mode having f_r in MHz range is attributed to the flip-flop motion of the LC molecules about their short axis [45-46].

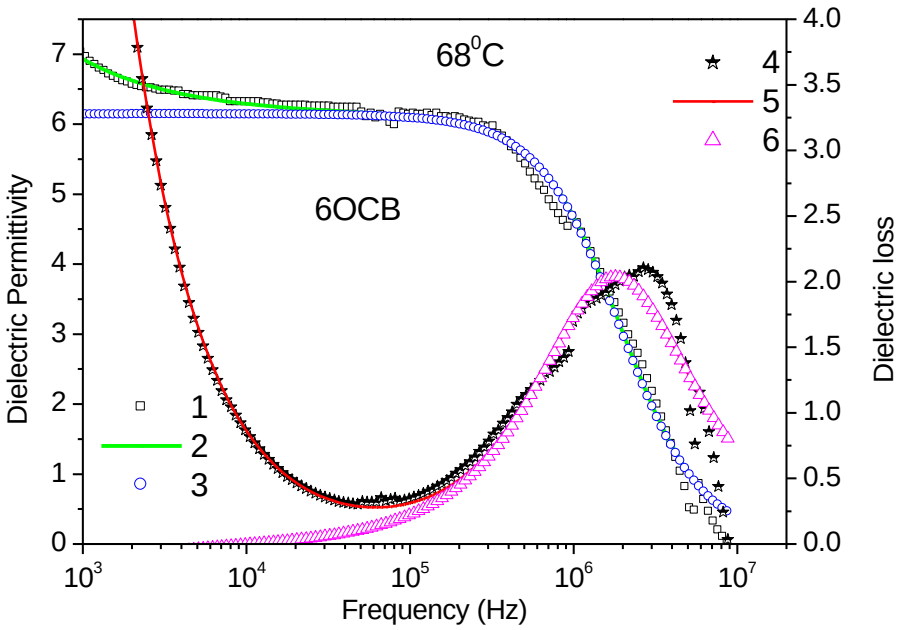

(a)

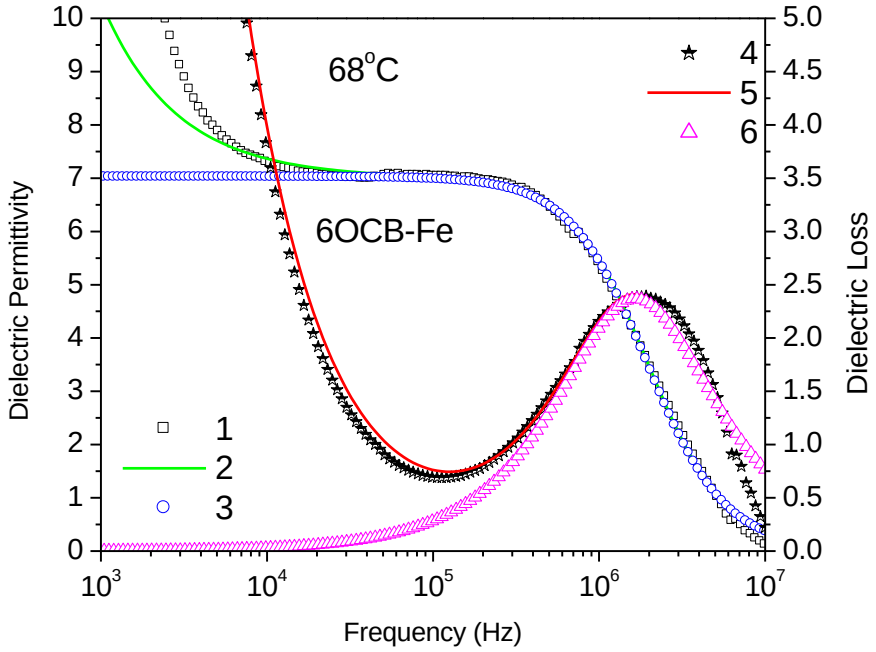

(b)

Figure 4.5 Frequency dependence of dielectric permittivity and dielectric loss (a) 6OCB and (b) 6OCB-Fe samples at 68°C. Curve 1 (□) - measured data, curve 2 (green solid line) show the fitted data, curve 3 (○) - corrected value of permittivity; Curve 4 (*) - measured data, curve 5 (red solid line) show the fitted data and curve 6 (Δ) represent corrected value of dielectric loss.

The f_r corresponding to flip-flop motion follows the Arrhenius behavior and expressed in the form of equation [47].

$$Logf_r = Logf_o - \frac{E_a}{RT} \tag{4.4}$$

where, E_a- activation energy corresponding to flip-flop motion of axes. R - gas constant (8.314 J/mole-K) and T is absolute temperature. E_a is obtained by calculating a slope of straight line between (1/T) versus $Logf_r$. The slope was measured using least square fit method. The inverse of temperature (1/T) with $Logf_r$ behavior is shown in Figure 4.6. It is found that E_a decreases from 8.56 kJ/mole (6OCB) to 2.32 kJ/mole (6OCB-Fe). This decrease in E_a after dispersion of Fe in 6OCB suggests that presence of Fe NPs facilities the flip flop motion of LC molecules, and results a decrease in E_a. The value of E_a and its temperature dependence variation are in good agreement with reported data [48].

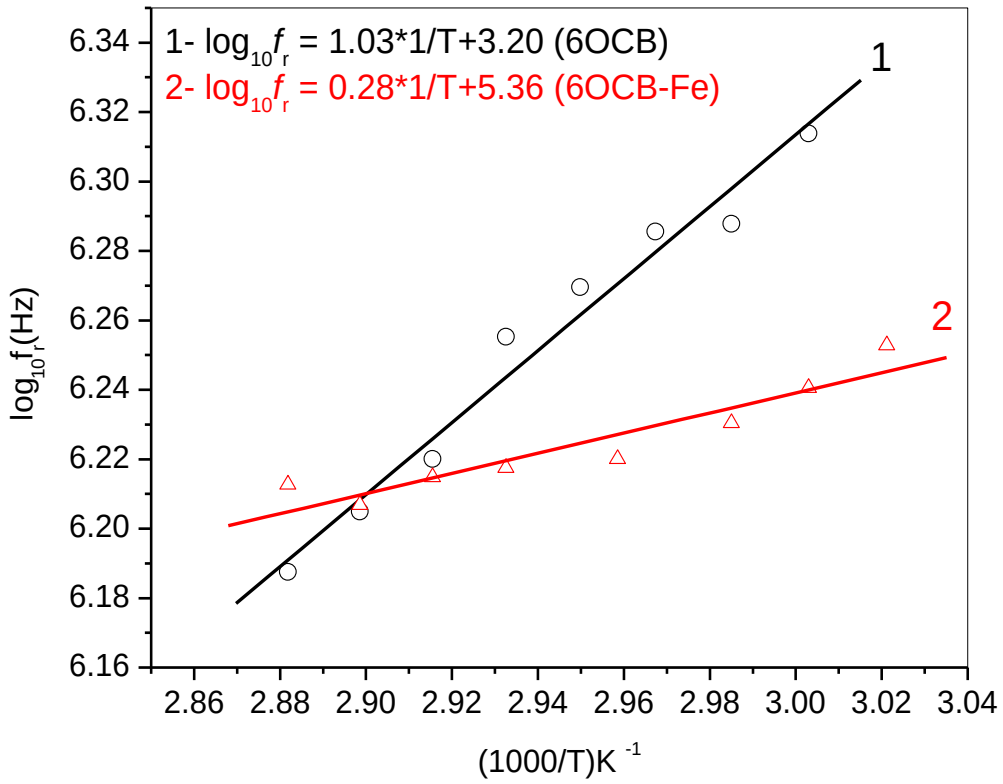

Figure 4.6 Arrhenius plots for 6OCB and 6OCB-Fe samples.

4.4.5 Optical absorption spectra and band gap

Figure 4.7 shows the UV-visible absorption spectra for 6OCB and Fe-6OCB composite. In Figure 4.7, a single peak was observed in the visible spectrum at 319 nm, 315 nm, for 6OCB and Fe-6OCB cells respectively. The absorbance spectrum was shifted slightly towards the lower wavelength side after doping with Fe. The optical band gap (E_g) has been calculated using the Tauc relationship [49].

$$\alpha h\nu = A(h\nu - E_g)^n \tag{4.5}$$

$$\alpha = -\frac{\ln T}{d} \tag{4.6}$$

Where, α - absorption coefficient, *d*- denotes the film thickness, *hν* – incident photon energy, *A* – constant and E_g corresponds to the particular transition in the material, n is an index having 1/2, 3/2, 2 and 3 depending on the nature of transition. Here, n = 1/2 is taken for direct allowed transition. E_g is analyzed by plotting a graph between $(\alpha h\nu)^{1/n}$

and *hv* as presented in Figure 4.8. An extrapolation of linear region at α = 0 give corresponding value of E_g. The intercept of the linear fit on the x- axis gives E_g. Here E_g is found 3.68 eV and 3.69 eV for 6OCB and 6OCB-Fe sample, respectively.

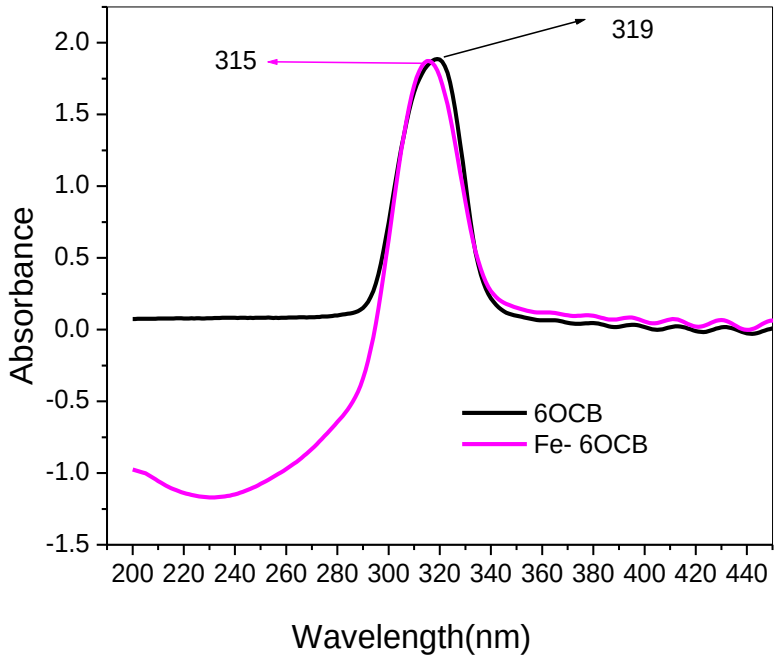

Figure 4.7 Optical absorption spectra for 6OCB and Fe-6OCB composite.

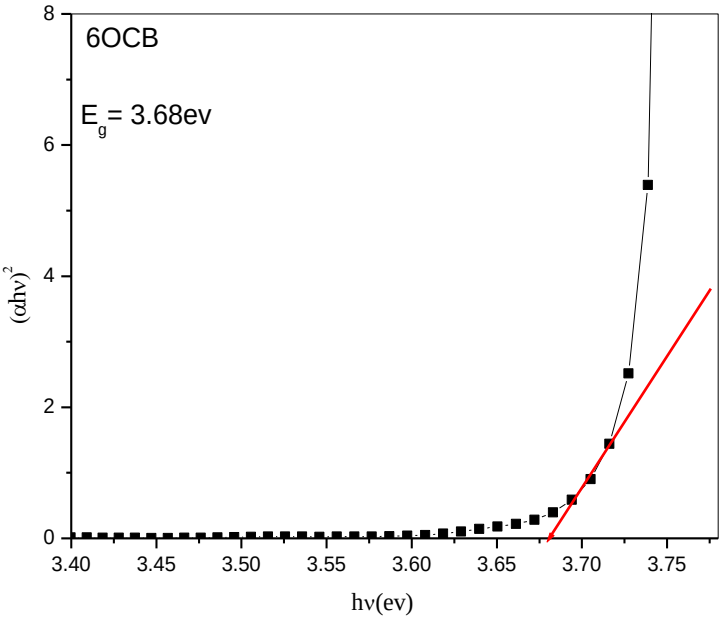

(a)

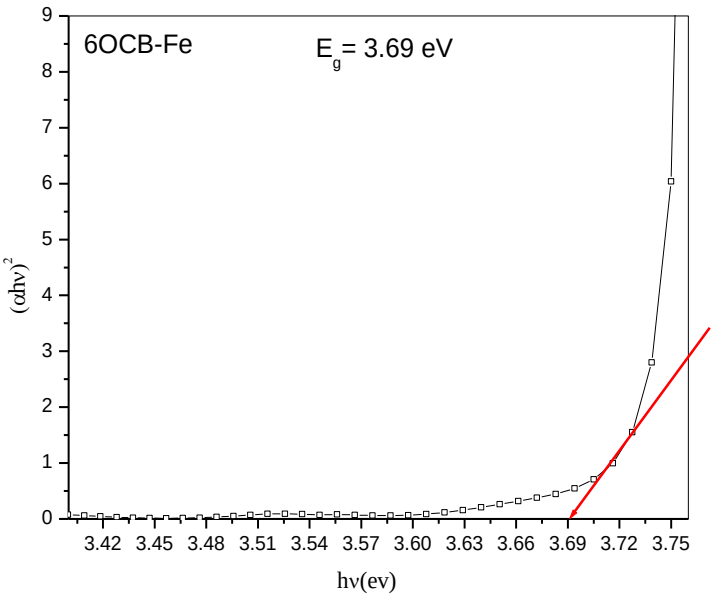

(b)

Figure 4.8 Band gap of (a) 6OCB and (b) 6OCB-Fe sample

4.4.6 Conductivity Measurement

The AC conductivity (σ_{ac}) as a function of frequency for both samples is shown in Figure 4.9. The AC conductivity has been evaluated using the expression;

$$\sigma_{ac}(\omega) = \sigma_0 + A\omega^n, \quad (4.7)$$

where $\sigma_{ac}(\omega) = \omega\, \varepsilon_0 \varepsilon''$; $\omega = 2\pi f$ and σ_0 is DC conductivity. It is seen that addition of Fe NPs in 6OCB increases the ac conductivity. This increase in ac conductivity may be due to enhancement in ion concentration after Fe NPs dispersion.

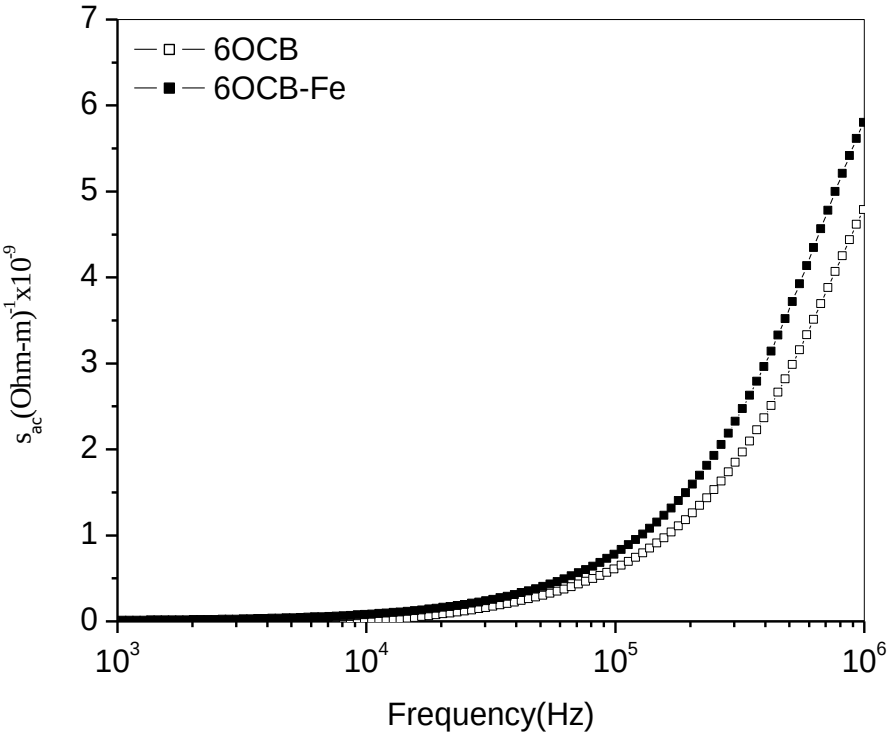

Figure 4.9. Variation of frequency dependence with AC conductivity for 6OCB and 6OCB-Fe samples in nematic phase at 68ºC.

References:

[1] H. Qi, T. Hegmann. J Mater Chem. 2008; 18: 3288-3294.

[2] P.J. Collings. Liquid crystals: Nature's delicate phase of matter. Princeton University Press;1990.

[3] H.K. Bisoyi, S. Kumar. Chem Soc Rev. 2011; 40: 306-319.

[4] J. P. F Lagerwall, G. Scalia. Curr Appl Phys. 2012; 12: 1387-1412.

[5] J. P. F. Lagerwall, G. Scalia. Liquid Crystals with Nano and Microparticles, Series in Soft Condensed Matter 7: World Scientific Press; 2016.

[6] O. Stamatoiu, J. Mirzaei, X. Feng, et al. Top in Curr Chem. 2012;318:331-394.

[7] H. Duran, B. Gazdecki, A. Yamashita, et al. Liq Cryst. 2005; 32: 815-821.

[8] A.S. Pandey, R. Dhar, S. Kumar, et al. Liq Cryst. 2011;38:115-120.

[9] M. Mishra, R. Dabrowski, R. Dhar, et al. Liq Cryst. 2015;42:1580-1590.

[10] P. Blake, P.D. Brimicombe, R.R. Nair, et al. Nano Lett. 2008;8(6):1704-1708.

[11] B. Senyuk, N. Behabtu, B.G. Pacheco, et al. ACS Nano. 2012;6(9):8060-8066.

[12] S. Javadian, N. Dalir, J. Kakemam. Liq Cryst. 2017; DOI: 10.1080/ 02678292. 2016. 1278051.

[13] N. Topnani, V. Hamplova, M. Kaspar et al. Liq Cryst. 2014; 41: 91-100.

[14] H.Y. Jung, H.J. Kim, S. Yang, et al. Liq Cryst. 2012; 39: 789-793.

[15] E. Ouskova, O. Buchnev, V. Reshetnyak, et al. Liq Cryst. 2003;30:1235-1239.

[16] P. Kumar, A. Sinha. Phase Trans. 2015; 88: 605-620.

[17] U.B Singh, M.B. Pandey, R. Dhar, et al. Liq Cryst. 2016; 43: 1075-1082.

[18] J. Mirzaei, M. Urbanski, K. Yu, et al. J Mate Chem. 2011; 21: 12710-12716.

[19] F. Brochard, P. G De Gennes. J of Phys. 1970;31:691-708.

[20] S.H. Chen, N.M Amer. Phys Rev Lett. 1983;51:2298.

[21] S.H. Chen, B.J Liang. Opt Lett. 1988;13:716-718.

[22] M. Koneracka, V. Kellnerova, P. Kopcansky, et al. J Magn Magn. Mat. 1995;140:1455–1456.

[23] P. Kopcansky, I. Potocova, M. Koneracka, et al. Phys Stat Sol (b). 2003;236:450-453.

[24] P. Kopcansky, I. Potocova, M. Koneracka, et al. J Magn Magn. Mat. 2005;289:101-104.

[25] I. Potocova, P. Kopcansky, M. Koneracka, et al. J Magn Magn. Mat. 2002;252:150-152.

[26] P. Kopcansky, N. Tomasovicova, M. Koneracka, et al. Phys Rev E.2008; 78: 011702.

[27] N. Podoliak, O. Buchnev, O. Buluy, G. DAlessandro, M. Kaczmarek, Y. Reznikov, T.J. Sluckin, Soft Matt. (2011);7:4742-4749.

[28] N. Tomasovicova, P. Kopcansky, N. Eber, Nova Science Pub Incorporated (2012).

[29] P. Kopcansky, N. L. Tomasovicov, M. Konerack, et al. IEEE Transactions on magnetics, 2011;47:4409-4412.

[30] E. Ouskova, O. Buluy, C. Blanc, H. Dietsch, A. Mertelj, Mol. Cryst. Liq. Cryst. 2010;525:104-111.

[31] G. Cordoyiannis, L.K. Kurihara et al., Phy Rev.E. (2009);79:011702

[32] L.M. Lopatina, J.V. Selinger, Phys Rev Lett, (2009);102:197802.

[33] S. Urban, B. Gestblom et al. Naturforsch. 1996; 51a:834-842.

[34] Khushboo, P. Sharma, P. Malik, et al. Phase Trans. 2015;89:144-154.

[35] A. Prasad, M.K. Das J. Phys. Cond. Mat. 2010;22:195106.

[36] T. Scharf Polarized Light in Liquid Crystals and Polymers. Hoboken, NJ: Wiley; 2007.

[37] J. L. West, G. Zhang , A. Glushchenko, et al. Appl Phys Letts. 2005;86:031111.

[38] T. Yoshida, A. Sugimoto et al. Liq. Cryst. 2015;45:463-472.

[39] J. Jadzyn, G. Czechowski, Liq. Cryst. 1989;4:157-163.

[40] A. Yoshizawa, Y. Kato et al. Soft Matt. 2015; DOI: 10.1039/C5SM02121A.

[41] M. K. Das, P. C. Barman, S. K. Sarkar Liq Cryst. 2016; DOI: 10.1080/ 02678292. 2016.1167262.

[42] K. S. Cole, R.H. Cole, J Chem Phys. 1941; 9: 98-105.

[43] F. Gouda, K. Skarp, S.T. Lagerwall. Ferro. 1991;113:165-206.

[44] M. Mishra, R. S. Dabrowski, R. Dhar et al. J Mol Liq. 2016; 213: 247-254.

[45] S. Urban et al. Liq Cryst. 2000;27:1675-1681.

[46] S. Mohyeddine, M. B. Pandey, D. Revannasiddaiah. Phas. Trans. 2009; 47: 12182.

[47] P. Yaduvanshi, A. Mishra, S. Kumar, et al. J Mol Liq. 2015; 208: 160-164.

[48] J. Jadzyn, G. Czechowsk. J. Phys. Condens. Matter. 2001;13:261–265.

[49] Khushboo, P. Sharma, P. Malik, et al. Liq Cryst. 2016;43:1671.

CHAPTER - 5

Nickel ferrites nanoparticles doped ferroelectric liquid crystal

Overview

In the present study, effect of nickel ferrite doping concentrations on electro-optic, dielectric and optical properties of FLC mixture were investigated and discussed. An improvement in spontaneous polarization, response time in nickel ferrite- FLC doped samples compared to FLC is observed and is explained on the basis of dipole moment and anchoring phenomena. The Goldstone mode (GM) is detected in all samples and follows a Debye-type relaxation behavior. A twofold increase in relaxation frequency for doped sample rather than pure sample has been observed. The bandgap was found more or less independent of doping concentration. The activation energy also decreases with increasing the amount of dopant.

5.1 Introduction:

Ferroelectric liquid crystals (FLCs) have received extensive interest owing to their distinctive properties and promising applications in optical antennas, spatial light modulators for optical storage, flat panel and switching displays. These materials have fast response time, low threshold voltage, better contrast ratio, wide viewing angle and memory [1-3]. Research in LC- nanoscience has received scientific curiosity in the field of self- assembled functional materials [4]. The interest in this area is due to the blend of two active field's namely Nano science and soft materials. The unique features of nanoparticles (NPs) e.g. anisotropic behavior and their thermal, electrical, magnetic properties, make them a suitable candidate to be used as guests for LCs. In recent years, the focus on understanding and investigations of NPs-induced effects in LCs on textures, phase transitions temperature, order parameter, dielectric responses and electro-optic properties have been thoroughly studied [5-10]. The main objective behind the investigation of NP-FLC hybrid systems is to study or alter/ modify the existing properties like switching time, spontaneous polarization, tilt angle, phase transition temperature, permittivity, conductivity etc. of FLCs. Dispersion of small amount of numerous type of NPs e.g. carbon nanotubes (single/ multiwalled) [11], ferroelectric ($BaTiO_3$) [9,12], metal (Au, Ag, Cu, Si), oxides (MgO, SiO_2, Y_2O_3, Ag, Pd, CdS, Au, Pt) [13-16], quantum dots (CdSe, CdTe, ZnO, ZnS) [17-19], graphene, in FLCs were studied by different research groups. Doping of these NPs does not induce much distortions in LC phases however modify or improve the response time, photoluminance properties, threshold voltage, contrast of LC devices, which may be beneficial in designing and fabrication of modern and advanced devices. The improvement in LC properties are governed not only on the doping of NPs, but also depends on shape, size, doping concentration, mutul interactions, anchoring energy, stability, purity and synthesis of NPs.

Soft magnetoelectric materials have received great scientific attention due to their fascinating properties and prospective applications [20]. A soft magnetoelectric material comprise a mixture of LC and MNPs and identified as *Ferrosmectic* (Dispersion *of fine ferromagnetic particles in smectics).* Firstly, Brochard and De Genes theoretically predict the idea of doping of fine magnetic particles into nematics but later experimentally established by Chen and Amer. [21,22]. Various MNPs, γ-Fe_2O_3, Fe_3O_4, Ni, Co-ferrite of different size, shape and coated with oleic acid, were

dispersed in FLCs mixtures and show a better transmittance, memory effect and improved electro- optical responses [23-29]. In the present work, dispersion of nickel ferrite NPs (NFNPs) in FLC is prepared and investigated. The effect of doping concentration on the polarization, switching time, viscosity and anchoring energy coefficient's varying phase of FLC are discussed. The effect of doping concentration on the dielectric and optical properties of FLC is also discussed.

5.2 Experimental

Materials

A FLC mixture, W206E of phase sequence SmC* - 86.6^{o}C – SmA – 92.5^{o}C - N* - 97.6^{o}C – Iso, was used. NFNPs were synthesized in our laboratory and details of the synthesis are given in chapter 3.

Preparation of NFNPs/ W206E mixtures

In this work, three doped samples were prepared by dispersion varyig amounts (0.12, 0.25, 0.5 wt. %.) of NFNPs into W206E mixture. Initially, few drops of oleic acid as a surfactant was added into NFNPs followed by ultrasonification. After that, these NFNPs were added into W206E and then ultrasonification was carried out for 1 hour to avoid the formation of an agglomeration. The prepared mixtures of NFNPs and W206E were kept at room tempearture for 24-36 hours to evaporate the surfactant.

Liquid crystal cell fabrication and measurements

Planar aligned LC cells (Instec, USA) made of highly transparent indium tin oxide (ITO) coated glass substrates of cell gap 5.0 μm & active area 0.5×0.5 cm^2 were used. The prepared mixture (W206-NFNPs) was introduced into an empty space of LC cell by capillary action at a slightly higher temperature than isotropic temperature of W206E. A pure sample (undoped) consisting of the same FLC mixture (W206E) and similar cell configuration was also prepared and studied. These filled LC cells were placed in hot stage and studied. The micro-textures and phase transition temperatures were observed through polarizing microscope at a magnification of 10x. The output responses through undoped and doped LC cells were recorded on a digital storage oscilloscope. Dielectric investigations were also carried out by an impedance analyzer in the frequency range of 20Hz-10MHz. The dielectric results were corrected after subtracting the low- and high-frequency correction data from the experimental data. For this, cells were calibrated with air and benzene as standard solvents. The optical band gap was measured by UV-visible spectrometer in the wavelength range of 200-

550 nm at room temperature.

5.3 Results and Discussion

5.3.1 *Electro-optic measurement*

The electro-optic properties were studied by field reversal technique and details are discussed in Chapter 3 [8].

Figure 5.1 show the temperature dependence on spontaneous polarization at an applied voltage of 30V (frequency~ 200 Hz) in SmC* phase. It is found that P_s decreases with increasing the temperature in all samples and have minimum value near the SmC*- SmA transition temperature and also follows a first- order phase transition behaviour. The value of P_s at 30 ^oC for pure FLC is found to be 18 nC/cm^2, which reduced to 12.2 nC/cm^2 for 0.5% NFNPs-doped sample, respectively. The temperature dependence behaviour with P_s was fitted using the relationship

$$P_s(T) = P_o(T_c - T)^{\beta} \qquad T < T_c \qquad (5.1)$$

Here, β is critical exponent and its value is 0.5. P_o is constant. T_c is the SmC*- SmA transition temperature. The fitted parameters (P_o, β) as calculated from Equation (5.1) are given in Table 5.1.

Table 5.1

Fitted parameters as a function of NFNPs doping concentration

Samples	***P_o***	β
FLC	7.213	0.231
FLC + 0.12	4.388	0.314
FLC + 0.25	4.105	0.311
FLC + 0.5	3.285	0.316

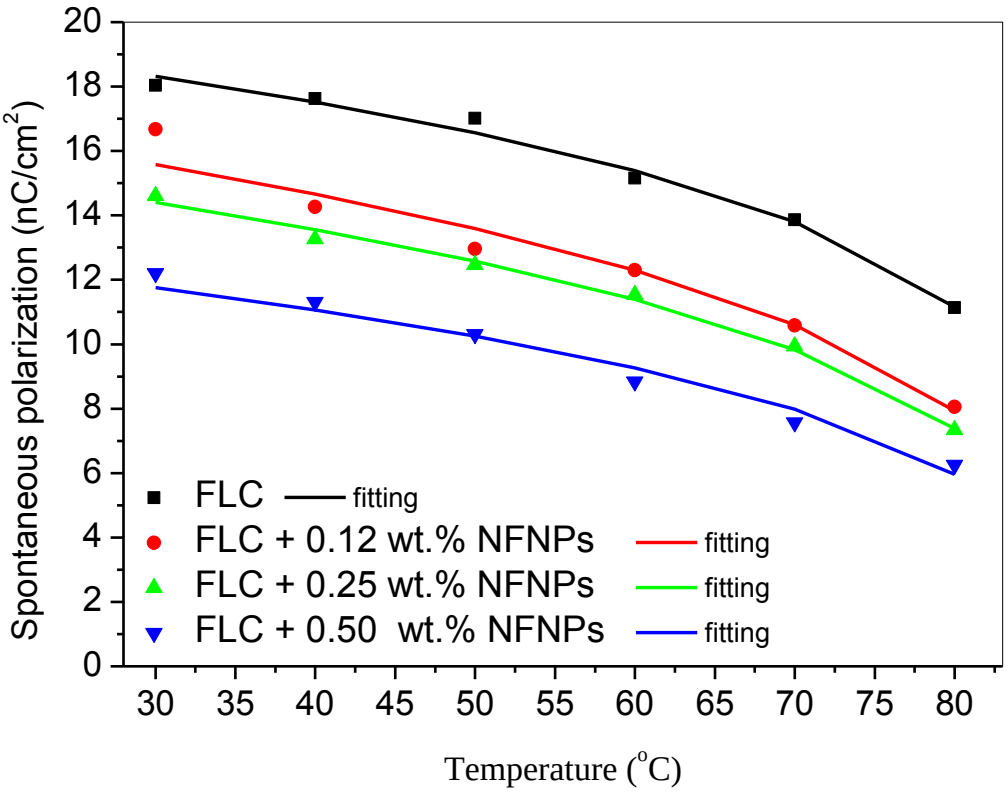

Figure 5.1. Temperature dependence of spontaneous polarization at 30V in SmC* phase.

The response time (τ_s), which is defined as the time taken by the molecules between two stable states (ON to OFF), has been evaluated using the relationship

$$\gamma = (P_s.E.\tau_s) \qquad (5.2)$$

The behavior of τ_s with temperature at 30 V square wave for different NPs concentration-based samples is shown in Figure 5.2. Figure 5.2 shows that τ_s decrease in all samples on increasing the temperature. The observed response time for pure FLC is 478 µsec and decreases to 166 µsec in 0.5 wt. % NFNPs -doped FLC sample. It implies an improvement in response time with doping of NFNPs into FLC. The rotational viscosity, which is an important property of FLC and related to the rotation of molecule about the SmC* cone, has been calculated using Equation (5.2). The temperature dependence behaviour of γ at 5 V/µm is illustrated in Figure 5.3. A decrease in γ after doping NFNPS is also seen.

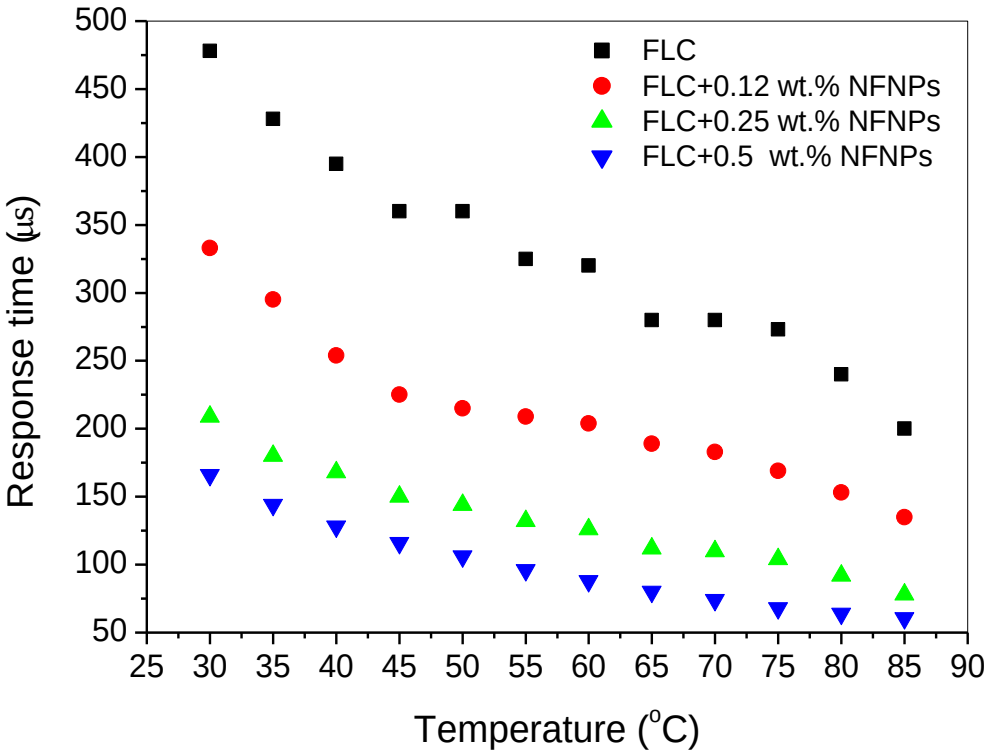

Figure 5.2 Temperature dependence of response time for FLC and NFNPs doped FLC samples at square wave (30V)

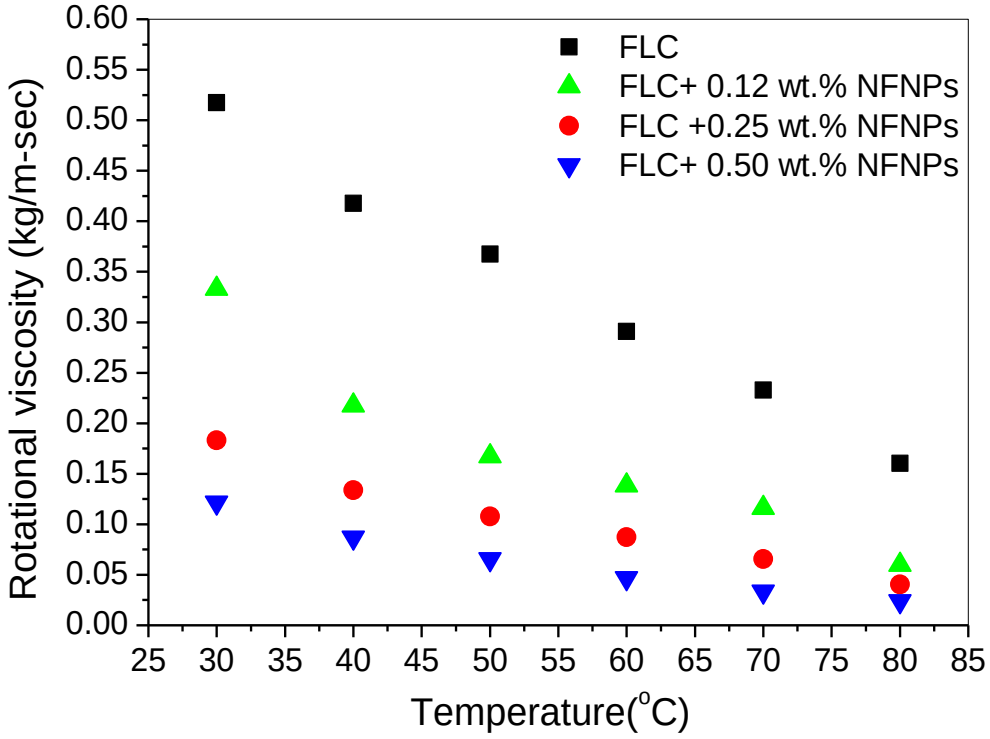

Figure 5.3 Temperature dependence of rotational viscosity for FLC and NFNPS doped FLC samples.

A decrease in electro- optic parameters P_s, τ_s and γ at different concentrations of NFNPs has been discussed on basis of (i) dipole- dipole interactions (ii) FLC molecular arrangement after dispersion (iii) anchoring phenomena. For geometrical point of view, it is assumed that NFNPs misfit between FLC molecules and smectic layers in such a way that added NPs perturbs the molecular arrangement of FLC and as a consequence modifies the FLC order. The change in molecular arrangement of FLC also decreases a tilt angle and results a low magnitude of P_s ($P_s \propto$ tilt angle) than pure FLC (undoped sample).

The other probable cause of reduction in P_s value is due to the decrease in the net effective dipole-moment. Here in doped sample, the FLC and NFNPs dipole-moments are just anti-parallel to each other and overall effective dipole-moment/volume decreases to some extent [30]. Besides these anti-parallel dipole-dipole interactions, screening of the polarization by external charges may also be accountable for the decrease in P_s [31]. The combined effects of P_s and viscosity decrease the response time in doped samples. The decrease in physical parameters of FLC after dispersion of quantum dots NPs [32], CdTe quantum dots in LAHS 19 [33], ZnO nanorods in Felix 17100 [34] gold nanorods in phenylpyrimidines based FLC [35] was also reported by several research groups. The alteration in smectic layer ordering produced by addition of NPs (spherical) was also described by Pratibha et al. [36].

5.3.2 Anchoring energy

The anchoring energy (F) has been calculated, which consist of polarization and dispersion contributions and can be expressed as

$$F = \int_s (\bar{W}_D + \bar{W}_P)\, dn \qquad (5.3)$$

where

$\bar{W}_D = -W_D(P_s\, n)^2 \qquad \& \; \bar{W}_P = -W_P(P_s\, n)$

Here W_D and W_P are the dispersion and polarization anchoring energy coefficient's, respectively. The polarization anchoring is due to the electrostatic forces between the dipole moments of the surface and LC molecules and dispersion anchoring is related to the non-electrostatic portion of the interaction between the surface and LC. n is layer normal. W_D and W_P can be measured using the following equations [37-38]

$$W_D = \frac{\gamma d}{4\tau} \qquad 5.3(a)$$

$$W_P = \sqrt{P_s W_D}^{1/2} \qquad 5.3(b)$$

A typical dispersion and polarization energy coefficients behavior with temperature is plotted in Figure 5.4 (a, b). It is seen that both W_P and W_D decrease on increasing the temperature and NFNPs concentrations. At 30° C, W_D decreases from 13.6×10^{-4} J/m^2 to 9.15×10^{-4} J/m^2 and W_P varies from 25.7×10^{-6} J/m^2 to 19.2×10^{-6} J/m^2 at 0 and 0.5% NFNPs, respectively. A concentration dependence of W_D and W_P is also shown in Figure 5.4(c). The decrease in anchoring energy behaviour with NFNPs concentration supports the reduction in viscosity for doped samples compared with pure samples. The decrease in anchoring energy with NFNPs doping means lower threshold voltage ($E_{th} = \frac{\sqrt{W_D}}{K} = \frac{W_P^2}{KP_s}$) is required to switch the FLC molecules between OFF and ON states. The decreasing nature of W_D and W_P with temperature also indicate that enthalpy of molecule continuously increased with temperature and thus broke their interaction barrier [38].

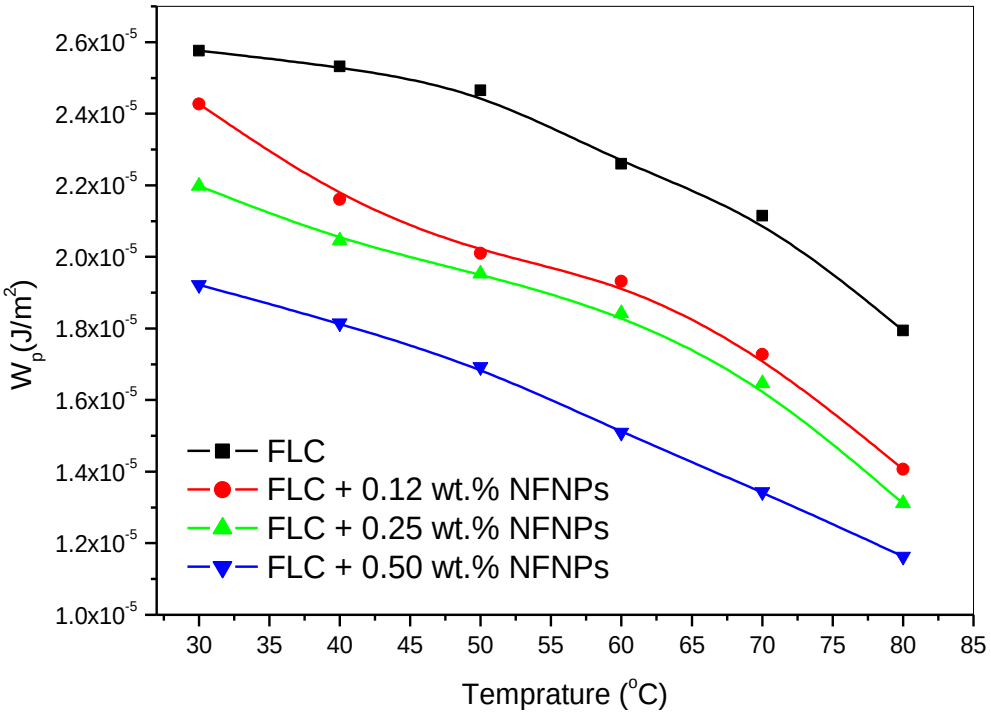

(a)

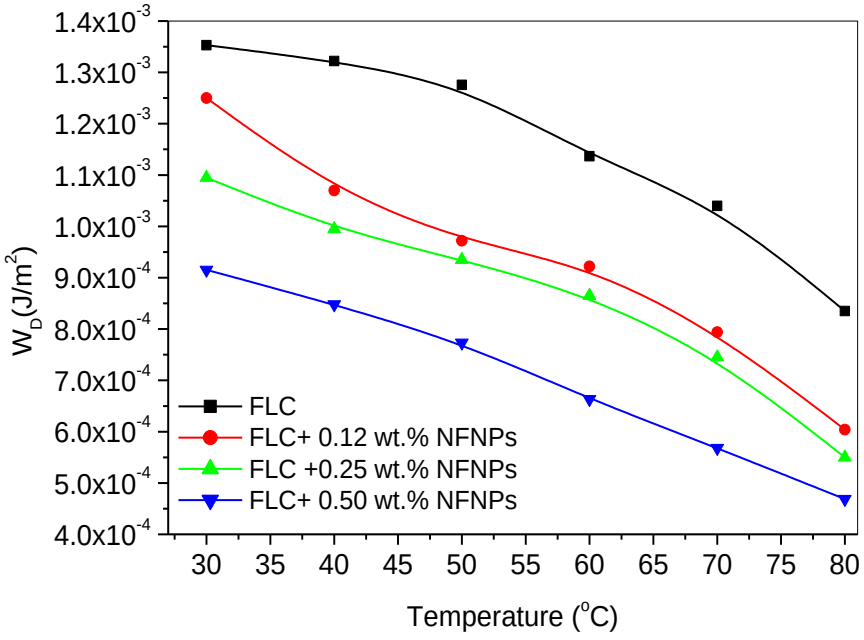

(b)

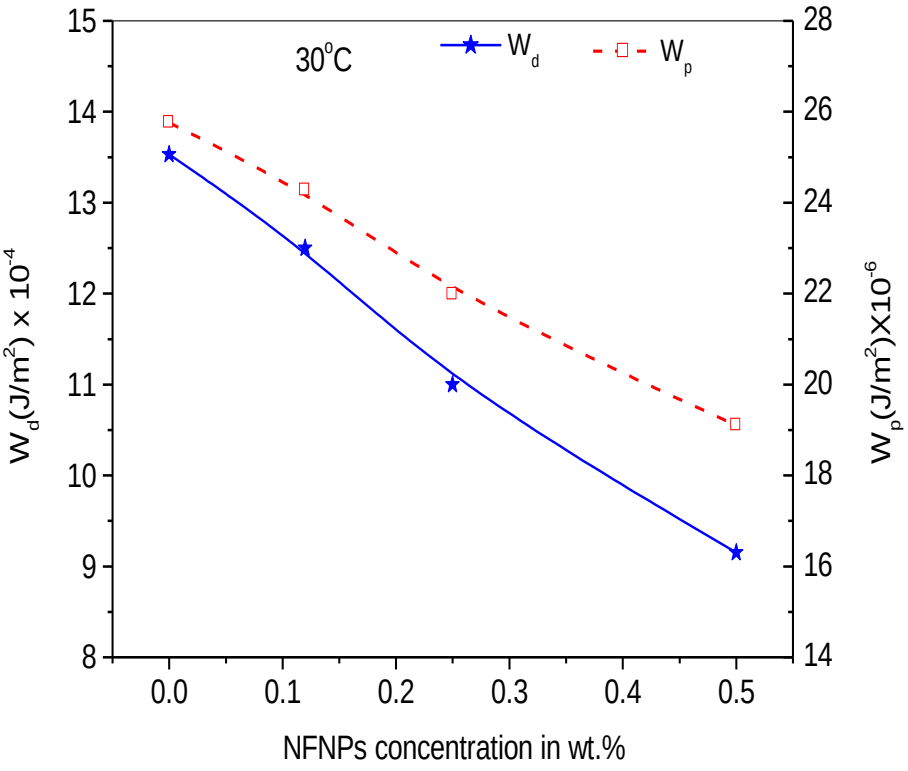

(c)

Figure 5.4 Temperature dependence of (a) anchoring energy coefficient's (b) dispersion energy coefficient's for pure and doped sample; (c) NFNPs concentration dependence on anchoring and dispersion energy at 30°C.

5.3.3 Dielectric studies

Generally in FLCs, during molecular processes two modes namely Goldstone mode (GM) which arises due to the azimuthal angle fluctuations in SmC* phase and Soft mode (SM) which is related to fluctuation of molecules in the tilt direction angle. Due to relatively small amplitude, SM occurs in the close vicinity of SmA*- SmC* phase transition. Usually GM is found in SmC* phase of relaxation frequency < 1 kHz. The dielectric relaxation spectrum can be described with the help of the following generalized Cole– Cole equation as [39].

$$\varepsilon^* = \varepsilon'(\infty) + \sum \frac{\delta\varepsilon}{1+(j\omega\tau)^{(1-\alpha)}} + \frac{A}{\omega^n} - j\frac{\sigma_{ion}}{\varepsilon_0\omega^k} - jB\omega^m \tag{5.4}$$

The real (ε') and imaginary part (ε'') of equation (5.4) can be written as

$$\varepsilon' = \varepsilon'(\infty) + \sum \frac{\delta\varepsilon[1+(\omega\tau)^{(1-\alpha)}\sin(\alpha\pi/2)]}{1+(\omega\tau)^{2(1-\alpha)}+2(\omega\tau)^{(1-\alpha)}\sin(\alpha\pi/2)} + \frac{A}{\omega^n} \tag{5.4.1}$$

$$\varepsilon'' = \sum \frac{\delta\varepsilon(\omega\tau)^{(1-\alpha)}\cos(\alpha\pi/2)}{1+(\omega\tau)^{2(1-\alpha)}+2(\omega\tau)^{(1-\alpha)}\sin(\alpha\pi/2)} + \frac{\sigma_{ion}}{\varepsilon_0\omega^k} + B\omega^m \tag{5.4.2}$$

Where, $\varepsilon_0, \varepsilon_\infty$ are the low and high frequency limiting values of dielectric permittivity, $\delta\varepsilon$, α (0 < α < 1) represents the dielectric strength and distribution parameter respectively. The third and fourth terms in equation 5.4, represent the contribution due to electrode polarization capacitance and ionic conductivity at low frequencies. The measured dielectric absorption contains a contribution above 100 kHz due to finite resistance of electrodes and lead inductance. Therefore, an additional imaginary term ($B\omega^m$) is included in equation 5.4 in order to partially to account for high frequency effect. The fitting parameters *A*, *B*, *m*, *n* and *k* are defined earlier. The frequency dependence behaviour of dielectric permittivity at 30^{o}C in the pure and doped samples is shown in Figure 5.5. Figure 5.5(a) shows that primarily a considerable decrease in permittivity (ε') was observed in doped samples and such a decreasing behavior in permittivity on increasing the frequency is up to 1 kHz. However, beyond 1 kHz almost no significant change in permittivity is seen. A similar type of behaviour in the imaginary part of permittivity (ε'') on increasing the doping concentration is also noticed [Figure 5.5(b)]. A single relaxation peak occurs at ~ 200 Hz in pure FLC sample slightly shifted to the high-frequency side at ~ 400 -500 Hz. Cole-Cole plots extracted from permittivity for pure and doped samples at 30^{o}C are presented in Figure 5.6. A single relaxation mode in cole-cole plots reveal a Goldstone mode (GM)

in the SmC* phase. The distribution parameter (α) was also obtained in the range of 0.23-0.28 < 0.5, which suggests a Debye-type relaxation [40].

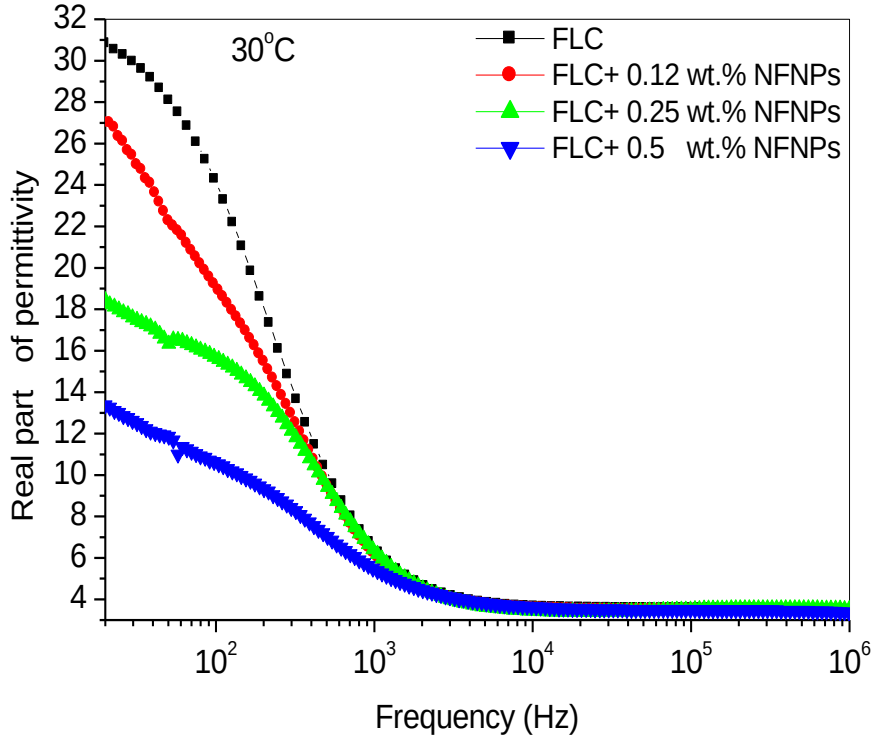

(a)

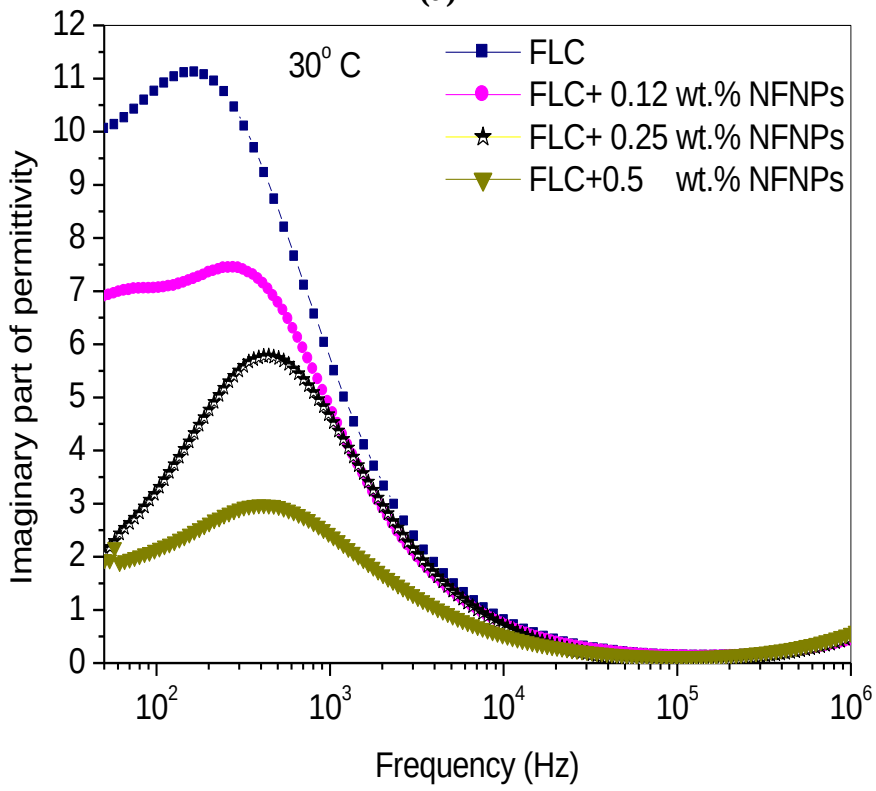

(b)

Figure 5.5 Frequency dependence of dielectric permittivity at 30°C (a) real part of permittivity (b) imaginary part of permittivity for pure FLC and doped samples.

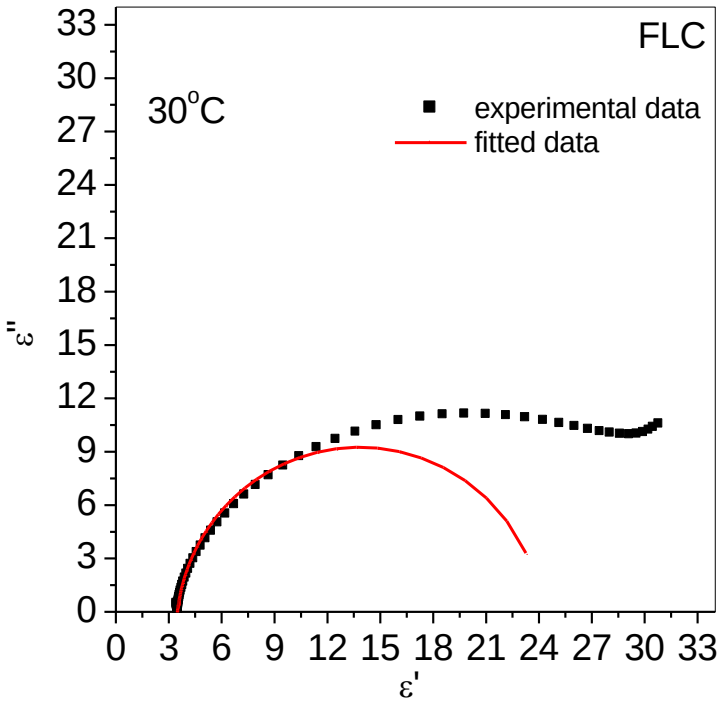
FLC
30°C
experimental data
fitted data
ε"
ε'
0 3 6 9 12 15 18 21 24 27 30 33

(a)

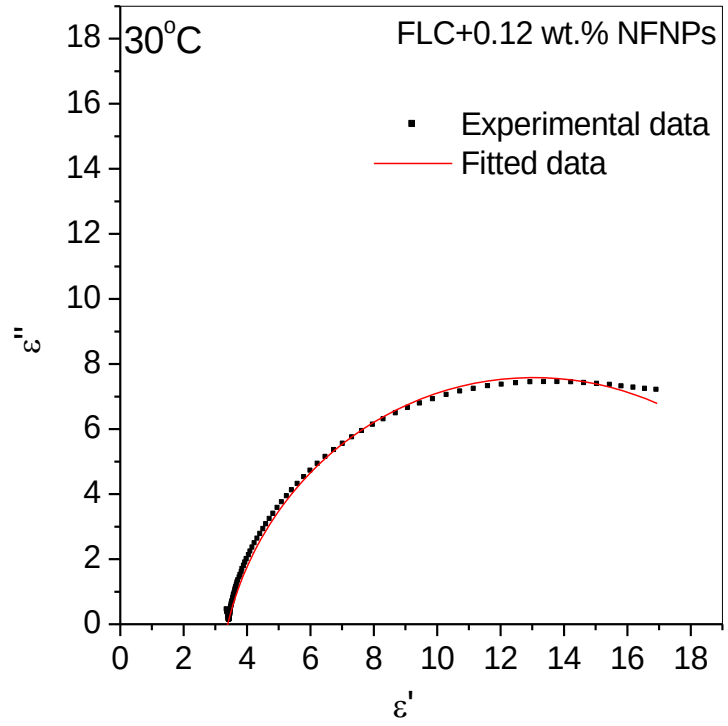
30°C
FLC+0.12 wt.% NFNPs
Experimental data
Fitted data
ε"
ε'
0 2 4 6 8 10 12 14 16 18

(b)

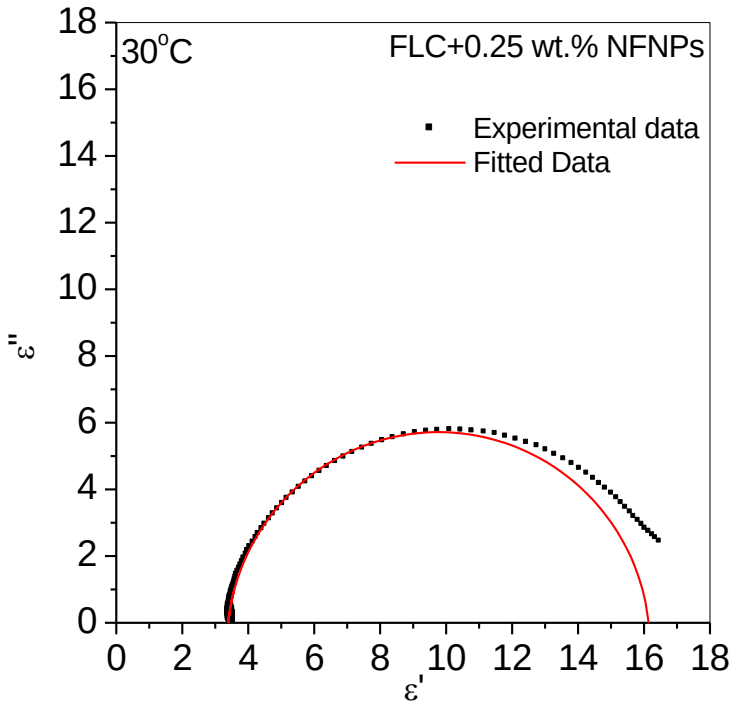

(c)

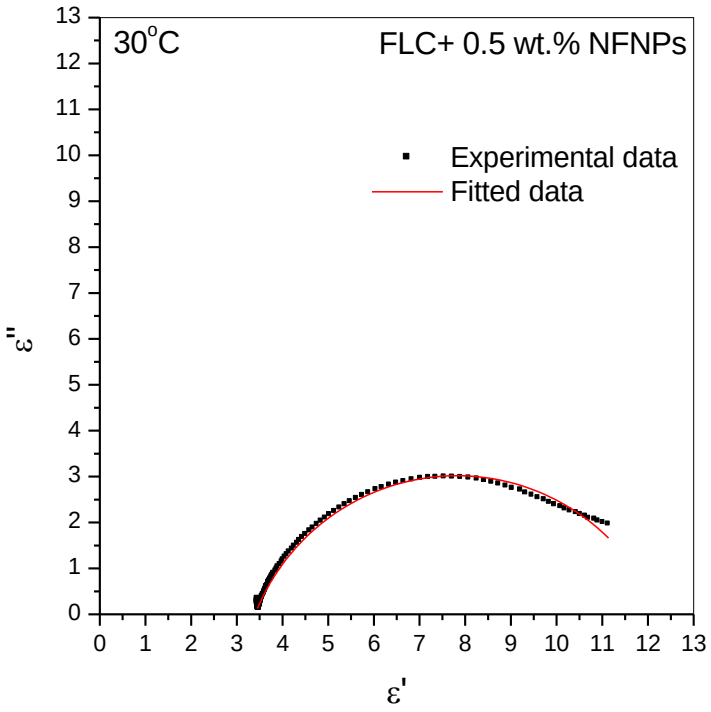

(d)

Figure 5.6. Cole-Cole plots at 30°C for (a) FLC, (b) 0.12 % (c) 0.25 %, and (d) 0.5 %, NFNPs doped samples, here redline show fitted data and square black symbol show- experimental data.

Temperature dependence of dielectric permittivity at 566 Hz is presented in Figure 5.7. Initially, ε' more or less increases in SmC* phase and decrease to low value as temperature approaches towards SmC*- SmA transition. A slight decrease (~5^{o}C) in SmC*-SmA transition temperature in doped samples over pure FLC has been observed. Probably, this decrease in transition temperature is due to the NP doping into FLC mixture, which may modify the order of FLC molecules. A decrease in permittivity (ε'') for the doped samples (Figure 5.7(b)) also indicates that losses are reduced to some extent after doping.

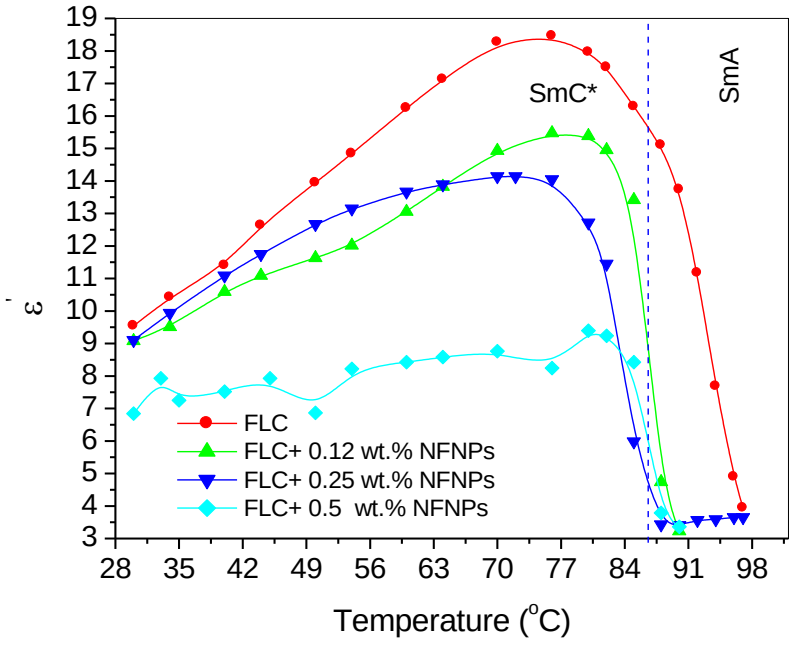

(a)

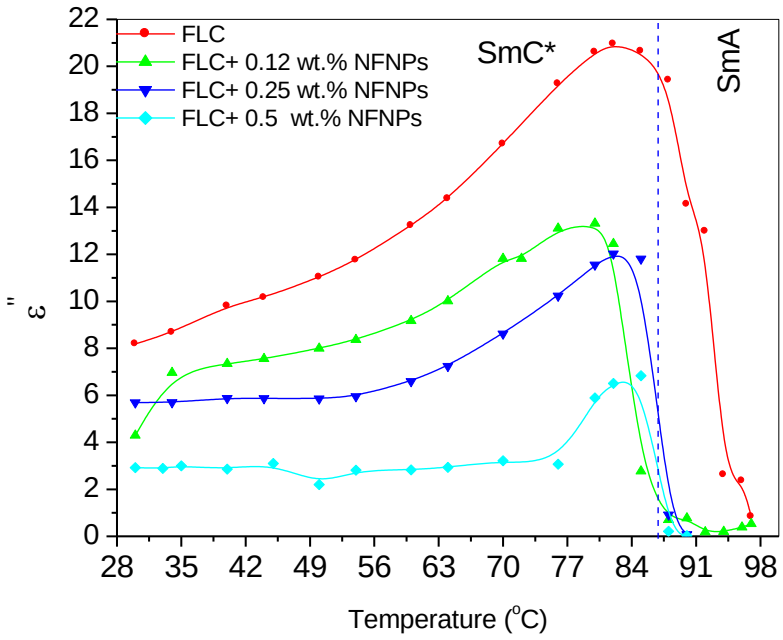

(b)

Figure 5.7. Temperature dependence of dielectric permittivity at a frequency of 566 Hz real part of permittivity (b) imaginary part of permittivity for pure FLC and doped samples

The relaxation frequency (f_r) measured for pure and doped samples is represented in Figure 5.8. It is clearly seen that f_r increases in SmC* phase and decreases near the SmC*- SmA transition temperature. This behavior may be explained using Landau free energy expression:

$$f_r = \frac{K_{33}q^2}{2\pi\gamma} \tag{5.5}$$

$$\Delta\epsilon_{GM} = \frac{P_S^2}{2\varepsilon_0 K_{33} q^2 \theta^2} \tag{5.6}$$

where K_{33} is the elastic constant and q is the wave vector corresponding to helical pitch of material. It can be seen from Equation (5.5) and (5.6) that f_r depends on γ, whereas $\Delta\epsilon_{GM}$ varies withP_s, q, θ and K_{33}. It is found that f_r increases on increasing the doping amount and temperature in SmC* phase; however f_r starts decreasing near the SmC*- SmA transition temperature. The value of f_r is found to be from 234 Hz-516 Hz and supports the GM relaxation frequency. This decrease in f_r near the transition temperature may be attributed to the change in order parameter on inclusion of NFNPs.

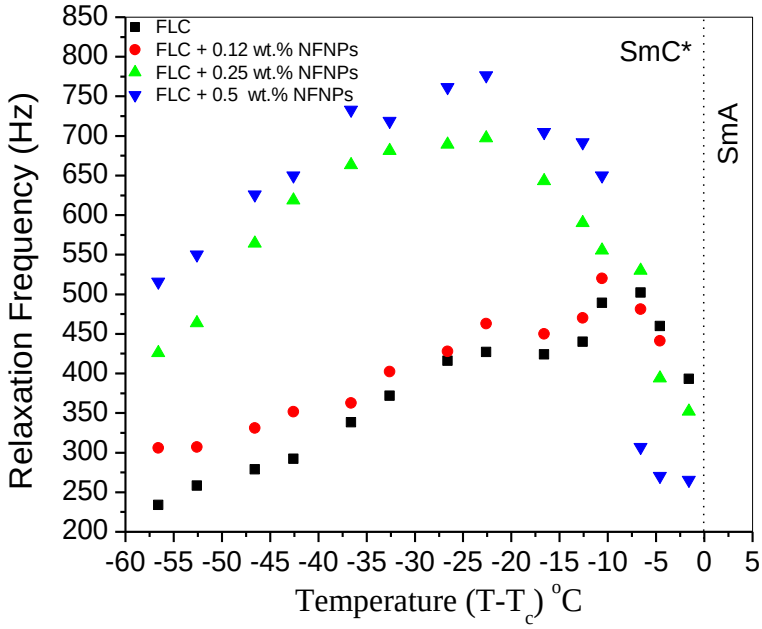

Figure 5.8. Temperature dependence of relaxation frequency in SmC* phase for FLC and NFNPs doped samples.

The temperature dependence on dielectric strength ($\Delta\epsilon_{GM} = (\varepsilon_0 - \varepsilon_\infty)$) at different doping concentrations is shown in Figure 5.9. Almost one-third decrease in $\Delta\epsilon_{GM}$ value was noticed on increasing the NFNPs concentration in FLC. A rise in $\Delta\epsilon_{GM}$ on increasing the temperature is also seen in SmC* phase, which decreases to a considerable low value near SmC*-SmA interface.

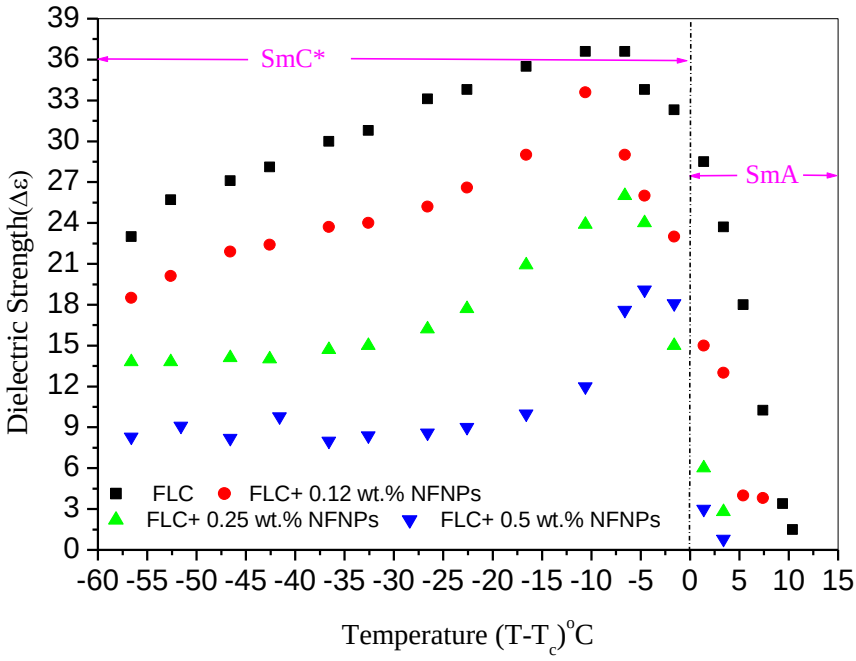

Figure 5.9. Temperature dependence on goldstone mode dielectric strength in pure FLC and NFNPs doped samples

The activation energy (E_a) for the pure and doped samples was evaluated using the Arrhenius equation:

$$Logf_r = Logf_o - \frac{E_a}{RT} \quad (5.7)$$

where E_a is the activation energy, R is the Gas constant (8.134 J/mole-K) and T is the absolute temperature. E_a was obtained by calculating a slope of straight line between the inverse of T versus$Logf_r$. The slope was measured using the least square fit method. The inverse of T with $Logf_r$ behavior as shown in Figure 5.10 depicts that E_a is found to be 5.41 kJ/mole for pure FLC and 4.25 kJ/mole, 5.36 kJ/mole, 4.42 kJ/mole for 0.12 wt. %, 0.25 wt. % and 0.5 wt. % NFNPs doped FLC samples, respectively.

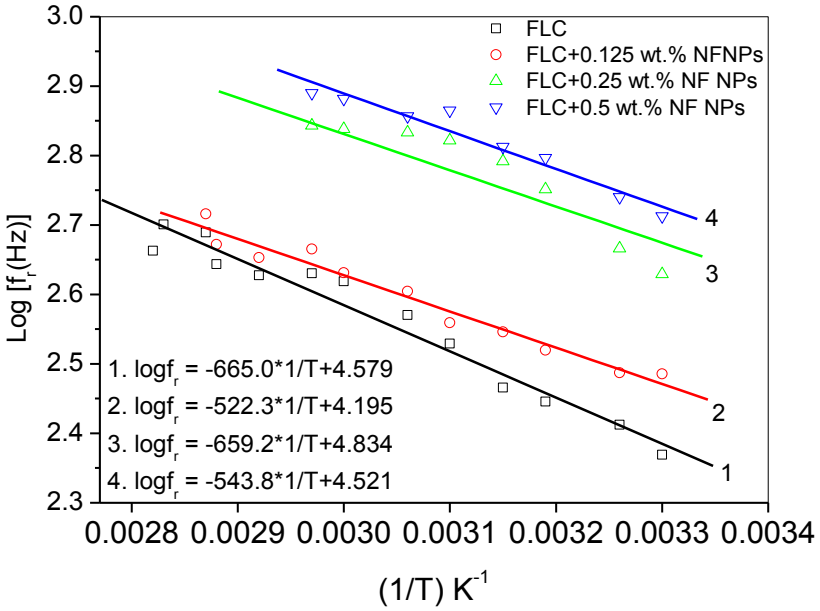

Figure 5.10. Variation of relaxation frequency (logarithm) with inverse of absolute temperature showing Arrhenius behavior of observed mode.

5.3.4 UV-Vis Studies

The UV-visible absorption spectra for pure and NFNPs doped FLC samples are shown in Figure 5.11. In Figure 5.11 a single peak was observed in the visible spectrum at 290 nm, 301 nm, 317 nm and 319 nm for pure and doped samples. The absorbance spectrum was shifted slightly towards the higher wavelength side with

increasing the NFNPs. The optical band gap (E_g) has been calculated by the Tauc relationship [41]. The details are discussed in Chapter 4. Here E_g was found to be 3.78, 3.58, 3.84 and 3.66 eV for pure and doped samples, respectively. The effect of doping concentration on FLC properties is summarized in Table 5.2.

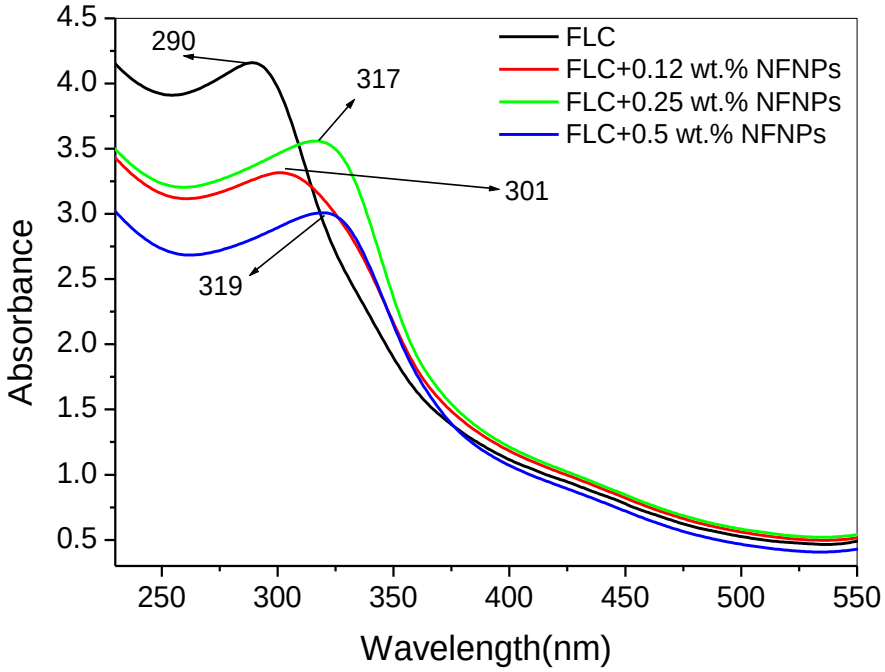

Figure 5.11. UV-Vis spectra of pure and doped samples

5.3.5 Magnetic behaviour

The effect of applied magnetic field on the magnetic properties i.e. magnetization value was studied using VSM. It is seen that NFNPs show a typical hysteresis behaviour as shown in Figure 3.6. It is worthmenthing here that doping of NFNPs has not effect on magnetization values.

Table 5.2

Physical parameters of the pure and doped samples.

Sample (FLC+NFNPs)	Ps (nC/cm^2)	τ_s (μs)	γ (kg/ms)	α	$\Delta\varepsilon_{GM}$	f_r (Hz)	E_a (kJ/mole)	E_g (eV)
FLC + 0.0	18.0	478	0.52	0.26	25.4	234±10	5.41	3.78
FLC + 0.12	16.6	333	0.33	0.23	18.7	306±10	4.25	3.58
FLC + 0.25	14.6	209	0.18	0.28	14.2	426±10	5.36	3.84
FLC + 0.50	12.2	166	0.12	0.25	8.3	516±10	4.42	3.66

References

[1] P Malik, K K Raina, A Bubnovb, et al. Phase Trans. 2006;79:889-898.

[2] P Malik, K K Raina, A K Gathania. Thin Sol. Film. 2010;519:1047-1051.

[3] J. P. F. Lagerwall, G. Scalia. Curr Appl Phys. 2012;12:1387-1412.

[4] O. Stamatoiu, et al.Topics in Curr Chem. 2012; 318:331-394.

[5] T. Joshi, A. Kumar, J. Prakash, et al. Liq Cryst. 2010;37:1433-1438.

[6] P. Malik, A. Chaudhary, R. Mehra, et al. Mol Cryst Liq Cryst. 2011;541:243-251.

[7] H. Duran, B. Gazdecki, A. Yamashita, T. Kyu. Liq Cryst. 2005;32:815-821.

[8] A. Chaudhary, P. Malik, R. Mehra, et al. J Mol Liq. 2013;188:230-236.

[9] E. Ouskova, O. Buchnev, V. Reshetnyak, et al. Liq Cryst. 2003; 30:1235-1239.

[10] M.S. Zakerhamidi, S. Shoarinejad, S. Mohammadpour. J Mol Liq. 2014;191:16-19.

[11] R. K. Shukla, K. K. Raina, V. Hamplová, et al. Phase Trans. 2011;84:850-857.

[12] P. Kumar, A. Sinha. Phase Trans. 2015;88:605-620.

[13] A. Kumar, G. Singh, T. Joshi, et al. Appl Phys Lett. 2012;100:054102.

[14] Y. Garbovskiy, I. Glushchenkko. Liq Cryst. 2015;5:501-533.

[15] A. Chandran, J. Prakash, K. K. Naik, et al. J Mat Chem C. 2014; 2: 1844-1853.

[16] A. Chaudhary, P. Malik, R. Mehra, et al. Phase Trans. 2012;85(3):244-254.

[17] D. P. Singh, S. K. Gupta, S. Pandey, et al. Liq Cryst. 2015,42:1159-1168.

[18] D. P. Singh, S. Pandey, Jour Lum. 2016;173:250-256.

[19] N. Topnani, V. Hamplova, M. Kaspar, et al. Liq Cryst. 2014;41:91-100.

[20] V. Novotna, J. Vejpravova, V. Hamplova,et al. RSC Adv. 2013;3:1091910926.

[21] F. Brochard, P. G. J. De. Gennes of Phys. 1970;31:691-708.

[22] S. H. Chen, N. M. Amer. Phys Rev Lett. 1983;51:2298.

[23] P. Ganguly, A. Kumar, K. Muralidhar, et al. App Phys Lett. 2016; 108:182905.

[24] Neeraj, K. K. Raina. Opt Mat. 2013**;**35:531-535.

[25] P. Goel, G. Singh, R. P. Pant, A. M. Biradar. Liq Cryst. 2012;39:927-932.

[26] V. Gdovinova, N. Tomasovicova, N. Eber, et al. Liq Cryst. 2014;41(12):1773-1777.

[27] E. V. Popova, S. A. Gamzaeva, A. I. Krivoshey, et al. Liq Cryst. 2015; 42(3): 334-343.

[28] G. Cordoyiannis, S. Gyergyek, B. Rozic, et al. Liq Cryst. 2016; 43(3): 314-319.

[29] Khushboo, P. Sharma, P. Malik, et al. Phase Trans. 2015;89:144-154.

[30] A. Mikulko, P. Arora, A. Glushchenko, et al. Europhys Lett. 2009; 87: 27009.

[31] R. K. Shukla, Liebig C M, Evans D R, et al. RSC Adv. 2014;4:18529-18536.

[32] S. Pandey, T. Vimal, D. P. Singh et al. J Mol Liq. 2015; 211: 157-163.

[33] A. Kumar, A. M. Biradar. Phys Rev E. 2011; 83: 041708.

[34] R. Manohar, A. K. Srivastava, P. K. Tripathi, et al. J Mat Sci. 2011;46:5969-5976.

[35] R. K. Shukla, X. Feng, S. Umadevi, et al. Chem Phy Lett. 2014;599:80-85.

[36] R. Pratibha, W. Park, I. I. Samlyukh. J Appl Phys. 2010; 107: 063511.

[37] A. K. Mishra, A. K. Srivastava, J. P. Shukla, et al. Phys Scr. 2008;78:065602.

[38] F. J. Lyuu, C. C. Chen, J. Y. Lee. Mol Cryst Liq Cryst. 1999;329:99-112.

[39] K. S. Cole, R. H. Cole. J Chem Phys. 1941**;** 9: 98- 105.

[40] M. Maeda, H. Kihara, A. Makino, et al. J. Appl. Phys. 1998; 37: 6465**–** 6471.

[41] P. Yaduvanshi, A. Mishra, S. Kumar, et al. J Mol Liq. 2015;208:160-164.

Chapter - 6

Nickel nanoparticle doped ferroelectric liquid crystal

Overview

In the present study, ferromagnetic (nickel) nanoparticles (NPs) of size (~ 20 nm, 40 nm) into ferroelectric liquid crystal (FLC) mixture were dispersed and investigated in planar cell. Effect of size of nickel NPs on the electro-optic, dielectric and optical properties of FLC mixture have been studied and discussed. A minor improvement in spontaneous polarization, rotational viscosity and faster response time in NiNPs/ FLC dispersed samples than pure FLC is observed. A Goldstone mode of relaxation frequency ~100 Hz is detected in all samples and follow a Debye type relaxation behavior. In addition, it is observed that size of NiNPs does not have any remarkable effect on spontaneous polarisation, relaxation frequency and dielectric strength. A single relaxation peak at 363, 362 Hz is also noticed in pure FLC and NiNPs/ FLC samples.

6.1. Introduction

Ferroelectric liquid crystals (FLCs), a special class of liquid crystals have been a subject of intense research due to its promising applications in fast respond electro-optic (EO) devices. Compared to NLCs that are widely used for LC-based devices, FLCs show faster switching time (μsec), low threshold voltage, better contrast ratio, wider view angle and memory effect [1-4]. In spite of its remarkable features, researchers have synthesize new FLCs mixtures which possess enriched intrinsic physical properties. Indeed, these new synthesized functional materials have great potential and practical applications in displays, photonics, and spatial light modulators. Synthesis of FLC mixture with desired characteristic is not so easy and always a challenge due to its complexity arises during synthesis process. Therefore, to enhance the LC physical properties of desired applications, continuous efforts have been made by several researchers.

In the past decade, a quantum of research work is focused on nanoparticles – ferroelectric liquid crystal composites. In this context, several type of NPs (for instance silica, zinc oxide, multiwall carbon nanotubes, single wall carbon nanotubes, ferroelectric, gold (both spherical and rod-like particles), capped with different organic layers, quantum dots, oxides) were investigated in FLCs and found exciting results [5-11].

Out of several kind of nanostructured materials used as dopants in FLC, *ferrosmectics* has created scientific curiosity due to the orientation coupling between MNPs and FLC director and notable response to magnetic fields. A number of MNPs ($\gamma - Fe_2O_3$, spherical shaped Fe_3O_4 (average diameter ~10 nm), iron oxide, nickel, cobalt, nickel ferrite) were doped in different FLCs mixtures and studied their electro-optical, electrical, optical properties [12-17]. Various research groups observed a substantial change or improvement in LCs properties and produce reasonable NP-LC theories. The enhancement in these properties depends on number of factors such as concentration of dopant, synthesis method of NPs, nanoparticle surface conditions, thermal and chemical stability, mutual interaction between NPs and LCs, shape and size of NPs. It has been observed that to improve the LC properties, NPs should not much disturb the FLC layer spacing and LC director. To confirm the same, low concentration (< 1%) and small size (≤ 10-50 nm) are the two main prerequisite of NPs to be used as guest in LCs. Mostly high concentration of NPs distracts the order

of LC molecules and form aggregates of NPs.

In a recent work, reported by A. Ruzdzki *et al.* have studied that harvested barium titanate ($BaTiO_3$) NPs of particle size 9, 15, 26 nm affect the electro-optic properties of FLC mixture [18]. Almost negligible change in phase transition temperature and tilt angle was detected after dispersion of $BaTiO_3$, however a decrease in electro-optic parameters in doped sample were observed than pure FLC mixture. i.e. (P_s , τ in doped sample) $_{9nm\ size}$ < (P_s , τ in doped sample $_{26\ nm\ size}$) < (P_s, and τ in pure FLC mixture).

Two different sizes (5-10 and 50-60 nm) of $BaTiO_3$ NPs were also dispersed in another FLC mixture ($6F_6T$) and observed that size of NPs also improve the electro-optic and dielectric properties of FLC [19]. R. K. Shukla *et al.* also consider the different sizes (1.77 and 5.5 nm) of gold NPs doped FLC mixture on clearing temperature, switching, polarisation and dielectric parameters [20]. As far as literature is concerned, the effect of different size of ferromagnetic NPs in FLC mixture is rarely studied.

In this chapter, effect of size of nickel NPs dispersion on the electro-optic, dielectric and optical properties of multicomponent FLC mixture are investigated and discussed.

6.2 Experimental

A multi-component FLC mixture, ZLI-4851-000 of phase sequence;

Cryst. $\xrightarrow{-10^oC}$ SmC* $\xrightarrow{64^oC}$ SmA $\xrightarrow{70^oC}$ N* $\xrightarrow{74^oC}$ Isotropic was used. This FLC has wide chiral (SmC*) phase. The other properties of FLC is also shown in Table 3.1. NiNPs of sizes (~ 20, 40 nm) were purchased from M/s Sigma-Aldrich. For TEM analysis, small amount of Ni were dissolved in ethanol and then ultrasonication was done for about 30 minutes. A drop of this solution containing NiNPs was put on carbon coated grid (400 mesh) for study. The size, shape and morphology of NiNPs were confirmed using TEM. Microscopy shows that NiNPs are of spherical shape of average size 20 and 40 nm. The magnetic properties of NiNPs were also measured and found a saturation magnetization of 1.35 emg/gm at a magnetic field of ~ 8800 Oe as shown in Figure 3.3.

Preparation of NiNPs dispersed FLC mixtures

The surface properties of doped NPs are very crucial for the manifestation of a well dispersed medium. The purpose of surface modification of NPs is mainly to achieve long-term stability, minimize the effect of NPs aggregation in the host (LC) medium

and to smoothen director distortions around NPs, thus reducing the cost of elastic energy. Among other surfactants like oleic acid, selenium docosane and dodecylbenzenesulphonic acid are widely used for surface modification of NPs. It is imperative to note here that oleic acid show best results to prevent the NPs aggregates problem. To study the size dependent properties of NiNPs of two different size ~ 20 and 40 nm and similar shape (spherical) were chosen. Initially, one drop of oleic acid was added into NiNPs followed by untrasonication. Now a fix amount of NiNPs (0.5 wt. %) was dispersed in a FLC mixture. The obtained mixture (NiNPs/FLC) was thoroughly mixed using ultrasonication (1hr, frequency- 1 kHz) process to get complete and uniform dispersion of NPs in FLC medium. The prepared mixtures of NiNPs/FLC were then kept at room temperature for 1-2 days to evaporate the excess amount of surfactant.

6.3 Results and Discussion

To study the effect of size of NiNPs on the physical properties of ZLI-4851-000, two different size of NiNPs (~ 20 nm and 40 nm size) were doped in FLC mixture and studied. Two doped samples consisting of NiNPs/ FLC and undoped (pure FLC) sample of same configurations (cell thickness, dimensions) were prepared.

For electro-optic and dielectric measurements, planar aligned LC cells (Instec, USA) of cell configurations (cell gap 5.0 μm & active area 0.5×0.5 cm^2) were used. The prepared mixture of NiNPs/FLC was then injected into an empty space of LC cell. A pure sample (undoped) consisting of ZLI-4851-000 was also fabricated and studied.

6.3.1. Electro-optic properties

P_s, τ_s and γ are the essential electro-optic parameters to determine the performance of LC based displays. These parameters were studied using field reversal technique [21].

Temperature dependence on material parameters

Figure 6.1 show the temperature dependence behavior on polarisation for FLC and NiNPs/FLC samples in SmC* phase at 30V (frequency~100 Hz). It is found that dispersion of NiNPs, increases the P_s as compared to pure FLC samples. For instance at room temperature, P_s is ~1.0 nC/cm^2 for pure FLC and increased to ~ 1.6, 1.9 nC/cm^2 (experimental error ± 0.2 nC/cm^2) for 20 nm and 40 nm size NiNPs doped FLC samples respectively. The increase in P_s value after dispersion of NiNPs is a consequences of increase in net dipole moment as compared to FLC sample.

Moreover, in the case of doped sample the effect of NP size on P_s value is more predominant for 20 nm containing NiNPs/FLC sample. Further, on increasing the temperature towards SmC*- SmA phase transition, P_s show a decreasing trend in the SmC* phase and as we approaches near the SmC*- SmA transition P_s reaches to a minimum value. The decreasing behavior of P_s with temperature follow a first-order phase transition. Using power law both β, P_o were estimated and their values are shown in Table 6.1. The value of β was found to be ≤ 0.5 in pure FLC as well as in NINPs/FLC samples and confirm a first-order phase transition.

The response time (τ_s) an important parameter for display application has been measured as a function of temperature at 30V (square wave) using the relationship $\gamma = P_s E \tau_s$. The temperature dependence on τ_s for different size of NINPs is demonstrated in Figure 6.2. Figure 6.2 infers that τ_s decreases with increasing the temperature in all samples. As one can see, the dispersion of NiNPs into FLC sample reveal significantly faster τ_s than FLC. The calculated values of τ_s for FLC is 600 µsec and reduce to 390 µsec (size 20 nm), 552 µsec (size 40 nm) in NiNPs/ FLC samples. γ is related to the rotation of molecule about the SmC* cone has also been calculated in SmC* phase and its temperature dependence behavior is also presented in Figure 6.3. The experimental result indicates a small increase in γ for doped samples over pure FLC sample, which decreases with increasing the temperature, as expected. However size of NPs does not affect the value of γ to a considerable extent. A more repaid decrease in γ is seen in the vicinity of the SmC*-SmA transition, which can be attributed to the softening of the potential and the electro-clinic effect. In doped samples, no clear trends or considerable impact except at low temperature region in γ is seen as a function of NiNPs size.

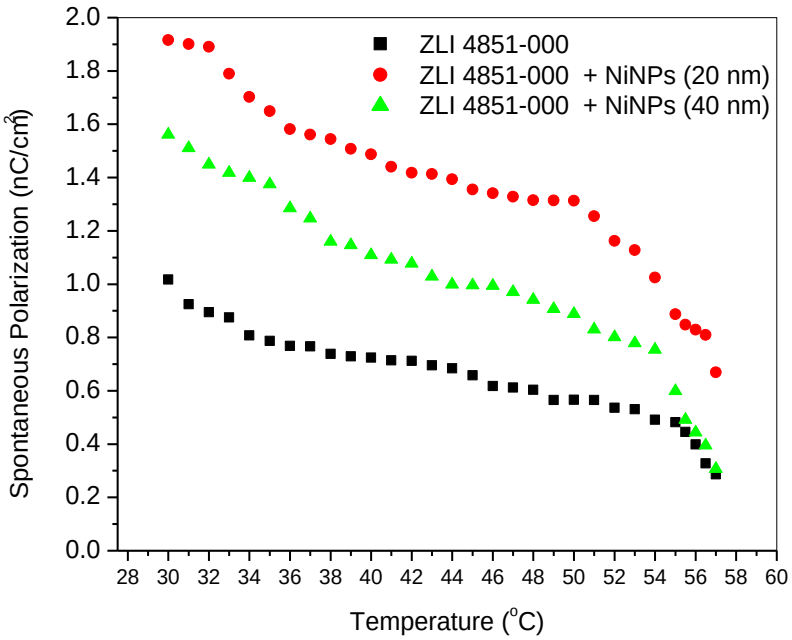

Figure 6.1. Variation of temperature with spontaneous polarisation at 30Vin SmC* phase.

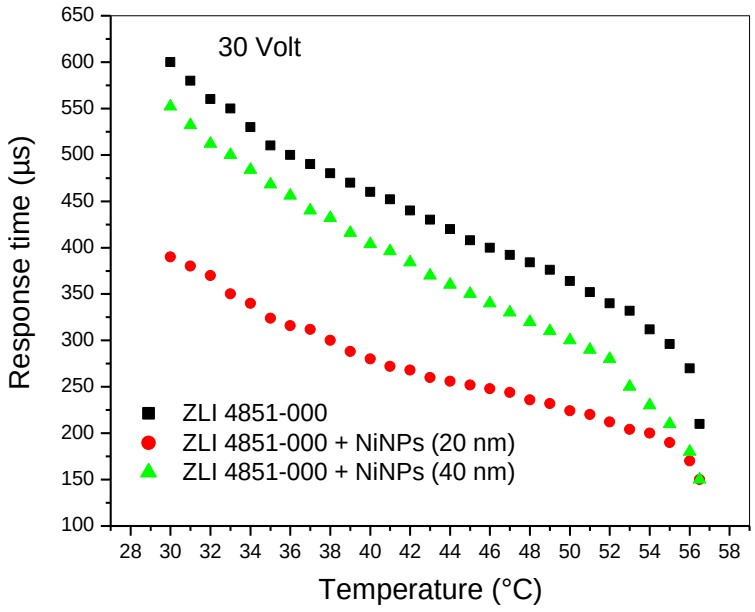

Figure 6.2. Temperature dependence of response time for FLC and NiNPs doped FLC samples at square wave (30V)

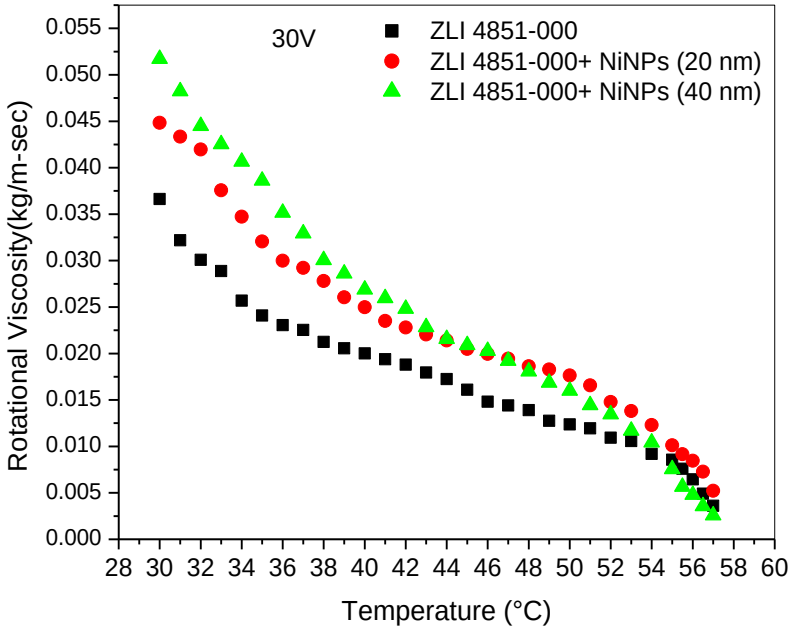

Figure 6.3 Temperature dependence of rotational viscosity for FLC and NiNPs doped FLC samples

Bias Voltage Dependence

The effect of applied voltage on EO parameters in SmC* phase for pure FLC and NiNP/ FLC samples is also shown in Figure 6.4 (a-c). It is seen that in all samples P_s more or less increases with the applied voltage up to ~30V and beyond this voltage, a saturation state is reached. It is expected that around this voltage the dipoles of LC and NPs preferably aligned along the electric field direction and consequently attain a saturation. In case of doped sample the saturation occurs slightly at 3-4 V less than the voltage required to get saturation in case of pure FLC sample. An improved τ_s after dispersion of NiNPs is seen in Figure 6.4 (b). A more pronounced faster response time is observed in larger NP size sample as compared to smaller NP sized sample. The improvement in electro-optic parameters (P_s and τ_s) in NiNPs/FLC samples is attributed to the interaction between NiNPs and FLC molecules. We expect that in doped samples, NiNPs is surrounded by the FLC molecules and a long range interaction is established between Ni and FLC molecules. NiNPs are ferromagnetic in nature and their dipoles are parallel to FLC dipole orientations. In the presence of applied electric field, the dipole moment of Ni gets aligned and adds up to the FLC dipoles. Thus, overall effective dipole moment per unit volume increases in

comparison to pure FLC sample and show a corresponding improvement in polarisation. The combined effects of P_s and γ decrease the response time in NiNPs/FLC as illustrated in Figure 6.4(b). The effect of NiNPs size on P_s and τ_s is also studied which is very low or almost negligible. Recently Zangana *et al.* also disperse $BaTiO_3$ NPs into FLC system and found that size of $BaTiO_3$ NPs has very low or negligible effect on FLC switching properties [22].

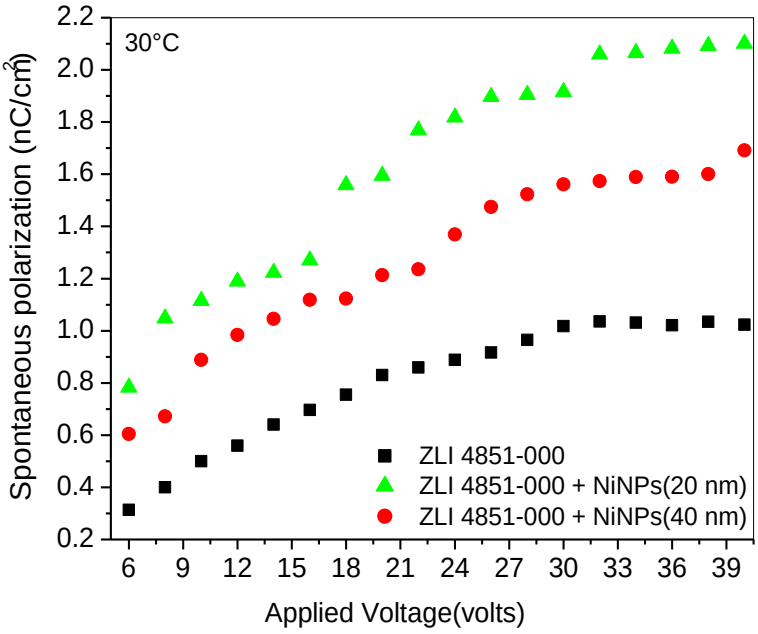

(a)

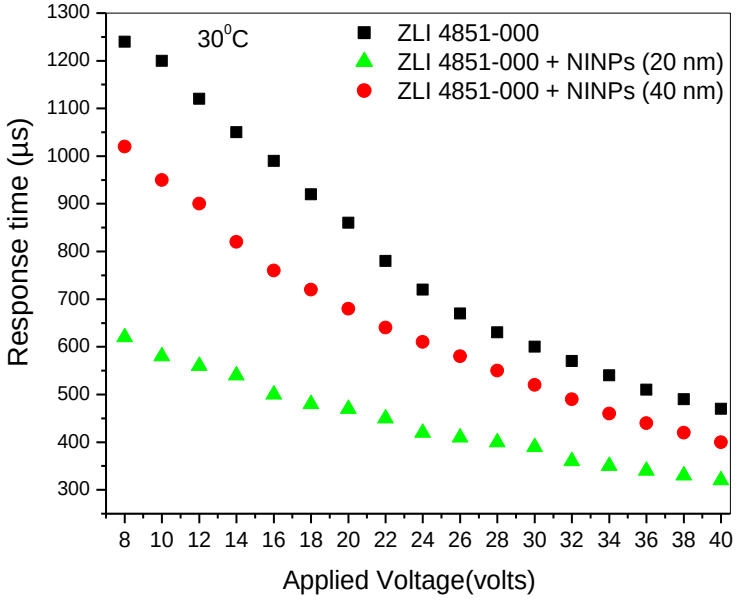

(b)

Figure 6.4 Applied voltage dependence of (a) polarisation (b) response time for pure FLC and NiNPs/FLC samples at 30°C.

Anchoring energy

A temperature dependence behavior on dispersion and polarisation energy coefficients are plotted in Figure 6.5(a, b). These coefficients are measured by the Equations, 5.3 (a, b) as mentioned in chapter 5. [23, 24] It is seen that W_P and W_D decreases with increasing the temperature. Doping of NiNPs increase the amount of W_P and W_D in comparison to pure FLC sample, However a trivial increase in anchoring energy contribution is noticed with increasing the size of NiNPs which is almost negligible. The rise in anchoring energy behavior with NiNPs size support the enhancement in viscosity in case of NiNPs-FLC sample than pure FLC sample.

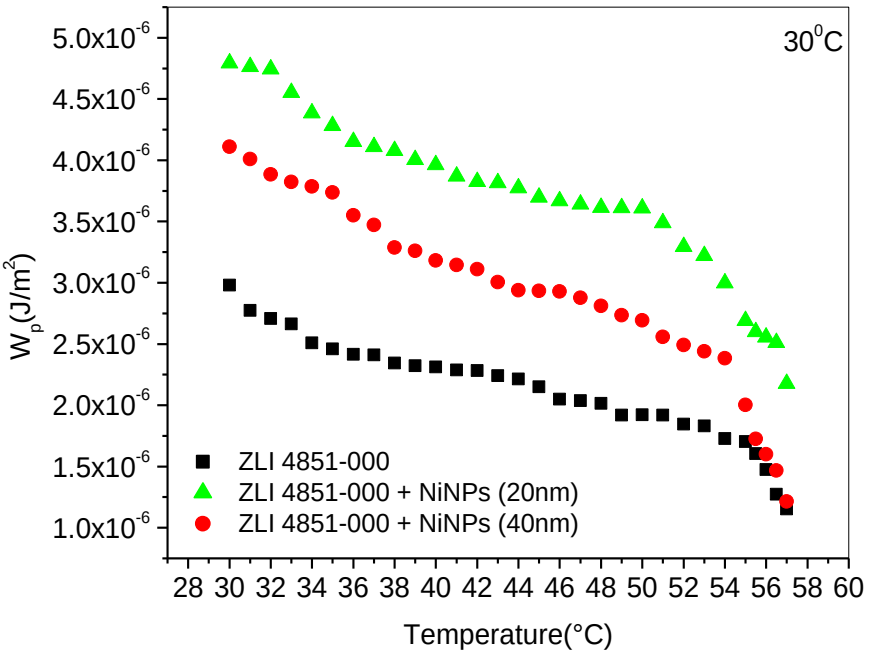

(a)

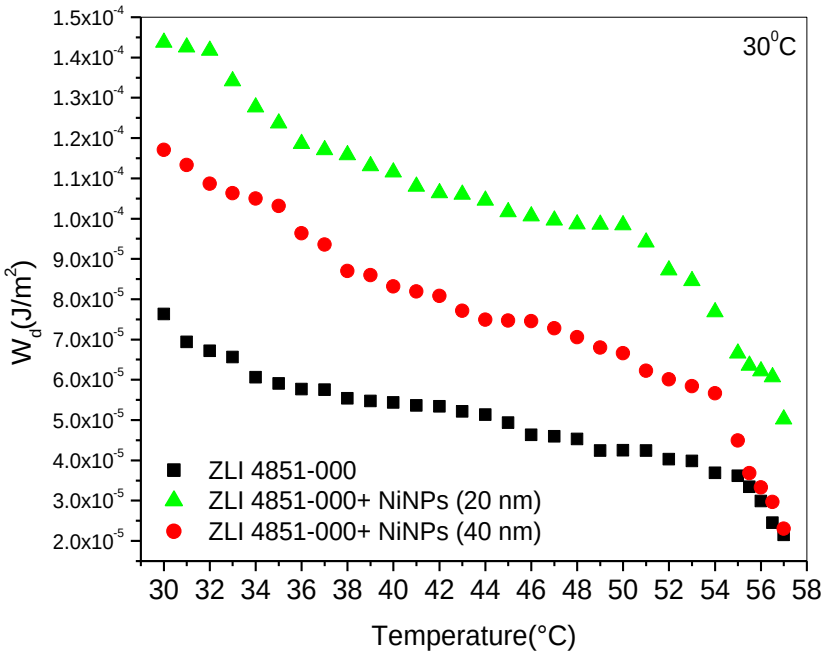

(b)

Figure 6.5 Temperature dependence on (a) anchoring energy coefficient's (b) dispersion energy coefficient's for pure FLC and NiNPs/FLC samples at 30°C.

6.3.2 Dielectric studies of NiNPs/FLC composites

Temperature dependence on permittivity

Temperature dependence on permittivity ($\varepsilon', \varepsilon''$) for neat FLC and NiNPs/FLC samples at 217 Hz are shown in Figure 6.6 (a, b). In SmC* phase initially ε' increases with increasing the temperature and then decrease to a minimum value as we approaches towards the SmC*- SmA phase transition temperature. It is clearly seen that this behavior is observed not only in pure FLC sample but also exist in NiNPs/ FLC samples. Figure 6.6 (a) indicates that ε'slightly increase with Ni dispersion and this increase with the size (average ~ 20, 40 nm) of NiNPs is within the limit of error. Since in the present work, the NiNPs size difference is not large (~20nm) and these size of NPs does not have any measurable effect on the permittivity as well as on the SmC*- SmA phase transition temperature. It specifies that different size of NiNPs does not disturb the order of FLC molecules and respective layer spacing. In a recent work, Zangana *et al.* have also reported that size of doping NPs does not have much impact on dielectric properties of FLC [22]. A temperature dependence on permittivity (ε'') for pure FLC and NiNPs/ FLC samples are also represented in

Figure 6.6(b). A similar type of temperature dependent behavior of permittivity in pure ZLI 4851-000 mixture was also obtained in planar aligned cells (5, 7.5 µm) [25].

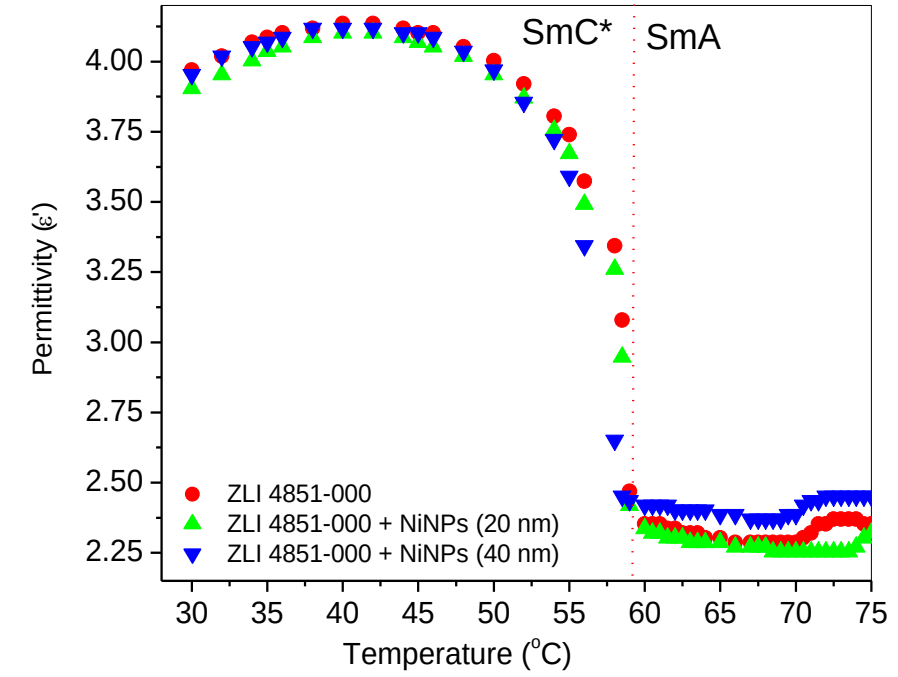

(a)

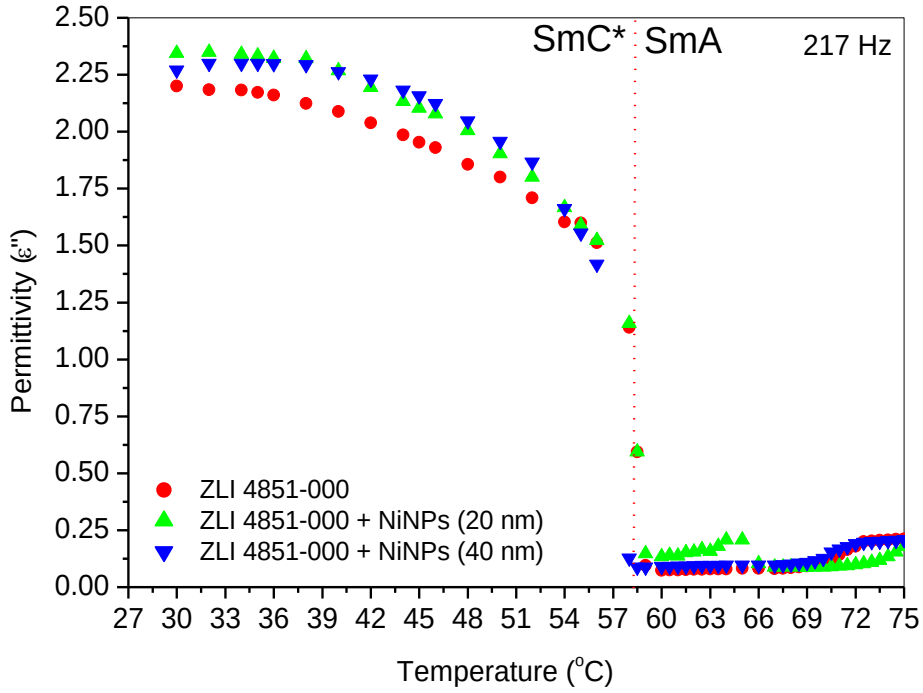

(b)

Figure 6.6 Temperature dependence of dielectric permittivity at a frequency of 217 Hz (a) real part of permittivity (b) imaginary part of permittivity for pure FLC and NiNPs/ FLC doped samples.

The relaxation frequency (f_r) and dielectric strength ($\delta\epsilon$) for GM is expressed using Landau free energy expression [26].

$$f_r = \frac{K_3 q^2}{2\pi\gamma} \quad (2)$$

$$\delta\epsilon_{GM} = \frac{P_s^2}{2\varepsilon_0 K_3 q^2 \theta^2} \quad (3)$$

Where, K_3 is Frank elastic constant and q is the wave vector ($q = \frac{2\pi}{p_0}$) where p_0 denotes helical pitch of material. The temperature dependence of GM f_r for pure FLC and doped samples is shown in Figure 6.7. It is clearly seen that in SmC* phase, f_r increases and on further increase in temperature it decreases near the SmC*- SmA transition. This increase in f_r with temperature and then decrease near the transition temperature might be caused by the competition between the temperature dependence on k_3 and γ in SmC* phase as given by $f_r \sim \frac{K_3}{\gamma}$. A small decrease in f_r with the dispersion of NiNPs is also noticed however size of NiNPs does not have any significant effect. The measured value of GM f_r at 30^0C is ~113, 112, 91 Hz in pure FLC and 20, 40 nm size NiNPs/ FLC samples, respectively. The obtained relaxation frequency is in good agreement with the previously reported relaxation frequency of GM in FLCs [27,28]. The temperature dependence on dielectric strength of GM ($\delta\epsilon_{GM} = (\varepsilon_0 - \varepsilon_\infty)$) is shown in Figure 6.8. Figure 6.8 infers that $\delta\epsilon_{GM}$ decreases with increasing the temperature up to the transition temperature. The $\delta\epsilon_{GM}$ of NiNPs/FLC samples is higher as compared to pure FLC sample and more pronounced at smaller size (20nm) of NiNPs. From Equation 3, $\delta\epsilon_{GM} \propto P_s^2$; it indicates that an increse in dielectric strength depends on polarisation factor which is higher in doped sample than pure FLC sample. The effect of size of NPs on the electro-optic and dielectric parameters are presented in Table 6.2.

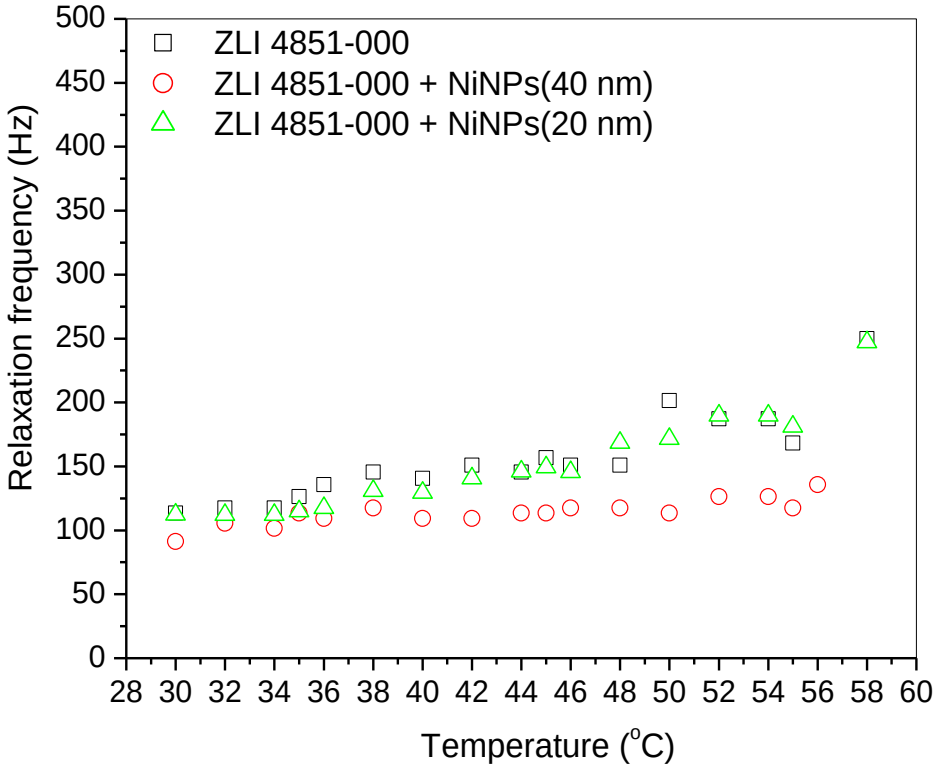

Figure 6.7. Temperature dependence of relaxation frequency in SmC* phase for pure FLC and NiNPs/FLC samples.

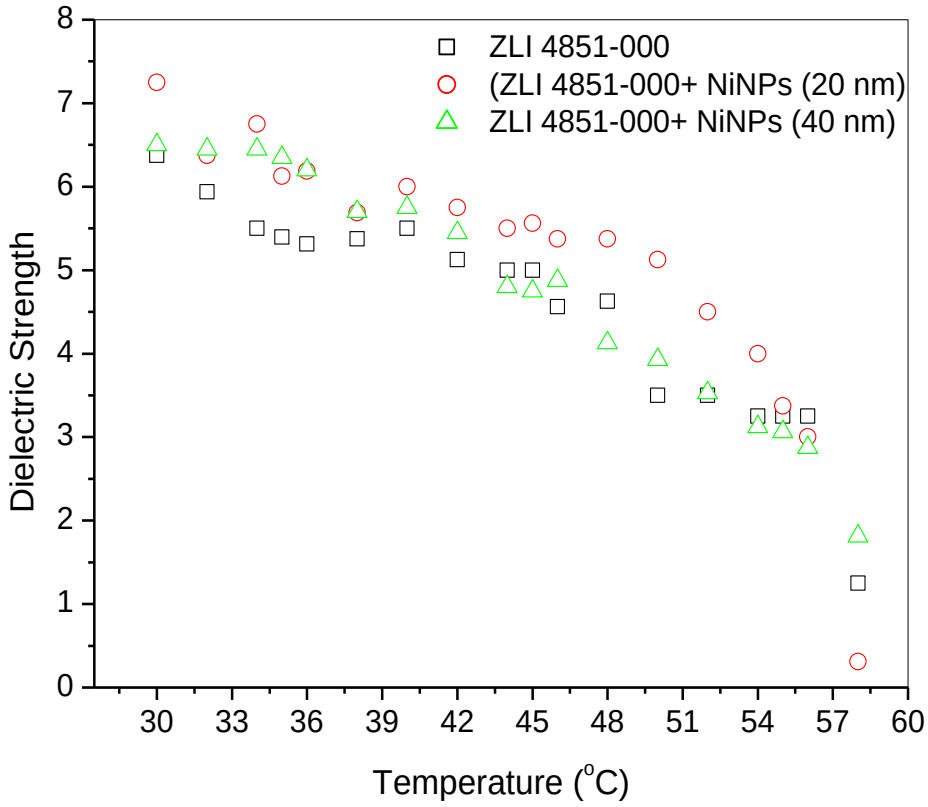

Figure 6.8 Temperature dependence of goldstone mode dielectric strength in pure FLC and NiNPs/FLC samples.

6.3.3 UV-Vis spectroscopy studies

The UV-Visible absorption spectra for pure and NiNPs doped FLC samples is shown in Figure 6.9. In Figure 6.9 a single absorption peak is observed in the visible spectrum at a wavelength of 363 and 362 nm for pure FLC and NiNPs-FLC samples respectively.

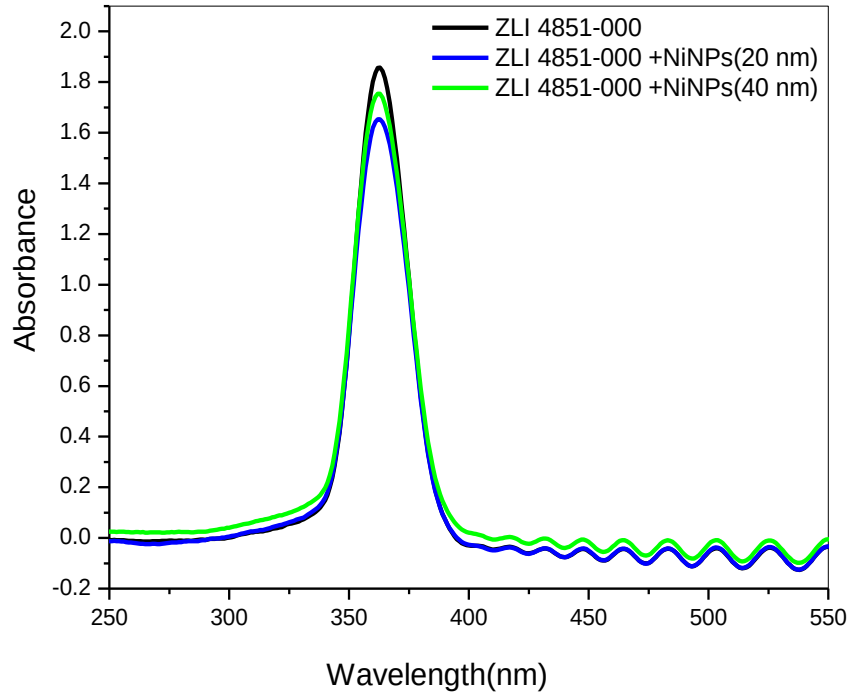

Figure 6.9. UV-Vis spectra of pure FLC and NiNPs/FLC samples

Table 6.1

Effect of NiNPs size on critical exponent and constant

Samples	P_o	β
ZLI 4851-000	0.18	0.43
ZLI 4851-000+ NiNPs (20 nm)	0.30	0.50
ZLI 4851-000+ NiNPs (40 nm)	0.23	0.49

Table 6.2

Physical properties of Pure FLC and NiNPs dispersed FLC mixtures at 30°C

Sample	P_s (nC/cm^2)	τ_s (μs)	$\boldsymbol{\gamma}$ (kg/ms)	$\boldsymbol{\delta\varepsilon_{GM}}$	f_r (Hz) ±10 Hz
ZLI 4851-000	1.0	600	0.036	6.4	113
ZLI 4851-000+ NiNPs (20 nm)	1.6	390	0.044	7.2	112
ZLI 4851-000+ NiNPs (40 nm)	1.9	552	0.051	6.5	91

References:

[1] P. Malik, K. K. Raina, A. J. Bubnov, et al. Phase Trans. 2006; 79: 889-898.

[2] S. T. Lagerwall, Ferroelectric and Antiferroelectric Liquid Crystals, WILEY-VCH Verlag GmbH, Weinheim-Germany, 1999.

[3] J. P. F. Lagerwall, G. Scalia, Curr Appl Phys. 2012; 12:1387-1412.

[4] R. B. Meyer, L. Liebert, L. Strzelecki, et al. J de Physique. 1975; 36: 69- 71.

[5] T. Joshi, A. Kumar, J. Prakash, et al. Liq Cryst. 2010; 7: 1433-1438.

[6] P. Malik, A. Chaudhary, R. Mehra, et al. Mol Cryst Liq Cryst. 2011; 541: 243-251.

[7] H. Duran, B. Gazdecki, A. Yamashita, T. Kyu. Liq Cryst. 2005; 32: 815-821.

[8] A. Chaudhary, P. Malik, R. Mehra, et al. J Mol Liq. 2013; 188: 230-236.

[9] E. Ouskova,Buchnev O, Reshetnyak V, et al. Liq Cryst. 2003; 30:1235-1239.

[10] M.S. Zakerhamidi, S. Shoarinejad, S. Mohammadpour. J Mol Liq. 2014; 191: 16-19.

[11] R. K. Shukla, K. K. Raina, V. Hamplová, et al. Phase Trans. 2011;84:850-857.

[12] E. V. Popova, S. A. Gamzaeva, A. I. Krivoshey, et al. Liq Cryst. 2015; 42(3): 334- 343.

[13] G. Cordoyiannis, S. Gyergyek, B. Rozic, et al. Liq Cryst. 2016; 43(3): 314-319.

[14] Khushboo, P. Sharma, P. Malik, et al. Phase Trans. 2015; 89: 144-154.

[15] A. Mikulko, P. Arora, A. Glushchenko, et al. Europhys Lett. 2009; 87: 27009.

[16] R. K. Shukla, C. M. Liebig, D. R. Evans, et al. RSC Adv. 2014; 4: 18529-18536.

[17] Neeraj, K. K. Raina. Opt Mat. 2013; 35:531-535.

[18] A. Rudzki, D. R. Evans, G. Cook et al. App Opt. 2013; 52: E6-E14.

[19] P. Kumar, A. Sinha. Phase Trans.2015; 88: 605-620.

[20] R. K. Shukla, A. Sharma, T. Mori et al. Liq Cryst. 2016; 43: 695-703

[21] P. Malik, K. K. Raina, A. K. Gathania. Thin Solid Films. 2010; 519: 1047-1051.

[22] S. Al Zangana, M. Tuner, et al. Appl. Phys., 2017; 121: 085105-1.

[23] Khushboo, P. Sharma, P. Malik. 2016; 43: 1671-1681.

[24] F. J. Lyuu, C. C. Chen, J. Y. Lee. Mol Cryst Liq Cryst. 1999; 329: 99- 112.

[25] R. Singh, K. K. Raina, Int J of Mod Phys. 2008; 22: 2263-2273.

[26] T. Carlsson, B. Zeks, C. Filipic et al. Phys. Rev. A 1990; 42: 877–889.

[27] P. Malik, A. Chaudhary, R. Mehra et al. Liq Cryst 2011; 541: 243–481.

[28] Neeraj, K. K. Raina, Phase Trans. 2010; 83: 615–626.

Chapter - 7

Conclusions

Overview

In this chapter, we have summarized the main finding and results obtained from the textural, thermal, dielectric and electro-optic studies of magnetic nanoparticles dispersed liquid crystal composites. The effect of magnetic nanoparticles dispersion on physical properties of nematic and ferroelectric liquid crystal composites have been thoroughly investigated in planar cell and discussed in Chapters 4, 5 and 6. The future scope have been explored on the basis work presented in this thesis from basic and applied research point of view.

In this thesis, efforts have been made to prepare, understand and systematic study of magnetic nanoparticles dispersed liquid crystal composites. The prepared materials were characterized using polarizing and thermal microscopy; electro-optic; thermal and dielectric spectroscopy.

The main results of the present work are summarized in the following points:

- The effect of small amount (0.25%) of Iron nanoparticles dispersion on the micro-texture, phase transition temperature, electro-optical and dielectric properties of 6OCB nematic LCs in planar cell configuration cell is investigated.
- Dispersion of Fe NPs significantly improve the transmission characteristic and decrease the threshold voltage from 1.4 V to 1.0 V. An increase in birefringence is notice in 6OCB-Fe.
- The DSC and polarizing microscopy confirm that inclusion of Fe NPs affect the Cr-N and N-I transition temperature which is almost negligible.
- Addition of Fe NPs also decreases the f_r from 1.80-1.65 MHz. This decrease is due to the flip-flop motion of the LC molecules about their short axis. A decrease in activation energy is also observed. The band gap and ac conductivity increases with the addition of Fe NPs.
- Doping a NFNPs into FLC mixture has substantial effect on spontaneous polarization, response time and rotational viscosity. The polarisation decreases with increasing the temperature and NFNPs concentration. The response time was observed to be 478 µsec and 166 µsec for the pure and doped (at 0.5 wt. %) samples, respectively.

- ❖ Decrease in electro- optic parameters is explained on the basis of dipole-dipole interaction, change in FLC order after doping and anchoring phenomena. The anchoring energy coefficient's decreases with increasing the NFNPs concentration.
- ❖ The dielectric strength of pure FLC decreases to one-fourth for NFNPs-doped sample [at 0.5wt. %]. In addition, relaxation frequency increase in SmC* phase and declines near the SmC*- SmA transition temperature. Nearly twofold increase in f_r for doped sample compared to the pure FLC sample is found. The GM is observed in all samples at ~ 400 Hz to ~500Hz and a Debye type relaxation behavior is confirmed.
- ❖ The measured value of E_g was found to be ~3.7 eV and virtually independent of NFNPs doping concentration. The activation energy decreases from 5.41 kJ/mole to 4.42 kJ/mole for pure FLC to doped FLC (0.5 wt. % NFNPs) samples, respectively.
- ❖ Dispersion of NiNPs show a small increase in spontaneous polarization and faster response time. The improvment in polarisation is due to net increase in dipole moment with the dispersion of NiNPs. The size of NiNPs has almost negligible effect on spontaneous polarization, rotational viscosity but show faster response time.
- ❖ The effect of applied voltage indicates that dispersion of NiNPs reduces the saturation voltage up to 3-4 volts than in pure FLC sample. The anchoring energy coefficients decreases with increasing the temperature.
- ❖ The relaxation frequency increases with the increase of temperature in SmC* phase and declines near the SmC*-SmA transition temperature. It is also observed that both relaxation frequency and $\delta\epsilon_{GM}$ are more or less independent of size of NiNPs. The Goldstone mode is observed in all samples at a relaxation frequency of ~100 Hz.

Future Scope

In this report, it is concluded that dispersion of magnetic nanoparticles in LCs show an enhancement in physical properties of liquid crystals. The improvement in LC characteristic suggests that blend of magnetic nanoparticles with liquid crystals may helpful to develop a soft magneto-electric materials which can tune with magnetic and electric fields. In the next phase, we would like to explore and study soft magneto-electric materials for magneto-optical applications. The deep understanding of these systems and coupling between magnetic nanoparticles and soft materials will promote us to develop soft materials for fast respond display devices.